Engineering Complex Kidney Structures for Disease Modelling, Drug Testing, and Studying Kidney Development

Thesis

ENGINEERING COMPLEX KIDNEY STRUCTURES FOR DISEASE MODELLING, DRUG TESTING, AND STUDYING KIDNEY DEVELOPMENT

Thesis submitted by

Valerio Brizi

For the degree of

Doctor of Philosophy (PhD)

Discipline of Life Sciences

The Open University, Milton Keynes, United Kingdom
IRCCS - Istituto di Ricerche Farmacologiche 'Mario Negri', Bergamo, Italy

Director of Studies
Dr. Susanna Tomasoni, PhD

Internal Supervisor
Dr. Christodoulos Xinaris, PhD

External Supervisor
Prof. Neil Turner, PhD, FRCP

September 2017

ENGINEERING COMPLEX KIDNEY STRUCTURES FOR DISEASE MODELLING, DRUG TESTING, AND STUDYING KIDNEY DEVELOPMENT

Valerio Brizi

IRCCS - Istituto di Ricerche Farmacologiche 'Mario Negri', Bergamo, Italy

The Open University, Milton Keynes, United Kingdom

Doctor of Philosophy (PhD)

September 2017

ABSTRACT

Although existing kidney tissue engineering systems and cell-based strategies favoured significant advances in the field, they cannot reproduce the organ's complex architecture. This prevented the use of these tissues in studying kidney development realistically, modelling diseases, and establishing therapeutic approaches.

To fill these gaps, we devised a 3D engineering system for rapid generation of custom-made geometrically predefined kidney units that more faithfully resemble their counterparts *in vivo*.

Combining 3D printing and PDMS prototyping, we fabricated differently sized and shaped scaffolds into which MDCK cells were seeded and cultured under tubulogenic conditions. Cells grew and self-assembled into branched tubules with single lumen delimited by a polarised monolayered epithelium, exhibiting kidney-specific functions.

To model polycystic kidney disease (PKD), we pharmacologically induced cyst formation within engineered tubules. Next, we tested and quantified different compounds' effect on cyst regression, identifying new potential pharmacological treatment; we showed that 2-deoxy-D-glucose is more effective than other compounds and discovered that berberine possesses high therapeutic potential for PKD treatment.

Optimising the protocol and using different human iPSC lines, we successfully engineered functional human ureteric bud (UB)-like tubules capable of recapitulating early steps of UB morphogenesis. Exploiting these developmental capacities, we used tubules to identify a novel growth factor combination that induces budding events in a way comparable to mouse embryonic kidneys and that may therefore be involved in human UB development. Observing a marked reduction of ramified buds in tubules derived from a patient with heterozygous *PAX2* mutation affected by focal segmental glomerulosclerosis, we speculated that such developmental disorder might have contributed to the patient's condition.

Overall, these findings document that our innovative and robust technology for controlled tubule engineering provides a valuable and reliable platform for kidney disease modelling, drug discovery and developmental studies, and may lay the groundwork for creating anatomically correct kidney tissue *in vitro*.

ACKNOWLEDGEMENTS

I am grateful to Professor Silvio Garattini, Director of the IRCCS - Istituto di Ricerche Farmacologiche 'Mario Negri', Professor Giuseppe Remuzzi, Research Coordinator of the 'Mario Negri' Laboratories in Bergamo, and Dr. Ariela Benigni, Head of Molecular Medicine Department for giving me the opportunity to undertake the PhD course, broadly strengthening my specialist knowledge and professional skills.

I am indebted to my Director of Studies, Dr. Susanna Tomasoni, for having carefully supervised my work, for her suggestions, scientific support, and, above all, for believing in me.

I would also like to express my special gratitude and appreciation to my Internal Supervisor, Dr. Christodoulos Xinaris, for his precious support in overseeing my research over these years and constantly encouraging me with his unique and special advice, allowing me to grow not only scientifically, but also on a personal level. You have been a remarkable mentor for me, and I feel honoured to have worked by your side.

I am thankful to my External Supervisor, Professor Neil Turner, for his outstanding courtesy and continuous availability in supervising my work and progresses.

Many thanks to Dr. Valentina Benedetti and to the colleagues of my Laboratory, in particular Dr. Lorena Longaretti and Dr. Osele Ciampi, who have been constantly to my side and incited me to strive towards my goal.

I am also grateful to the patient L.S. for the kindly blood donation, thus allowing the execution of the patient-related studies in my research.

Finally, heartfelt thanks to my family. No words can express how grateful I am to my parents, my brother and my beloved fiancée Giusy for everything they have made on my behalf, and for their limitless love and patience with me. You all sustained me in every single moment when there was no one to answer my queries. I love you, from the depths of my heart.

CONTENTS

Table of Contents

CHAPTER 1 - INTRODUCTION

1.1 Chronic kidney disease: a public health problem

Chronic kidney disease (CKD) is a leading cause of morbidity and mortality in modern society. Currently, CKD affects hundreds of million people worldwide and has a consistent estimated global prevalence of between 11 to 13% (Hill *et al.*, 2016). Its global incidence and prevalence are rapidly increasing, particularly in developing countries, thus making CKD, without a doubt, a major global public health issue.

Major causes of CKD are diabetes, hypertension, infectious diseases and acute kidney injury as consequence of several drug exposure, and polycystic kidney disease (PKD), the most common genetic renal disease affecting all ethnic groups (Ong *et al.*, 2015; Brunelli *et al.*, 2015; Mao *et al.*, 2016).

In most patients, CKD eventually progress towards kidney failure, also called end-stage renal disease (ESRD) that, being characterised by irreversible loss of nephrons and deterioration of renal function, is incurable.

The only treatment for ESRD is renal replacement therapy (RRT), which aims to substitute the critical kidney functions and sustain life in affected people. RRT consists of hemodialysis, peritoneal dialysis and kidney transplantation.

Although dialysis keeps patients alive by replacing exclusively the non-endocrine kidney functions such as removal of molecular waste products from the blood, the patients' quality of life is severely impaired by life-threatening complications (Rodrigues-Díez *et al.*, 2017). The global healthcare costs for dialysis patients are between $150,000 and $200,000 per year and will exceed $1 trillion this decade. This significant economic burden, combined with the ongoing 7% annual increase in patients who need dialysis, will make this treatment impractical and unaffordable even in developed countries (Perico and Remuzzi, 2012).

The alternative to dialysis is kidney transplantation, which, at present, represents the most effective treatment for patients with ESRD. In fact, both quality of life and life expectancy in people who underwent kidney transplantation are better than in long-term dialysis patients (Wolfe *et al.*, 1999). Unfortunately, almost every patient who receives kidney transplant undergoes non-specific immunosuppressant treatments, with increased risk of developing malignancies, opportunistic infections, cardiovascular and metabolic diseases, all of which negatively influence graft function and outcome. In addition to these problems, the critical shortage of compatible donor organs for transplantation makes it extremely hard to meet the existing demand for renal replacement, so that the vast majority of patients die on the waiting list before receiving a kidney (Rodrigues-Díez *et al.*, 2017).

The high costs associated with RRT, combined with the rising imbalance between the number of patients waiting for kidney transplantation and the availability of donor organs, make indispensable the development of alternative therapeutic approaches. The establishment of effective therapies for CKD is also hindered by the lack of experimental models systems that faithfully reproduce the disease and the kidney's extremely complex cellular composition, intricate anatomy and physiology.

1.2 Early kidney development

The posterior primitive streak, a linear band of cells that forms at the caudal edge of the embryo epiblast, gives rise to the intermediate mesoderm (IM), a narrow cell population comprised between paraxial and lateral plate mesoderm, from which mammalian kidney originates. The IM differentiates, in turn, into the nephric duct (ND) epithelium and the adjacent metanephric mesenchyme (MM), the two key renal precursor tissues that will form the metanephric kidney through reciprocal and finely orchestrated interactions (Saxén, 1987; Little *et al.*, 2016; Takasato *et al.*, 2016) **(Figure 1)**.

In mice, at 10.5 embryonic days (E10.5), and E35 in humans, morphogenetic signals from the MM induce the outgrowth of the ureteric bud (UB) as a lateral branch at the caudal end of the ND epithelium. The UB is a tubular structure endowed with a lumen delimited by a polarised epithelium and a basement membrane (Meyer *et al.*, 2004; Chi *et al.*, 2009). UB formation occurs in correspondence of a single area, so that only one UB arises from the ND, thus guaranteeing the development of a single and unique collecting duct system. The UB stalk between the MM and the ND epithelium develops into the ureter that joins the kidney with the bladder.

At E11, the UB invades the adjacent MM and, through direct cell-cell contact and secretion of morphogens by its cells, induces the condensation of a subset of MM cells surrounding the bud tip. These condensed mesenchymal cells form the cap mesenchyme (CM), which comprises nephron progenitor cells morphologically distinguishable from the surrounding un-induced metanephric blastema (Davidson, 2008) **(Figure 1)**.

At E11.5, the CM induces the UB epithelium to branch for the first time and generate a T-shaped bifurcation consisting of two UB tips, each at the end of a stalk. Concomitantly, the newly formed UB tips induce condensation of surrounding un-induced MM cells, leading to the formation of a CM in correspondence of each bud tip (Vainio and Lin, 2002; Hendry *et al.*, 2011; Krause *et al.*, 2015). From this time onwards, each CM will induce the UB tips to branch and, simultaneously, undergo mesenchymal-to-epithelial transition (MET) to form a primitive polarised epithelium, the renal vesicle (RV). The RV grows, elongates and forms a comma-shaped body, which then develops into an S-shaped body that undergoes segmentation and eventually gives rise to the nephron **(Figure 1)**. In particular, the S-shaped body's distal portion, which fuses to a UB branch, becomes the distal tubule of the nephron, the middle region gives rise to both the loop of Henle and the proximal

tubule of the nephron, and the other end develops its own vascularisation to form the glomerulus (Davidson, 2008).

As kidney development proceeds, the UB epithelium continues to grow, elongate and branch, with each new UB tip acting as an inductive centre for nephrogenesis (Vainio and Lin, 2002). Through its developmental program, named branching morphogenesis, which consists of iterative budding and branching events, the UB eventually forms the tree-like collecting duct system of the kidney with the typical cortical-medullary organisation.

These MM and UB derivatives will develop a network of interconnected epithelial tubules consisting of polarised monolayered epithelia of aligned and tightly adhering cells surrounding a single central lumen. This complex structural organisation arises through the formation of specialised junctions between cells, which establish apical domains oriented toward the lumen, and basal and lateral domains in contact with the basement membrane and adjacent cells, respectively (Andrew and Ewald, 2010). In order to assemble into appropriately polarised tissue, cells must also interact with the extracellular matrix (ECM) through different types of receptors, such as integrins, and with neighbouring cells through diffusible molecules, such as morphogens, chemoattractants and chemorepellants (Bryant and Mostov, 2008; Bryant *et al.*, 2010). Therefore, the combination of cell-cell and cell-ECM interactions drives the apical-basal polarity establishment by segregating membrane components into different cell domains.

As every epithelial tubular structure, kidney epithelial tubules can form through the mechanisms of cord hollowing, cell hollowing and cavitation (Andrew and Ewald, 2010; Lubarsky and Krasnow, 2003).

In cord hollowing, small multiple lumens form at the apical membrane contact sites - following cell polarity establishment within tissue primordia - and then fuse together to create a single and continous lumen.

In cell hollowing, luminal spaces originate within individual cells as large cytoplasmic vesicles, which then fuse together and, ultimately, with the plasma membrane to connect with lumens formed within the adjacent cells of the developing tubular epithelium.

The mechanism of cavitation begins with polarisation of unpolarised primordia's peripheral cells that will constitute the mature tubular epithelium, followed by death for apoptosis of the cells in the central region that are not in contact with the ECM, leading to the generation of a single lumen.

Kidney tubules are surrounded by supporting cells, also known as stromal cells, which originate from the MM and constitute a population of cells distinct from that of the nephrogenic precursors **(Figure 1)**. Shortly after UB invasion, stromal cells can be identified in the MM as spindle-shaped mesenchymal cells (Hatini *et al.*, 1996). Stromal progenitor cells can differentiate into various non-epithelial cells in the adult kidney, including interstitial fibroblasts responsible for synthesizing collagen and producing erythropoietin (Bachmann *et al.*, 1993; Li *et al.*, 2014; Maxwell *et al.*, 1993), endothelial cells that form the peritubular capillaries (Sims-Lucas *et al.*, 2013), vascular smooth muscle cells, pericytes and glomerular mesangial cells (Humphreys *et al.*, 2010). Furthermore, by secreting ECM proteins and signalling molecules, stromal cells play pivotal roles for the appropriate nephrogenesis and collecting duct system formation. In particular, stromal cells are involved in regulating MM epithelialisation, UB growth and branching morphogenesis, and, by antagonising inductive signals from MM, in inhibiting budding from inappropriate or multiple sites of the ND epithelium (Al-Awqati and Oliver, 2002; Cullen-McEwen *et al.*, 2005).

Overall, cell populations and tissues described above interact in a spatiotemporally regulated manner to develop an intricate architecture, which supports the functional and physiologically active adult kidney.

1.3 Overview of kidney anatomy and functions

The kidney is a vital organ with an exceptionally complex morphology and highly specialised in maintaining body fluid homeostasis. Indeed, by filtering blood, kidney regulates the body's water balance and chemical composition, controls levels of electrolytes and metabolites, and removes metabolic waste products to finally produce and excrete urine. Additional major kidney functions are reabsorption of essential nutrients, regulation of blood volume and pressure, and production of hormones indispensable for regulating erythropoiesis and the bones' density.

1.3.1 Kidney anatomy

In vertebrates, kidneys are two bean-shaped organs located on the left and right sides of the body retroperitoneal space. Each kidney shows a convex and a concave side. The narrow opening on the concave side, through which the renal artery enters the kidney and the renal vein and the ureter leave, is called renal hilum. A thin layer of connective tissue, known as the renal capsule, envelopes the whole kidney's surface (Rodrigues-Díez *et al.*, 2017) **(Figure 2)**. Beneath the renal capsule, the kidney can be divided in two main regions easily recognisable by observing the sagittal section of the organ: (*i*) the renal cortex on the outside, and (*ii*) the deeper medullary region (Taal *et al.*, 2011). In humans, the medulla is organised into 8 to 18 cone-shaped structures, the renal pyramids, spaced out by projections of the cortex, called renal columns. The base of each renal pyramid resides within the renal cortex, while its tip, the papilla, extends inward towards the renal pelvis, and empties the urine formed by each pyramid into a minor calyx **(Figure 2)**. The minor calyces coalesce to form 2 to 3 major calyces, which in turn fuse to form the renal pelvis - a funnel-like structure that exits the kidney through the renal hilum and drains the urine away into the ureter (Taal *et al.*, 2011). Renal pelvis, calyces and hilum are contained into

a fatty compartment, the renal sinus, which separates these structures from the renal medulla **(Figure 2)**. This structural organisation is crucial to the appropriate kidney function since it establishes an osmotic gradient from the cortex to the medulla that drives urine concentration.

1.3.2 The nephron

The nephron is the key structural and functional unit of the kidney. It filters blood and produces urine. Structurally, it can be subdivided in two main sections: *(i)* the renal corpuscle, needed for blood filtration, and *(ii)* the renal tubule, needed for reabsorption and secretion (Rodrigues-Díez *et al.*, 2017).

The renal corpuscle is composed of glomerulus, mesangium and Bowman's capsule **(Figure 3)**. The glomerulus is a tuft of capillaries (or capillary loops) surrounded by mesangial cells, and is located between an afferent arteriole, which supplies blood to the glomerulus, and an efferent arteriole, which drains blood away from the glomerulus. The region where renal arterioles enter and leave the glomerulus is called vascular pole. The Bowman's capsule envelops the glomerulus and consists of an inner layer of specialised epithelial cells, called podocytes, and an outer epithelial layer of parietal cells. The narrow cavity between these two epithelial layers is the Bowman's space, also known as urinary space. Podocytes are extremely specialised cells characterised by interdigitating foot processes wrapped around the glomerular capillary loops, and forming cell-cell junctions termed slit diaphragms. The latter are crossed by pores with heterogeneous size and shape, which are responsible for the selective passage of macromolecules (Gagliardini *et al.*, 2010). The Bowman's capsule connects to the renal tubule, which can be subdivided in three segments: *(i)* the proximal convoluted tubule, lined by a simple cuboidal epithelium of cells with brush borders that strongly increase the absorption surface; *(ii)* the loop of

Henle, a U-shaped epithelial conduit consisting of two portions: the descending limb and the ascending limb; *(iii)* the distal convoluted tubule that drains urine into the collecting duct via the connecting tubule **(Figure 3)**. The human kidney contains up to 1.5 million nephrons, each of them spans the renal cortex and medulla. Specifically, the renal cortex contains glomeruli, proximal and distal convoluted tubules, and the first trait of the collecting ducts; the renal medulla contains both the loops of Henle and the collecting ducts. Since the collecting duct system's initial portion is located in the renal cortex, whereas the rest extends inwards, towards the renal medulla, it is characterised by cortical-medullary orientation **(Figure 3)**.

The fact that both nephron and collecting duct epithelia consist of cells with well-defined morphological and functional properties, explains why they are competent at exerting diverse and specific physiological roles.

1.3.3 Kidney functions

The kidney is responsible for regulating body fluids' composition and volume by filtering the blood to eliminate metabolic waste products, such as creatinine, ammonia, urea, uric acid, and toxins, and by reabsorbing water and essential nutrients. Blood filtration begins in the glomerulus and leads to the production of urine (Rodrigues-Díez *et al.*, 2017). The filtration barrier that divides blood and Bowman's space consists of the fenestrated monolayered endothelium lining glomerular capillaries, the glomerular basement membrane, and the slit diaphragm's pores between the interdigitated foot processes of the podocytes enveloping the capillary tuft (Haraldsson *et al.*, 2008).

In physiological conditions, only molecules of lower molecular size than albumin (68 kDa), for instance water and small molecules, can pass through this filter and reach the Bowman's space, forming the glomerular ultrafiltrate. The latter, flows through the

sequential segments of the renal tubule where it is modified by the highly regulated processes of reabsorption and secretion. In fact, together with waste and toxic products, the ultrafiltrate also contains metabolically useful solutes that require reabsorption.

Most of the ultrafiltrate reuptake (65-70%) occurs in the proximal convoluted tubule and allows water, electrolytes, amino acids, glucose, vitamins, and other essential macromolecules to come back to the bloodstream through peritubular capillaries. Additional ultrafiltrate concentration takes place along the loop of Henle's descending and ascending limbs via water, sodium and other ions reabsorption. This process results from the osmotic difference existing between the hypotonic ultrafiltrate and the hypertonic medullary interstitium (Rodrigues-Díez *et al.*, 2017).

As the ultrafiltrate passes through the distal convoluted tubule, reabsorption of sodium chloride, calcium and magnesium, and secretion of potassium takes place (Subramanya and Ellison, 2014). This is followed by further acidification of the ultrafiltrate since water and bicarbonate are reabsorbed as it passes from the distal convoluted tubule to the medullary collecting duct. Once at the end of the collecting duct, in the renal papilla, the modified ultrafiltrate, now called urine, is composed exclusively of a minimum amount of water and non-reabsorbed compounds, reaching the renal pelvis to be finally drained away to the bladder through the ureter.

In virtue of these sophisticated mechanisms, kidneys play a central role in the regulation of water and electrolyte homeostasis, and blood pH level and pressure. Kidneys can also regulate blood pressure through the production of the proteolytic enzyme renin secreted by the juxtaglomerular cells of the juxtaglomerular apparatus located between the glomerular vascular pole and the distal convoluted tubule of the same nephron. By triggering the renin-angiotensin system, a hormonal cascade that exerts the homeostatic control of arterial

pressure, renin raises blood pressure in response to hypotension (Rodrigues-Díez *et al.*, 2017).

In virtue of its ability to synthesize and secrete hormones, the kidney also exerts multiple endocrine functions. The two main hormones produced by kidney are erythropoietin and calcitriol. The first is a glycoprotein secreted by the peritubular cortical interstitial fibroblasts that stimulates red blood cell production in response to anemia. The second is the biologically active form of vitamin D produced by the proximal convoluted tubular cells. Calcitriol has been shown to be involved both in suppression of renin production and in maintenance of calcium homeostasis by regulating calcium reabsorption in distal convoluted tubules and medullary collecting ducts (Freundlich *et al.*, 2008; Wang *et al.*, 2012).

1.4 Engineering approaches to regenerate the kidney

Many investigation groups aimed at creating 3D kidney tissue *ex vivo* by exploiting the MM and UB cells' innate ability to reciprocally interact and instruct each other, as well as the mouse embryonic kidney's capacity to reconstruct itself after single-cell dissociation and reaggregation. Specifically, these studies - overviewed in the following paragraphs and summarised schematically in **Figure 4** - employed embryonic kidney fragments and renal progenitor cells obtained either from rodent embryonic kidneys or human pluripotent stem cell (hPSC) directed *in vitro* differentiation.

1.4.1 Tissue-based approaches

The pioneering studies by Grobstein, dated early 1950s, demonstrated that MM and UB tissues could be grown *ex vivo* and partially recapitulate the kidney's developmental program, giving rise to nephron formation and collecting duct branching morphogenesis,

respectively (Grobstein, 1953). Based on such discoveries, other groups co-cultured isolated intact MM with various inductors in order to attain nephrogenesis *in vitro* (Ekblom *et al.*, 1981; Barasch *et al.*, 1996). Specifically, isolated intact MM grew and matured into glomerular and renal tubular epithelia when cocultured with exogenous embryonic spinal cord explants used as nephrogenesis inductors (Ekblom *et al.*, 1981). In another study, Barasch *et al.* showed that isolated MMs could be induced to undergo nephrogenesis when cultured in direct contact with UB cell pellets, without the need of spinal cord or any other exogenous tissues (Barasch *et al.*, 1996).

With regard to UB branching morphogenesis, it was demonstrated that uninduced intact rat UB isolated from surrounding MM could undergo branching morphogenesis in a 3D culture system (Qiao *et al.*, 1999a). Specifically, UB was embedded in ECM-mimicking gel, and cultured in conditioned medium from an E11.5 mouse MM-derived cell line (BSN cells), which was supplemented with glial cell line-derived neurotrophic factor (GDNF) (Qiao *et al.*, 1999a). This molecule is expressed by the MM during the early stage of kidney development and is essential for UB formation, growth and morphogenesis (Sainio *et al.*, 1997). Under these culture conditions, the UB developed into 3D polarised and extensively branched epithelial tubular structures endowed with a single lumen, without the need of direct contact with MM tissue. These branched tubular structures were capable of inducing nephrogenesis when recombined with E13.5 rat MMs *in vitro*. Remarkably, MM-derived nascent nephrons were connected to the UB tubular structures to form a continous lumen, and, in turn, UB responded to the morphogenetic inductive effects of the adjacent MM by further growing and extending branches into the MM tissue. These data demonstrated that *(i)* UB branching morphogenesis does not require direct contact with MM, *(ii)* the *in vitro*-derived branched tubular structures retain their intrinsic ability to induce nephrogenesis as occurs *in vivo*, and *(iii)* the regulation of branch elongation, as

well as the appropriate branching pattern establishment, take place only when UB was physically combined *in vitro* with MM (Qiao *et al.*, 1999a).

This 3D culture system was also used to propagate isolated rat UBs *in vitro* (Steer *et al.*, 2002). The isolated intact UBs were cultured and induced to undergo branching morphogenesis, then after 8 days of culture were subdivided into thirds and each portion cultured independently for additional 8 days. This process was repeated for several UB generations. Of note, propagated UBs recombined with freshly isolated MMs were able to induce nephrogenesis and retained the ability to connect with the MM-derived tubules, leading to the formation of 'neokidneys' containing tubular structures comparable to those of whole rat embryonic kidney cultures (Steer *et al.*, 2002). Building on this strategy, Rosines *et al.* devised an approach that sequentially induced an isolated ND to bud and branch *in vitro*, demonstrating that the capacity to undergo branching morphogenesis *in vitro* is not retained exclusively by the UB (Rosines *et al.*, 2007). When freshly isolated MM was recombined with a ND-derived branched structure, the 3D nephron formation occurred, similarly to that obtained in UB-derived branched tubular structures and MM recombination experiments. The MM derivatives appeared phenotypically normal, expressed tubular transporters and were capable of organic ion transport, all features demonstrating maturation and functional capacity of the recombined tissue. Moreover, when the recombined kidney-like tissue was implanted beneath the renal capsule of a rat host, it developed multiple glomeruli positive for endothelial markers and containing erythrocytes. Finally, through global gene expression pattern analyses, it was demonstrated that the transcriptome of the nephron structures that had developed within the recombined tissue bore a resemblance to the transcriptome of the E18 rat kidney (Rosines *et al.*, 2007).

1.4.2 Creating 3D kidney tissue using embryonic kidney cells and cell lines

One of the most promising approaches in the field of tissue engineering is the generation of 'foetal' organs by exploiting the progenitor cells' intrinsic capacity to organise themselves into 3D structures typical of early organogenesis (Xinaris *et al.*, 2015).

Traditional reaggregation experiments revealed that embryonic kidney cells are able to differentiate and self-organise to form 3D tubular structures. In these pioneering studies, Auerbach and Grobstein developed a method for *in vitro* generation of a 3D tissue containing rudimental nephron-like structures through MM dissociation into single cell suspensions followed by reaggregation and co-culture onto embryonic dorsal spinal cord cell layer (Auerbach and Grobstein, 1958). Other early studies focused on kidney tissue generation via cell-based strategies demonstrated that adult renal epithelial cell lines, cultured in ECM gel-based 3D culture systems, could undergo tubulogenesis in the presence of conditioned media or embryonic kidneys (Montesano *et al.*, 1991a, 1991b; Steer and Nigam, 2004)

These studies showed that when Madin-Darby canine kidney (MDCK) cells and murine inner medullary collecting duct (mIMCD3) cells were embedded in ECM gel and cultured with fibroblast-conditioned medium (Montesano *et al.*, 1991a, 1991b) or with embryonic kidneys in the absence of direct contact (Santos *et al.*, 1994; Barros *et al.*, 1995) underwent branching tubulogenesis.

Using a similar approach, Machiguchi and Nakamura implanted individual tubular epithelial cells and mesenchymal stem cells into the subcutaneous spaces of immunodeficient rats, and stimulated them with a combination of vascular endothelial- and tubular cell-derived conditioned media to form glomerular and renal tubular structures (Machiguchi and Nakamura, 2013).

A step forward was made through the derivation and *in vitro* propagation of immortalised cell lines from uninduced MMs (BSN cell line) and unbranched UBs, which were isolated from E11.5 mouse embryonic kidneys (Sakurai *et al.*, 1997). Using these cells, Sakurai *et al.* developed a method for establishing a tubulogenesis system *in vitro*. In particular, the authors reported that, when cultured in a 3D ECM-gel with BSN cell-conditioned medium, UB cells formed cell processes and then multicellular cord-like structures - morphogenetic changes peculiar of early *in vitro* branching tubulogenesis. The multicellular cord-like structures eventually branched and gave rise to ramified and polarised epithelial tubular structures endowed with lumen comparable to those observed in cultured intact embryonic kidneys.

A more recent *in vivo* study showed that MM and UB cell lines cocultured in 3D matrices and implanted in immunodeficient mice, organised into spheroid and tubuloid structures that matured to finally form epithelia with lumens surrounded by capillary-like structures (Velagapudi *et al.*, 2012). In particular, UB cells formed almost exclusively the tubuloid structures and expressed UB/collecting duct markers, whereas MM cells differentiated mainly into capillary-like cells. Although the tubuloid structures exhibited specialised epithelial features such as apical vacuoles, microvilli, junctional complexes and linear basement membranes, the formation of brush borders and the expression of aquaporin 1 - features of mature proximal tubular epithelium - were not observed (Velagapudi *et al.*, 2012).

In the last decade, several groups showed that kidney tissue could be generated using single cells freshly isolated from embryonic kidneys as starting material (Osafune *et al.*, 2006; Unbekandt and Davies, 2010; Xinaris *et al.*, 2012; Ganeva *et al.*, 2011; Xinaris and Yokoo, 2014).

By modifying previous culture protocols (Grobstein, 1953; Kispert *et al.*, 1998), Osafune *et al.* demonstrated that murine E11.5 MM progenitor cells strongly expressing *Sall1* - a zinc-finger nuclear transcription factor expressed in the MM and essential for kidney development (Nishinakamura *et al.*, 2001) - generated 3D colonies when cultured onto a feeder layer of a mouse embryonic fibroblast cell line stably expressing Wnt4, a glycoprotein required to trigger nephrogenesis in isolated MM (Kispert *et al.*, 1998; Osafune *et al.*, 2006). The colonies reconstituted a 3D kidney tissue consisting of glomerular- and tubular-like structures positive for the podocyte marker Wilm's tumor 1 (WT1) and the proximal tubule marker *Lotus tetragonolobus lectin* (LTL), respectively (Osafune *et al.*, 2006). Although functional features of these structures were not investigated *in vivo*, this bioengineering approach suggested that rudimental 3D kidney tissues could be obtained from single cell suspensions.

Building on Grobstein's group studies (Grobstein, 1955; Auerbach and Grobstein, 1958), Unbekandt and Davies set up a novel method to generate 3D embryonic kidney tissue through E11.5 mouse kidneys dissociation into single cell suspensions followed by reaggregation, without the need for any exogenous tissue (Unbekandt and Davies, 2010). A key innovation of this method was the transient culture (for the first 24 hours) of the cell reaggregates with a Rho-associated kinase inhibitor in order to enhance cell self-organisation and UB branching reactivation, and prevent cell death for apoptosis, which is due to the dissociation process (Schmidt-Ott, 2010; Unbekandt and Davies, 2010). Even though this protocol allowed the engineering of embryonic kidney tissue containing nephrons at different developmental stages and with normal anatomies, the UB developed as a multitude of small individual collecting duct trees, rather than a single highly branched UB/collecting duct tree, as normally occurs during kidney organogenesis. Furthermore, this would mean that, assuming that the tissue were vascularised and physiologically

active, the multiple individual collecting ducts would not be effective for draining urine away towards a common exit. To overcome the above limitation, the authors refined the system by culturing, for 3-4 days, MM cell reaggregates in combination with a single reformed UB dissected from a reaggregated tissue of a previous round of dissociation-reaggregation. This manoeuvre led to the engineering of 3D embryonic kidney tissue containing immature nephrons directed outwards and each distally connected to a branch of the single UB-derived collecting duct tree. Such configuration resembled the normal *in vivo* kidney tissue patterning (Ganeva *et al.*, 2011).

Although the dissociated and reaggregated MM (drMM) maintains its nephrogenic potential, if nephrogenesis is induced following the dissociation step, drMM degenerates and undergoes apoptosis (Koseki *et al.*, 1992; Saxén, 1987). To address this problem, a novel protocol that allows drMM to maintain its nephrogenesis competence *ex vivo* has been recently developed (Junttila *et al.*, 2015). In particular, drMM was cultured in the presence of bone morphogenetic protein 7 (BMP7) and fibroblast growth factor 2 (FGF2) - both showed to promote the survival of isolated intact MM - for 24 hours before nephric tubule induction (Junttila *et al.*, 2015). As a result, when cultured onto the dorsal piece of an E11.5 embryonic spinal cord as inducer of tubulogenesis, the uninduced drMM cells survived and assembled into segmented nephrons expressing markers of glomerular podocytes, proximal and distal tubules, and ascending loop of Henle. Furthermore, to evaluate potential for kidney organogenesis *in vitro*, the BMP7/FGF2-treated MM cell reaggregates were combined with one freshly isolated intact UB, which was previously stimulated with GDNF, to form explants. After 9 days, explants displayed a unique branching UB, multiple developing nephrons around the UB tips, and renal corpuscle-like structures, as occurs during normal kidney organogenesis. Consequently, the major advantage of this novel protocol for kidney tissue engineering was the extension of the *in*

vitro culture time of the uninduced drMM, which in the above-mentioned culture conditions survived and maintained its nephrogenic potential with no sign of apoptosis (Junttila *et al.*, 2015).

Despite the advances in the field, none of these cell-based strategies has favoured the development of vascularised glomeruli with appropriately structured glomerular filtration barrier, due to the avascular *in vitro* environment. Hence, this important impediment to the generation of mature and functional kidney tissue from renal progenitor cell suspensions persisted.

In order to overcome this obstacle, our group, building on previously reported technologies (Auerbach and Grobstein, 1958; Unbekandt and Davies, 2010), generated kidney organoids *in vitro* and implanted them into living recipients. Once *in vivo*, organoids further grew and matured, developing vascularised glomeruli and functional nephrons (Xinaris *et al.*, 2012). Specifically, organoids were constructed using single cell suspensions of fully dissociated E11.5 mouse kidneys and, after growing *in vitro* for 5 days - the time they develop elongating tubular profiles with distal poles connected to the adjacent branching UB/collecting duct epithelia - they were implanted below the renal capsule of unilaterally nephrectomised athymic rats. The unilateral nephrectomy - a surgical intervention known to enhance the expression of several mitogenic, prosurvival, and morphogenic genes in rodents (Siegel *et al.*, 1996; D'Agati, 2012) - was performed to promote growth and maturation of the grafted tissue.

Two pivotal steps introduced with this optimised reaggregation method were the generation of kidney organoids as large cell aggregates to allow survival and growth of the implanted tissues *in vivo* and, to promote endogenous vascular development, their pretreatment with vascular endothelial growth factor (VEGF) before implantation, followed by systemic VEGF injections into the host animals. This second manoeuvre

restored the podocyte-endothelial cell stimulation mediated by VEGF, which drives the formation of glomerular capillary loops (Kitamoto *et al.*, 1997, 2002; Tufro *et al.*, 1999; Guan *et al.*, 2006). Indeed, during kidney development, endothelial progenitor cells residing in the renal stroma express VEGF receptors and migrate into the vascular cleft of developing glomeruli - where they will form the glomerular capillary loops - in response to podocyte secretion of VEGF (Dressler, 2006; Jeffrey and Miner D.R.A., 2012).

As a result, the implanted organoids grew, became vascularised, and developed glomeruli with fenestrated capillaries and fully differentiated podocytes having foot processes spaced by slit diaphragms (Xinaris *et al.*, 2012). Furthermore, implanted tissues exhibited basic kidney-specific functions, including capacity for proximal tubular reabsorption of systemically injected labelled macromolecules that reached tubular lumen by transglomerular passage, and production of erythropoietin by stromal cells when recipient animals were made anaemic (Xinaris *et al.*, 2012). More in-depth investigations combining electron microscopy analysis and macromolecular tracing experiments revealed that, *in vivo*, the organoids recapitulated the extremely complex 3D structural framework of the glomerular slit diaphragm, and performed selective glomerular filtration and tubular reabsorption (Xinaris *et al.*, 2015).

The organoid system is a reliable tool to validate the renal differentiation potential of human stem cells from different sources. By using this technology, several groups determined the human stem cells' capacity to follow renal developmental program and their contribution to developing kidney compartments (Siegel *et al.*, 2010; Papadimou *et al.*, 2015; Xinaris *et al.*, 2016). Siegel *et al.* showed that, when mixed with suspension of mouse embryonic kidney cells and reaggregated to form 3D chimeric organoids, human amniotic fluid stem cells (hAFSCs) integrated into developing kidney structures positive for PAX2 - a marker expressed in UB and developing nephrons (Rothenpieler and

Dressler, 1993) - and calbindin - a specific marker for UB and distal tubules (Siegel *et al.*, 2010) - wherein they also started to express both markers.

More recently, our group applied the optimised technology described above (Xinaris *et al.*, 2012) to generate 3D chimeric organoids from E11.5 mouse kidney cells and hAFSCs that were genetically modified to express GDNF (Xinaris *et al.*, 2016; Benedetti* *et al.*, 2016) in order to enhance their contribution to developing nephrons (Yokoo *et al.*, 2005). This manipulation promoted hAFSCs integration in the caps of condensing MM positive for neural cell adhesion molecule (NCAM) - a specific marker of condensed MM (Bard *et al.*, 2001) - and PAX2 (Xinaris *et al.*, 2016). When implanted beneath the renal capsule of athymic rats, chimeric organoids grew, developed tubular structures and glomeruli that contained red blood cells, thus revealing the establishment of vascular connection between host and graft. In the implanted tissues, the majority of hAFSCs incorporated in glomerular structures, and differentiated into mature podocytes endowed with interdigitating foot processes separated by well-formed slit diaphragms (Xinaris *et al.*, 2016). Remarkably, the hAFSC-derived podocytes displayed active endocytosis of systemically injected fluorescent bovine serum albumin (BSA), a functional feature typical of normal podocytes *in vivo* (Eyre *et al.*, 2007).

This chimeric organoid system have been also applied by our group to validate renal differentiation and integration potentials of various cell types, such as the HK2 renal proximal tubular epithelial cell line, human bone-marrow mesenchymal stem cells (hBM-MSCs), and hBM-MSC-derived proximal tubular-like epithelial cells (Papadimou *et al.*, 2015; Benedetti* *et al.*, 2016). The latter cell type (CL17) was generated by direct hBM-MSC reprogramming using HK2 cell extracts. In 1-day chimeric aggregates, CL17 cells incorporated into the condensing MM. At 5 days, both CL17 and HK2 cells formed chimeric elongating tubular structures adjacent to early glomerular-like structures.

Otherwise, hBM-MSCs did not form or contribute to renal structures, thus indicating neither nephrogenic nor integration potential (Papadimou *et al.*, 2015).

1.4.3 Creating 3D kidney tissue from pluripotent stem cells

Pluripotent stem cells (PSCs) are able to self-renew indefinitely *in vitro* while maintaining the capacity of differentiating into specialised derivatives of all the three primary germ layers (Yu and Thomson, 2008). Due to these characteristics, human PSCs (hPSCs) emerged as an extremely valuable source for studying human development, modelling disease, testing drugs, and establishing strategies aimed at engineering human tissues *in vitro*. The hPSCs are classed as human embryonic stem cells (hESCs), which derive from the inner cell mass of a blastocyst (Thomson *et al.*, 1998), and human induced pluripotent stem cells (hiPSCs). The latter have been generated by the Shinya Yamanaka's group, first from mouse (Takahashi and Yamanaka, 2006) and then from human (Takahashi *et al.*, 2007) somatic cell reprogramming. Specifically, the authors induced adult terminally differentiated donor cells to revert to a pluripotency state by transfection of four selected transcription factors (OCT4, KLF4, SOX2 and c-myc). The hiPSCs possess morphology, proliferation capacities and differentiation potential highly comparable to hESCs and, as their generation does not entail destruction of human embryos, they allow circumventing all ethical issues associated with the use of hESCs. Importantly, hiPSCs, which can be derived from both healthy people and patients, are, accordingly, immunocompatible with the original donor, thus avoiding the need for immunosuppressants when transplanted back into the donor organism. For all these reasons, the discovery of hiPSCs gave way to a new era in stem cell biology and regenerative medicine, creating significant prospects for the *in vitro* generation of renal progenitor cells as source for engineering immunocompatible kidney tissue applicable to transplantation.

In the last few years, intense research has been dedicated to develop protocols for differentiating hPSC towards specific renal progenitor cell types.

Mae *et al.* differentiated hPSCs (both hESCs and hiPSCs) towards IM cells (Mae *et al.*, 2013) in a stepwise fashion. Initially, hPSCs were stimulated with Activin A and the Wnt agonist CHIR99021 for 3 days to differentiate into mesoderm, and then were treated with BMP7 and CHIR99021 for an additional 20 days to generate IM cells highly expressing OSR1, a specific marker of IM. The authors documented that these cells also expressed several markers specific to cell types of both embryonic (ND, UB, MM and metanephric stromal cells) and mature kidney. However, when hiPSCs-derived IM cells were cocultured with E11.5 mouse metanephric cells to generate 3D chimeric aggregates, they formed polarised proximal tubular-like structures with low efficiency and exhibited scarce differentiation capacity into UB cells, indicating a limited developmental potential.

In view of these limitations, the same group improved the efficiency of the protocol by skipping the stage of mesoderm induction and stimulating the hiPSCs exclusively with small molecules - CHIR99021 and retinoic acid receptor agonists - for 5 days. This modification significantly increased the capacity of hESC/hiPSC-derived IM cells to form proximal tubular-like structures within chimeric aggregates (Araoka *et al*., 2014).

Following a similar line of research, Lam *et al.* reported a robust protocol for hPSC differentiation into IM cells that spontaneously formed tubule-like structures (Lam *et al.*, 2014). Initial treatment of hPSCs with CHIR99021 for 1-2 days induced mesendoderm differentiation. Cells were then treated with a combination of FGF2 and retinoic acid for 3 days to generate PAX2- and LHX1-positive IM cells with high efficiency. When the authors withdrew growth factors from culture media, differentiated cells proliferated and formed polarised tubular epithelial structures positive for the proximal tubule markers LTL and N-cadherin, and endowed with primary cilia on the apical surface. Nevertheless, when

recombined with E12.5 mouse kidney cells to form chimeric kidney explants, these cells partially contributed to laminin-bounded tubular structures, indicating a low integration potential into developing kidney tissue. In another set of experiments, PAX2- and LHX1-positive IM cells were stimulated with FGF9 - a growth factor known to induce and maintain nephron progenitors *in vitro* (Barak *et al.*, 2012) - and Activin A to differentiate into CM cells expressing *SIX2*, *SALL1* and *WT1*. In chimeric kidney explants, these hPSC-derived CM cells were found in organising clusters of LTL-positive cells (Lam *et al.*, 2014).

Xia *et al.* established a rapid and efficient two-step protocol for hESCs and hiPSCs directed differentiation into UB progenitor-like cells (Xia *et al.*, 2013). In the first step, hPSCs were committed to mesodermal fate by exposure to BMP4 and FGF2 for 2 days. In the second step, combined treatment with BMP2, Activin A and retinoic acid drove cells to acquire a late IM/UB-like phenotype. After 4 days of differentiation, cells expressed high levels of IM and ND/ureteric epithelium markers (OSR1, LHX1, PAX2 and GATA3), and UB-specific markers (HOXB7, RET and GFRA1), rather than MM markers. To investigate the hPSC-derived UB-like progenitor cells for their propensity to contribute to complex 3D renal structures, the authors cocultured them with E11.5 mouse kidney cells to form 3D chimeric organoids. Under these culture conditions, the human cells exclusively integrated into the murine developing UB structures, indicating efficient *in vitro* UB-lineage commitment and *ex vivo* maturation capacity in response to renal developmental cues from mouse embryonic kidney cells (Xia *et al.*, 2013, 2014). Moreover, the chimeric UB epithelia became polarised along the apical-basal axis and induced MM condensation and nephrogenesis, as occurs *in vivo*. In agreement with the absence of MM marker expression, differentiated human cells did not integrate at all in the MM derivatives.

In the past few years, significant advances towards the generation of multilineage and/or functional kidney organoids have been made by exposing hPSCs to chemically defined culture conditions that more accurately mimic early kidney developmental cues *in vitro*.

Working on this approach, Takasato *et al.* established a protocol for the stepwise simultaneous differentiation of hESC monolayers towards UB and MM cells under chemically defined culture conditions (Takasato *et al.*, 2014). In the first step, hESCs were induced to posterior primitive streak by exposure to either BMP4 and Activin A or CHIR99021 alone. Next, these cells were differentiated into IM cells using FGF9 and heparin. Finally, IM cells were stimulated with a combination of FGF9, heparin, BMP7 and retinoic acid to derive MM cells. Otherwise, CHIR99021-treated cell lines were deprived of any growth factors for 12 days to generate a mixed population of both UB and MM progenitor cells. When reaggregated following monolayers' dissociation into single cell suspensions, UB and MM progenitor cells self-organised to form human 3D kidney tubular structures in the absence of any other supporting cell type or tissue. Furthermore, upon coculture with E12.5 murine kidney cells to form chimeric aggregates, the hESC-derived kidney progenitor cells integrated into all cellular compartments and epithelia of the developing kidney tissue (Takasato *et al.*, 2014).

In parallel, Taguchi *et al.* optimised a differentiation protocol to derive MM cells expressing *WT1*, *PAX2*, *SALL1* and *SIX2* from both mouse ESCs and hiPSCs, by first defining MM developmental origins through *in vivo* lineage-tracing studies, and then by accurately mimicking them *in vitro* (Taguchi *et al.*, 2014). The authors demonstrated that MM progenitor cells derive from the posterior nascent mesoderm expressing Brachyury - a primitive streak and posterior nascent mesoderm marker (Herrmann *et al.*, 1990) - and they established a combination of factors for inducing posterior mesoderm and its subsequent differentiation into MM. To induce posterior mesoderm differentiation, embryoid bodies

(EBs) from PSCs were initially treated with Activin A alone, and then with the combination of BMP4 and CHIR99021. Subsequently, IM identity was achieved by combined treatment with Activin A, BMP4, CHIR99021 and retinoic acid. Finally, differentiation into MM cells was accomplished using CHIR99021 and FGF9. Coculture of MM cell-aggregates with mouse embryonic dorsal spinal cords resulted in MM cell maturation and reconstitution of contiguous 3D glomerular structures, and proximal and distal tubules. When co-transplanted with dorsal spinal cords below the kidney capsule of immunodeficient animals, the EB-derived MM cell aggregates underwent massive tubulogenesis and developed vascularised glomeruli containing erythrocytes, indicating the graft's connection to host circulation (Taguchi *et al.*, 2014). Although vascularised glomeruli are required for blood filtration, neither urine production nor any other kidney functions were shown.

Later, the same group, generated hiPSC lines expressing green fluorescent protein (GFP) in the *NPHS1* locus - which encodes the podocyte slit diaphragm protein nephrin - and, differentiating these cells according to previous protocol, induced formation of 3D GFP-glomerular structures containing nephrin-positive podocytes with primary processes and immature slit diaphragm-like structures (Sharmin *et al.*, 2016). Next, the authors transplanted the sorted 3D GFP-positive glomerular structures beneath the host kidney capsule. Here, the glomerular structures further matured, were vascularised by host endothelial cells, and developed podocytes with foot processes wrapping the fenestrated endothelium (Sharmin *et al.*, 2016). Importantly, the hiPSC-derived podocytes displayed both gene expression pattern and structural features typical of *in vivo* podocytes.

By recapitulating metanephric kidney development *in vitro*, Morizane *et al.* have recently published a differentiation protocol to obtain MM cells expressing *SIX2*, *SALL1* and *WT1* from hPSCs. Moreover, the authors demonstrated that the hPSC-derived nephron

progenitor cells could spontaneously assemble into human kidney organoids in both 2D and 3D culture conditions (Morizane *et al.*, 2015). Specifically, to stimulate consecutive differentiation into primitive streak and posterior IM, hiPSCs were cultured in the presence of CHIR99021 and Noggin - a BMP4 signaling antagonist - for 4 days, and then with Activin A alone for additional 3 days, respectively. To establish MM identity and induce cell self-organisation, cells were stimulated with FGF9 for another 7 days, with transient 2-day treatment with CHIR99021 starting on day 9. Finally, cell culture in the absence of growth factors for additional 14 days led to the spontaneous formation of hPSC-derived 'nephron organoids' containing appropriately segmented nephrons, but completely lacking of UB derivatives. Remarkably, by exposing organoids to commonly used antibiotics and anticancer drugs, the authors demonstrated that they could be used as a tool to investigate mechanisms of proximal and/or distal tubular toxicity *in vitro* (Morizane *et al.*, 2015).

Almost simultaneously, the same group showed that hPSC-derived kidney cells could self-organise to generate tubular organoids, recapitulate kidney epithelial transport, and, following genome editing, could model human kidney disease (Freedman *et al.*, 2015). The authors developed a 3D culture system for sequential generation of hPSC-derived epiblast spheroids and kidney tubular organoids. In this system, hPSCs were first embedded in Matrigel to spontaneously form spheroids consisting of a polarised epithelium surrounding a hollow lumen in 3 days. Subsequent exposure to CHIR99021 for 1.5 days followed by incubation in B27-supplemented media for 11.5 days induced epiblast spheroid differentiation into kidney tubular organoids in which tubules positive for podocyte, vascular, proximal and distal tubular markers developed, and exhibited transport characteristics typical of proximal tubules. Interestingly, when biallelic truncating mutations in *PKD1* (polycystin-1) or *PKD2* (polycystin-2) genes were introduced in hPSCs through the CRISPR/Cas9 genome editing technology, kidney tubular organoids formed

large LTL-positive cyst-like structures alongside proximal tubular structures. Although this represents the first report of 3D kidney organoids capable of modelling human kidney disease *in vitro*, cysts formation was detected in only 6% of the self-forming organoids.

In parallel, Takasato *et al.* modified their previous protocol (Takasato *et al.*, 2014) in order to induce hiPSC differentiation and self-organisation into 3D kidney organoids composed of UB epithelia and MM-derived segmented nephrons, endothelial cells and renal stroma (Takasato *et al.*, 2015). The *in vitro* self-forming organoids resulted transcriptionally similar to first trimester human foetal kidneys. Moreover, from the bottom to the top regions, organoids showed multiple individual collecting ducts linked to the distal and proximal tubules, and glomeruli containing podocytes with primary and secondary foot processes. The proximal tubular cells were capable of absorbing labelled macromolecules and underwent specific apoptosis in response to cisplatin, indicating tubular functional maturation (Takasato *et al.*, 2015).

Very recently, by recapitulating kidney developmental stages *in vitro*, our group set up a robust three-step protocol for hiPSC differentiation into functional podocytes (Ciampi *et al.*, 2016). The hiPSCs were first specified into IM, then committed to nephron progenitor cells and, finally, differentiated into mature podocytes with typically low proliferation rate. The hiPSC-derived podocytes resulted able to endocytose and accumulate albumin in the perinuclear regions, and displayed cytoskeletal reorganisation when treated with Angiotensin II, a known inducer of podocyte damage. Moreover, when human podocytes from differentiation day 13 were reaggregated with E12.5 mouse kidney cells to form chimeric organoids, they incorporated into WT1-positive developing structures, where they also started to express *WT1* (Ciampi *et al.*, 2016).

The technologies described in the paragraphs above strongly fostered the creation of kidney epithelial tubular structures that, in part, resemble their counterparts *in vivo*, and

hPSC-derived kidney organoids displaying considerable structural complexity and functional maturation.

However, they cannot accurately replicate normal kidney tissue patterning, due to the organ's complex architecture and the finely orchestrated interactions occurring between ECM and several cell lineages during organogenesis. Indeed, as kidney tubule and organoid formation solely relied on cell-driven self-assembly - reason why cells were not geometrically directed to acquire appropriate spatial configuration - engineered tubules were heterogeneous in size and shape and far from being anatomically realistic, whereas kidney organoids displayed serious developmental anomalies and structural malformations. First and foremost, within the organoids, the UB was either totally missing or developed as a multitude of small individual ducts (Taguchi *et al.*, 2014; Freedman *et al.*, 2015; Morizane *et al.*, 2015; Takasato *et al.*, 2015; Xia *et al.*, 2013; Xinaris *et al.*, 2016) instead of a unique collecting duct system of tubules that could drain urine away to a single exit if the tissue were vascularised. These anatomical deficiencies prevented development and maturation of kidney tissue arranged organotypically around one single and branched UB/collecting duct system, as instead occur during normal kidney organogenesis. Another issue is the short viability (3-4 weeks) of the organoids *in vivo*, as they soon after begin to degenerate.

Additional technical insufficiencies of the existing tubule engineering systems are the requirement for extensive cell culturing - from several days to weeks (Montesano *et al.*, 1991a; Sakurai *et al.*, 1997) - as well as the need for other cell types (Montesano *et al.*, 1991a), tissues (Steer *et al.*, 2002; Santos *et al.*, 1994) or conditioned media (Montesano *et al.*, 1991b; Sakurai *et al.*, 1997).

Overall, the constrictions described above hinder the reliability, reproducibility, cost-effectiveness, and applicability of all these technologies. Moreover, systems for

engineering pure kidney units developed so far have not been adopted when using human cell sources, thus limiting investigations concerning human kidney developmental and pathophysiological mechanisms.

To summarise, the generation of renal tubular structures and hPSC-derived kidney organoids has created considerable advances in the field, providing opportunities for disease modelling and toxicology studies. However, the usefulness of these tissues is limited because of serious technical weak points and anatomical deficiencies related to the UB development, namely the lack of collecting ducts or their random formation as multiple disconnected units within the organoids.

Although Xia *et al.* attempted to derive collecting duct cells from hPSCs, they obtained UB-like cells that did not demonstrate significant UB tissue formation and maturation capacities (Xia *et al.*, 2013).

Therefore, developing 3D tissue engineering systems that could direct the generation and growth of unique and complex UB/collecting duct units from hiPSCs may be extremely helpful for creating more realistic human kidney tissue that *bona fide* resembles normal kidney anatomy and physiology, and that can be used for disease modelling and drug testing/discovery studies. Moreover, this kind of engineering system would allow the generation of patient-specific kidney tissue - an unresolved challenge in the field - useful for studying kidney diseases caused by abnormal developmental processes that cannot be investigated due to the shortage of suitable human samples.

1.5 Specific Aims

1) To develop and optimise a 3D culture method to engineer functional epithelial kidney tubules using micro-patterned scaffolds and a distal tubule/collecting duct renal cell line.

2) To use this method as a tool to:

- Model kidney disease and perform drug testing/discovery studies;
- Engineer human epithelial tubules using hiPSC-derived UB progenitor-like cells;
- Study human UB developmental processes and defects.

CHAPTER 2 - MATERIALS AND METHODS

2.1 PDMS scaffold fabrication

Polydimethylsiloxane (PDMS) scaffolds (Sylgard 184 Silicone elastomer kit, Dow Corning, Midland, MI) were fabricated by NanoMed Labs (University of Genova, Italy) using a 3-step prototyping approach: scaffold design, 3D printing and replica moulding. First, by using Computer Aided Design (CAD) software (Autodesk 123D® Design ©2014 Autodesk Inc.), scaffolds were designed with different geometries: *(i)* three scaffolds with width and depth of 1 mm: a linear one with a straight cavity, a bifurcated one with terminal 80° branching and an asymmetrical one with two 30° lateral branches extending from the central trunk; *(ii)* two more complex ramified and tree-like scaffolds, the latter containing a fractal-like pattern, both 0.7 mm in depth, and ranging in width from 0.7 to 0.5 mm, respectively; *(iii)* a multichannel scaffold containing 11 linear microchannels, which were 0.4 mm in depth x 0.4 mm in width x 9 mm in length, within a miniaturised culture chamber (1 mm in depth).

3D printing technology (Professional Desktop Pico Plus39 stereolithographic 3D printer, Asiga Global Helpdesk) was applied to build plastic masters (Asiga PlasWhite photopolymer resin). The printer uses an upside-down system with nominal XY pixel resolution down to 39 μm and servo resolution of 250 nm. The masters were printed at 0.5 seconds of exposure time, with a printing speed of 0.33 cm/hour and 10 μm vertical step size. After printing, masters were cleaned by rinsing with isopropyl alcohol for 5 minutes, washed in distilled water, dried and exposed to UV light (365 nm) (Bio-Link-BLX-365 nm, 80 W, Vilber Lourmat) for 40 minutes to complete curing. To facilitate the de-moulding of the polymeric replicas, masters were functionalised with an oxygen plasma treatment (Tucano plasma reactor Gambetti Kenologia) and with the deposition, from vapour phase, of an anti-sticking layer of Trichloro (1H,1H,2H,2H-perfluorooctyl) silane (FOTS, 448931-10G, Sigma-Aldrich, Saint Louis, Missouri, USA). Subsequent REplica

Moulding (REM) steps provide several polymeric replicas starting from a single master as previously described (Angeli *et al.*, 2015). Briefly, the PDMS base and the curing mixture (10:1 w/w) were cast into 3D printed masters, degassed using a vacuum desiccator for 20 minutes, cured at 60 °C in oven for 2 hours, and then peeled off the master mould. Finally, the bottom side of the cavities was closed up with a 20 μm-thick PDMS layer. After assembling, cavities were open-topped and completely made of PDMS. In order to enable high-resolution imaging, the thickness of the PDMS scaffolds was maintained between 0.7 and 1 mm. Scaffold hydrophobicity was preserved to avoid cell attachment. PDMS Scaffolds were re-used after standard sterilisation procedures.

2.2 Madin-Darby canine kidney (MDCK) cell culture

The MDCK type II cell line (MDCK II; 00062107; Lot Number 06D026; Origin: Canine Cocker Spaniel Kidney; European Collection of Authenticated Cell Cultures, ECACC, Salisbury, UK) was maintained in Minimum Essential Medium Eagle (MEM) (M5650; Sigma-Aldrich) supplemented with 10% Fetal Bovine Serum (FBS) (10270; Invitrogen Corporation, Carlsbad, CA, USA), 1% L-glutamine (25030024; Invitrogen), 1% penicillin and streptomycin (Pen-Strep) (15140122; Invitrogen). Cells were cultured as monolayers in tissue culture-treated T75 (75 cm^2) flasks (353136; Corning Falcon®, Corning, NY, USA) under standard conditions (37°C incubator, humidified atmosphere of 5% CO_2). For passaging, 70-80% confluent MDCK cells were washed once with sterile filtered pre-warmed BioWhittaker® 1x phosphate buffered saline (PBS) pH 7.2 without Ca^{2+} and Mg^{2+} (BE17-516F; Lonza, Verviers, Belgium), and then were treated with 3 ml of pre-warmed 0.25% Trypsin-Ethylenediaminetetraacetic Acid (EDTA) (25200056; Invitrogen) for 4 minutes at 37°C. Detached cells were gently pipetted 2-3 times to ensure complete dissociation of any remaining clumps and dislodgement of any cells still attached to the

bottom of the flask. Next, cells were collected in a 50 ml conical tube containing the appropriate volume of culture medium, counted and seeded in T75 flasks at a density of $1.6x10^4$ cells/cm^2 in 15 ml of fresh culture medium. Cells were maintained for 3 days without culture medium change until subsequent passaging.

2.3 Human induced pluripotent stem cell (hiPSC) culture

The hiPSC lines used in our experiments were derived from healthy donor somatic cells by different technologies and characterised as previously described (Imberti *et al.*, 2015; Ciampi *et al.*, 2016). Specifically, hiPSC clone IV was obtained from human dermal neonatal fibroblasts via STEMCCA lentivirus-mediated reprogramming (Imberti *et al.*, 2015), whereas hiPSC#16 cells were derived from peripheral blood mononuclear cells (PBMCs) through non-integrative Sendai virus-mediated reprogramming (Ciampi *et al.*, 2016). For feeder-free culture conditions, cells were maintained in mTeSR1 medium enriched with mTeSR1 5X Supplement (05850; Complete Kit; StemCell Technologies, Vancouver, Canada), and cultured as monolayers on Matrigel hESC-qualified Matrix (354277; Corning)-coated 100x20 mm dishes (353003; Corning) under standard conditions. Matrigel hESC-qualified Matrix was used following the manufacturer's instructions. Briefly, aliquots were prepared according to the dilution factor indicated on the Certificate of Analysis and frozen at -80°C. One aliquot was thawed on ice and added to 25 ml of ice-cold DMEM/F12+GlutaMAX (31331028; Invitrogen) to coat the dishes (5 ml/dish), which were then incubated at room temperature for at least 1 hour before use. The remaining coating liquid was aspirated from the dish just before hiPSC seeding on top of the thin gel layer.

When 80% confluent, hiPSCs were abundantly washed with PBS and then treated with 3 ml Accutase (a1110501; Invitrogen) for 4 minutes at 37°C for passaging. Detached cells

were gently pipetted 2-3 times to ensure complete dissociation of any remaining clumps and dislodgement of any cells still attached to the bottom of the dish. Next, cells were collected in 50 ml conical tube containing culture medium, counted, and seeded onto Matrigel hESC-qualified Matrix-coated dishes at a density of $4.5x10^4$ cells/cm^2 in the appropriate volume of fresh mTeSR1 complete medium supplemented with 10 μM Y-27632 dihydrochloride [Rho-associated protein (ROCK) inhibitor; 07172; Sigma-Aldrich] for the first 24 hours to avoid/reduce cell death for apoptosis. The hiPSCs were maintained in 10 ml of mTeSR1 complete medium for 3-5 days, with daily medium change, until subsequent passaging.

2.4 Isolation of peripheral blood mononuclear cells (PBMCs)

PBMCs (lymphocytes, monocytes, and thrombocytes) were isolated under sterile conditions from 40 ml of whole blood taken from a patient carrying a heterozygous mutation in the *PAX2* gene. Patient's whole blood was collected in sterile 50 ml conical tube and 10 U/ml heparin (Pharmatex Italia, Milan, Italy) were added to prevent blood coagulation. The blood was diluted 1:1 with saline solution (Pharmatex Italia) and 20 ml of diluted sample were delicately layered over 15 ml of Ficoll-Paque™ (17-1440-02; GE Healthcare Life Sciences, Little Chalfont, UK) in a total of 4 sterile 50 ml conical tubes, which were centrifuged 800x*g* for 20 minutes at room temperature without brake. Next, tubes were recovered from the centrifuge taking care of not disturbing the layering. The layer containing PBMCs, which was positioned at the interphase, was gently aspirated carefully avoiding Ficoll-Paque™ aspiration, and was transferred to new 50 ml conical tube. At this point, PBS was added to reach a final volume of 50 ml, and the suspension was centrifuged at 400x*g* for 8 minutes at room temperature. Then, supernatant was discarded and cell pellet was washed again using PBS. After discarding the supernatant, 2

ml of RPMI medium (11875093; Thermo Fisher Scientific, MA, USA) supplemented with 20% human serum-AB were added and PBMC pellet was resuspended to obtain a uniform suspension of single cells. After cell counting, aliquots of 5-10x10^6 PBMCs were gently dropped into cryovials containing 1-1.5 ml of freezing medium [RPMI medium supplemented with 20% human serum-AB and 10% dimethyl-sulphoxide (DMSO) (D2650; Sigma-Aldrich)]. After the cells were exposed to freezing medium containing DMSO, they were frozen within 2 minutes by placing cryovials in a cryofreezing container and transferring it to -80°C overnight. This manoeuvre allows freezing the cells at 1°C per minute. After overnight storage, cryovials were transferred into a liquid nitrogen tank vapour phase for long-term storage.

2.5 Generation of patient-derived iPSCs

The patient involved in this study is affected by an autosomal dominant form of Focal Segmental Glomerulosclerosis (FSGS) linked to a disease-segregating missense heterozygous genetic mutation in *PAX2* gene (c.G565A, p.G189R) (Barua *et al.*, 2014). FSGS patient-derived iPSCs were generated from PBMCs (the written informed consent was obtained from the patient in accordance with the Declaration of Helsinki guidelines) through Sendai virus-mediated reprogramming by using CytoTune-iPS 2.0 Sendai Reprogramming kit (A16517; Thermo Fisher Scientific) according to the manufacturer's instructions as follows:

2.5.1 PBMCs seeding. Four days before infection, cryopreserved PBMCs were thawed in 37°C water bath, gently transferred into 15 ml conical tube containing 10 ml of pre-warmed complete PBMC medium [StemPro®-34 medium (10639-011) supplemented with 2 mM L-Glutamine (25030), 100 ng/ml human recombinant

SCF (c-kit Ligand) (PHC2111), 100 ng/ml human recombinant FLT-3 Ligand (PHC9414), 20 ng/ml human recombinant IL-3 (PHC0034), and 20 ng/ml human recombinant IL-6 (PHC0065). All PBMC medium components were purchased from Thermo Fisher Scientific] and centrifuged at 200x*g* for 10 minutes at room temperature. An aliquot of cells was taken for cell counting before centrifugation. After centrifugation, supernatant was discarded, and pellet was resuspended in complete PBMC medium to $5x10^5$ cells/ml. Next, 1 ml per well was dropped in 24-well plates (3527; Corning), and PBMCs were cultured as suspension of not-proliferating cells under standard conditions for the next 3 days, with daily 500 µl (half) medium change without disturbing the cells.

2.5.2 PBMC infection. The day of infection (day 0), PBMCs were harvested, and brought to $3x10^5$ cells/ml into sterile, round-bottom and screw capped centrifuge tubes (352054; Corning). At this point, PBMCs were infected by adding 5 multiplicity of infection (MOI) of hKLF4-OCT4-SOX2 (hKOS) Sendai virus vector, 5 MOI of hc-Myc Sendai virus vector, and 3 MOI of hKLF4 Sendai virus vector in a total volume of 1 ml. Both Sendai reprogramming tubes' thawing and virus volume calculation were performed following the manufacturer's instructions. To increase transduction and reprogramming efficiencies, capped tubes were centrifuged at 2,250 rpm for 30 minutes at room temperature using the SL-16 centrifuge (Thermo Fisher Scientific). After centrifugation, PBMC pellets were resuspended in the same virus-containing medium, and 1 ml of fresh PBMC complete medium was added to each tube. At this point, PBMCs were seeded in 12-well plates (3513; Corning) and incubated overnight under standard conditions. The next day (day 1 post-infection), both cells and medium were harvested from

the wells and transferred into centrifuge conical tube. Each well was rinsed with 1 ml of PBMC complete medium to ensure harvesting most of the cells, and volumes were added to the centrifuge tube. PBMC suspension was centrifuged at 200x*g* for 10 minutes, supernatant was discarded, and cells were resuspended in 500 µl of PBMC complete medium per well of 24-well plate. Cells were seeded and cultured under standard conditions for the next 2 days (day 2 and 3 post-infection).

2.5.3 Cell seeding on mouse embryonic fibroblasts (MEFs). MEFs were isolated from CD1 mouse (Charles River Italia S.p.A., Calco, Lecco, Italy) embryonic day (E) 13.5 embryos, and used as feeder layers for hiPSC generation. MEFs were cultured in T75 flasks as monolayers under standard conditions in Dulbecco's Modified Eagle Medium (DMEM) (11960044; Invitrogen) supplemented with 10% FBS (16000; Invitrogen), 0.1 mM non-essential amino acids (11140050; Invitrogen) and 1% Pen-Strep. When 95% confluent, MEFs were mitotically inactivated by treating them with 0.01 mg/ml mitomycin-C (M4287; Sigma-Aldrich) for 2 hours, and then seeded on 6-well plates (353046; Corning) at a density of $8x10^4$ cells/cm^2. At day 3 post-infection, $1\text{-}5x10^4$ live PBMCs per well were seeded on mitotically inactivated MEFs in a total volume of 2 ml StemPro®-34 medium without cytokines, and cultured under standard conditions for other 3 days (day 4-6 post-infection). From day 4 to day 6, 1 ml (half) of StemPro®-34 medium without cytokines was replaced every other day with the same amount of fresh medium, taking care of not disturbing cells.

2.5.4 Transitioning-PBMC exposure to hiPSC-medium. On day 7 post-infection, 1 ml (half) of StemPro®-34 medium without cytokines was replaced with the same

amount of hiPSC-medium [DMEM/F12+GlutaMAX supplemented with 20% knock-out serum (10828028; Invitrogen), 0.1 mM non-essential amino acids, 0.1 mM 2-mercaptoethanol (M6250; Sigma-Aldrich), 10 ng/ml human fibroblast growth factor 2 (FGF2) (100-18B; PeproTech, NJ, USA), and 1% Pen-Strep]. The next day (day 8 post-infection), culture medium was completely replaced with 2 ml of hiPSC-medium, which was changed every day thereafter with the same amount of fresh medium, until the appearance of the first cell colonies (about day 10-12 post-infection), indicative of reprogrammed cells.

2.5.5 Picking of patient-derived iPSC colonies and cell expansion. When reprogrammed cell colonies grew to an appropriate size (~ 500 μm in diameter; day 21 post-infection), they were manually picked under an inverted microscope placed in a sterile cell culture hood. The colonies to be picked were cut in 4 similarly-sized pieces using a sterile 25-gauge $1^{1/2}$-inch needle (insulin-needle) directly in the cell culture wells. Cut pieces were gently aspirated with a 200 μl micropipette (Gilson, Inc., Middleton, USA), transferred into sterile Eppendorf® Safe-Lock microcentrifuge tubes (T9661; Sigma-Aldrich), containing 500 μl of hiPSC-medium and fragmented into smaller clumps by gently pipetting. At this point, clumps were aspirated and seeded onto newly prepared MEF feeder layers in wells of 6-well plates in 2 ml of hiPSC-medium - supplemented with 10 μM ROCK inhibitor for the first 24 hours - and cultured under standard conditions. Clumps were allowed to attach and grow as large hiPSC colonies, and culture medium was changed daily. In order to be expanded, 70-80% confluent hiPSC colonies were mechanically split (manual picking) for 4 passages, and seeded on freshly prepared MEF feeder layers.

2.5.6 Patient-derived iPSCs adaptation to feeder-free culture conditions. Patient-derived iPSCs grown and expanded on MEF feeder layers were cut and manually picked as described in the paragraph 2.5.5. Cut pieces were transferred into sterile Eppendorf® Safe-Lock microcentrifuge tubes containing 500 µl of mTeSR1 complete medium and fragmented into smaller clumps by firmly pipetting. At this point, clumps were aspirated and seeded onto Matrigel hESC-qualified Matrix-coated wells of 6-well plates in 2ml of mTeSR1 complete medium - supplemented with 10 µm ROCK inhibitor for the first 24 hours - and cultured in feeder-free conditions as described in the paragraph 2.3. Patient-derived hiPSC#1 clone was selected for characterisation and additional experiments (see the paragraph 2.6 below).

2.6 Characterisation of patient-derived iPSCs

To characterise patient-derived iPSCs (hiPSC#1 clone) we: *(i)* performed immunofluorescence and quantitative real-time PCR (qRT-PCR) analyses to evaluate pluripotency marker expression, *(ii)* tested cell capacity to form embryoid bodies (EBs) as a stringent assay to screen for pluripotency, (*iii*) investigated stochastic differentiation of the cells forming the EBs into all three somatic germ layers, and *(iv)* carried out karyotype analysis.

2.6.1 Immunofluorescence staining. For immunofluorescence analysis, patient-derived iPSCs were washed three times with 2 ml of PBS and fixed in PBS containing 4% paraformaldehyde (PFA) (157-8; Electron Microscopy Sciences, Hatfield, PA, USA) for 15 minutes at room temperature. Next, cells were permeabilised with 0.3% Triton X-100 (93418; Sigma-Aldrich) prepared in PBS for 10 minutes at

room temperature, blocked with PBS containing 5% bovine serum albumin (BSA) (A2153; Sigma-Aldrich) for 1 hour at room temperature, and incubated with the primary antibodies diluted in PBS containing 2% BSA (Sigma-Aldrich). Primary antibodies: rabbit anti-NANOG (sc-33759; Santa Cruz Biotechnology, Inc., Santa Cruz, CA, USA; 1:100), mouse anti-OCT4 (sc-5279; Santa Cruz Biotechnology; 1:100), mouse anti-TRA 1-60 (MAB4360; Merck-Millipore, NJ, USA; 1:200), mouse anti-TRA 1-81 (MAB4381; Merck-Millipore, 1:200), rat anti-SSEA3 (sc-21703; Santa Cruz Biotechnology; 1:100) and mouse anti-SSEA4 (sc-21704; Santa Cruz Biotechnology; 1:100) over night at 4°C.

The next day, samples were abundantly washed with PBS and incubated for 1 hour at room temperature in the dark with the appropriate secondary antibodies diluted in PBS containing 2% BSA (Sigma-Aldrich). Secondary antibodies: Donkey anti-Rabbit IgG Alexa Fluor® 546-conjugated (A10040; 1:300), Goat anti-Rat IgM Alexa Fluor® 488-conjugated (A21212; 1:300), Donkey anti-Mouse IgG Alexa Fluor® 546-conjugated (A10036; 1:300) and Goat anti-Mouse IgM Alexa Fluor® 488-conjugated (A21042; 1:300). All secondary antibodies were purchased from Thermo Fisher Scientific. After incubation with secondary antibodies, cells were washed twice with PBS for 5 minutes, and then nuclear staining was performed by incubating cells with 1 mg/ml 4',6-diamidino-2-phenylindole dihydrochloride (DAPI) (D9542; Sigma-Aldrich) for 10 minutes in the dark. DAPI was prepared and stored according to the manufacturer's instructions. Images were taken with the CF40 Axiovert fluorescence microscope (Carl Zeiss, Oberkochen, Germany) and are representative of three independent experiments.

2.6.2 Embryoid body (EB) formation and patient-derived hiPSC differentiation into the three germ layers. For EB formation, sub-confluent patient-derived iPSCs were harvested as described in paragraph 2.3, and counted. Before cell seeding, AggreWell^{TM}800 plates (27965; Stem Cell Technologies), which are endowed with microwells of 800 μm in diameter, were centrifuged at 2,000x*g* for 5 minutes in a swinging bucket rotor with plate-holders in order to remove any air bubbles from the microwells. To obtain 3,000-4,000 cell-sized EBs, the harvested hiPSCs were first resuspended in order to have $1x10^6$ hiPSCs/well in 1.5 ml/well of AggreWell^{TM} medium (EB medium; 05893; Stem Cell Technologies) supplemented with 10 μM ROCK inhibitor, and then were seeded. Soon after seeding, cell suspension in each well was gently pipetted several times to homogeneously distribute the cells. Next, plate was centrifuged at 100x*g* for 3 minutes at room temperature for capturing cells in the microwells and was finally incubated under standard conditions. EBs formed within 2 days of culture. At this point, EBs were displaced and harvested by firmly pipetting 2-3 times the EB medium in each well. Then, EBs were transferred into 6-well ultra-low-adherence plates (27145; Corning) (~ 800 EBs/well) in a total volume of 5 ml/well of EB medium, and were cultured in suspension under standard conditions, changing EB medium every 2 days. After 8 days as floating cultures, EBs were transferred onto 0.1% gelatine (G2500; Sigma-Aldrich)-coated plates [6-well plate coating was made by adding 2 ml/well of 0.1% sterile gelatine solution prepared in PBS (Lonza) and incubating plates at 37°C for 30 minutes] and cultured for another 8 days, by changing EB medium every 2 days. Under these culture conditions, EBs gradually adhered to the gelatine-coated well bottom and grew as monolayered cells. On culture day 16, cells were fixed in PBS containing 4% PFA, and

processed for immunostaining as described in paragraph 2.6.1. In particular, differentiation into the three germ layers was evaluated by immunostaining the EB-derived cells for Alexa Fluor® 488-conjugated mouse anti-β-Tubulin III (ectoderm marker; CBL412X; Merck-Millipore; 1:100), Cy3^{TM}-conjugated mouse anti-α-smooth muscle actin (SMA) (mesoderm marker; C6198; Sigma-Aldrich; 1:100) and rabbit anti-GATA4 (endoderm marker; sc-9053; Santa Cruz Biotechnology; 1:50).

2.6.3 Gene expression analysis. Gene expression level of pluripotency markers was analysed by performing qRT-PCR assays using predesigned Taqman probes (Thermo Fisher Scientific) specific to *OCT4*, *NANOG* and *SOX2* genes (Table 1) as described in the paragraph 2.8 below. Gene expression levels were normalised to the housekeeping gene hypoxanthine phosphoribosyltransferase-1 (*HPRT1*).

2.6.4 Karyotype analysis. When 60-70% confluent, patient-derived iPSCs were treated with 10 mg/ml Colcemid (10295892001; Roche, Basel, Switzerland) in mTeSR1 medium for 2 hours and a half, in order to induce cell cycle synchronisation and increase the yield of metaphase chromosomes. After treatment, cells were harvested as described in the paragraph 2.3 and centrifuged at 1000x*g* for 6 minutes at room temperature. Soon after, pellets were delivered to the Genetic Medicine Laboratory of the Azienda Socio-Sanitaria Territoriale (ASST) Papa Giovanni XXIII, Bergamo (Italy), where karyotype analysis was performed. Briefly, metaphase spreads (consisting of condensed metaphase chromosomes) were prepared onto microscope slides, and were processed for G-banding karyotype analysis. Twenty metaphases were analysed for the chromosomes' size, shape and number.

2.7 Differentiation of hiPSCs toward ureteric bud (UB) progenitor-like cells

The hiPSCs were induced to differentiate toward UB-like cells as previously described with minor modifications (Xia *et al.*, 2013). When 70-80% confluent, hiPSCs cultured in 6-well plates were abundantly washed with PBS and then treated with 2 ml of pre-warmed DMEM/F12+GlutaMAX (31331028; Invitrogen) containing 1 U/ml Dispase (1x Dispase; 07913; StemCell Technologies) for 4 minutes at 37°C. After treatment, 1x Dispase was removed and cells were washed twice with 2 ml of DMEM/F12+GlutaMax. Next, 2 ml of DMEM/F12+GlutaMAX were added to each well and the hiPSC sub-confluent colonies were fragmented through gentle manual scraping with a 5 ml glass pipette into small clusters (each consisting of about 200-400 cells), which were then split onto Basement Membrane Growth-Factor-Reduced (GFR) Matrigel (356231; Corning)-coated 6-well plates at a ratio of 1:4. Basement Membrane GFR Matrigel was used following the manufacturer's instructions. Briefly, 0.5 ml aliquots of Basement Membrane GFR Matrigel were prepared and frozen at -80°C. One aliquot was thawed on ice and added to 15 ml of cold DMEM/F12+GlutaMAX (31331028; Invitrogen) (1:30 dilution) to coat wells of 6-well plates (1 ml/well), which were then incubated at room temperature for 1 hour prior to be used. Just before hiPSC seeding and culturing on top of the thin gel layer, the unbound coating liquid was aspirated from each well.

After 24 hour-recovery in mTeSR1 complete medium supplemented with 10 μM ROCK inhibitor, cell colonies were grown in 1.5 ml of chemically defined basal differentiation medium [DMEM/F12+GlutaMAX (Invitrogen), 17.5 mg/ml BSA fraction V (126579; Merck-Millipore), 17.5 μg/ml human insulin (I9278; Sigma-Aldrich), 275 μg/ml human holo-transferrin (T0665; Sigma-Aldrich), 450 μM 1-thioglycerol (M6145; Sigma-Aldrich), 0.1 mM non-essential amino acids (Invitrogen), 1% Pen-Strep (Invitrogen)] supplemented with 50 ng/ml human fibroblast growth factor 2 (FGF2) (100-18B; PeproTech) and 30

ng/ml human bone morphogenetic protein 4 (BMP4) (120-05; PeproTech) for 2 days to induce mesoderm commitment. For the next 2 days, cells were exposed to the basal differentiation medium supplemented with 1 μM all-trans retinoic acid (R2625; Sigma-Aldrich), 10 ng/ml human Activin A (120-14E; PeproTech) and 100 ng/ml human bone morphogenetic protein 2 (BMP2) (H00000650-Q01; Abnova Corporation, Taiwan) for UB fate induction. 1.5 ml of appropriate differentiation medium was added daily. Activin A, all-trans retinoic acid, and all growth factors were reconstituted and stored in accordance with the manufacturer's instructions.

2.8 RNA isolation and gene expression analysis with quantitative reverse transcription-polymerase chain reaction (qRT-PCR)

Both undifferentiated (d0) and differentiated (d1-d4) hiPSCs were harvested with Accutase as described in the paragraph 2.3, and separately collected in 50 ml conical tubes. After cell counting, aliquots of 2-3x10^6 cells were transferred to 15 ml conical tubes, and centrifuged at 200x*g* for 5 minutes at room temperature. After centrifugation, supernatant was discarded, pellet was resuspended in 8 ml of PBS, and cell suspension was centrifuged again. Next, supernatant was carefully aspirated without disturbing the pellet, and dry pellets were stored at -80°C overnight or until RNA isolation procedure. Total cellular RNA was isolated with Trizol® Reagent (15596026; Invitrogen) according to the manufacturer's instructions using the appropriate precautions to avoid RNase contamination. The total RNA yields and purity were determined by measuring the absorbance at 260 nm and 280 nm ($A_{260/280}$ > 1.8), respectively, with NANODROP 1000 UV/VIS spectrophotometer (Thermo Fisher Scientific) following dilution of the isolated RNA samples in RNase-free water on ice. To avoid DNA contamination, 10 μg of total RNA were treated using the RQ1 RNase-free DNase kit (M6101; Promega Corporation,

Madison, WI, USA) [DNase treatment for 1 hour at 37°C in the presence of 1 U/µl of SUPERaseInh^{TM} RNase Inhibitor (AM2694; Invitrogen), followed by the addition of DNase STOP solution for 10 minutes at 65°C]. Purified RNA suspension volume was made up to 200 µl with RNase-free water, and was precipitated by adding 20 µl of 3M sodium acetate buffer pH 5.4 and 600 µl of ice-cold 100% ethanol, overnight at -80°C. The next day, samples were centrifuged at 13,200 rpm for 30 minutes at 4°C in the Eppendorf® 5415-R refrigerated microcentrifuge. After centrifugation, supernatant was discarded, pellets were washed by gently adding 500 µl of ice-cold 75% ethanol, and were centrifuged at 13,200 rpm for 5 minutes at 4°C. Subsequently, supernatant was aspirated, pellets were resuspended with RNase free-water on ice, and the absorbance at 260 nm and 280 nm was measured. At this point, 2.5 µg of purified RNA were reverse-transcribed using SuperScript VILO cDNA synthesis kit (11754050; Invitrogen) adhering to the manufacturer's instructions. No enzyme was added to reverse transcriptase-negative controls. Expression of pluripotency, early renal and UB-related markers was evaluated by TaqMan gene expression assay on ViiA 7 Real Time PCR system (Applied Biosystems, CA, USA) using predesigned TaqMan probes (Thermo Fisher Scientific) specific to *NANOG*, *T*, *LHX1*, *PAX2*, *GATA3* and *HOXB7* genes (Table 1) according to the supplier's instructions. Gene expression levels were normalised to the housekeeping gene glyceraldehyde-3-phosphate dehydrogenase (*GAPDH*). The ΔΔCt technique was adopted to calculate cDNA content in each sample using cDNA expression of the pluripotent state (d0) as a calibrator. Three independent experiments for each hiPSC line were performed, and samples were analysed in triplicate.

2.9 Kidney tubule engineering

Sub-confluent MDCK type II cells and *in vitro* differentiated hiPSCs were harvested, as

described in the paragraphs 2.2 and 2.3, using pre-warmed 0.25% Trypsin–EDTA and Accutase, respectively. Once detached, cells were counted, collected in sterile Eppendorf® Safe-Lock microcentrifuge tubes containing the appropriate culture medium, and centrifuged at 300x*g* for 3 (hiPSCs) or 4 (MDCK cells) minutes in the CL17-R Microcentrifuge (75002455; Thermo Fisher Scientific). Subsequently, supernatant was completely discarded, pellets were resuspended in 2.4 mg/ml rat-tail collagen type I (354236; Corning) on ice taking care to avoid air bubble formation and obtain a homogeneous cell suspension, which was finally seeded into the PDMS scaffold cavities. Prior to cell seeding, PDMS macro- and microscaffolds were placed into sterile 60x15 mm (353004; Corning) and 35x10 mm (DTC035; Sterilin® Ltd, British Plastics Federation, Parkway, UK) tissue culture dishes, respectively. Rat-tail collagen type I was stored according to the manufacturer's instructions and was gelled by bringing its pH to alkalinity following the gelation procedure described in the Certificate of Analysis provided by the producer. Optimal cell densities were set-up at $1.2x10^5$ cells/µl collagen and $2x10^5$ cells/µl collagen for macro- and microscaffolds, respectively. The total volume of seeded cell-collagen mixture vary according to the size of the PDMS scaffold cavities. After collagen polymerisation, which for macroscaffolds occurs after 30 minutes at 37°C and for microscaffolds occurs after 2 minutes at room temperature, the appropriate culture medium (6 ml for macroscaffolds and 200-250 µl for microscaffolds) was gently dropped to cover the scaffolds.

Culture media: DMEM/F12+GlutaMAX supplemented with 1% FBS, 1% Pen-Strep and 40 ng/ml hepatocyte growth factor (HGF) (100-39; PeproTech) for MDCK tubules; basal differentiation medium supplemented with 1% FBS, 40 ng/ml HGF and 100 ng/ml glial cell-derived neurotrophic factor (GDNF) (ab73450; Abcam, Cambridge, UK) for hiPSC-derived tubules.

Bright-field images of cultured tubules were obtained using Leica ZOOM 200 stereomicroscope (Leica Microsystems, Wetzlar, Germany) and Primo Vert inverted microscope (Carl Zeiss). Both HGF and GDNF were reconstituted and stored following the manufacturer's instructions. Tubules were cultured for up to 2 days in standard conditions without changing culture medium.

2.10 Kidney tubule histological staining

For cross-sectional histological analysis, 2-day cultured macrotubules were gently harvested with a 1000 µl micropipette (Gilson), transferred into sterile 60x15 mm dish, washed with PBS for 10 minutes, and then fixed in PBS containing 4% PFA for 15 minutes. After abundant washing with PBS, tubules were embedded in Optimal Cutting Temperature (OCT) compound (4583; Tissue-Tek, Sakura Finetek, Japan) and frozen at -80°C. After freezing, 3-µm serial tubule cryosections were cut using Leica CM1950 cryostat (Leica), mounted on Polysine® slides (J2800AMNZ; Thermo Fisher Scientific) and immediately placed at -80°C. Subsequently, slides were submerged in Harris's haematoxylin (05-M06004; Bio-optica) for 2 minutes, rapidly washed with distilled water, mounted with Ready-to-use Dako Faramount Aqueous Mounting Medium (S3025; DAKO Corporation, Carpinteria, CA, USA) and observed by light microscopy.

Tubules 3D-cultured in Transwell inserts (see paragraphs 2.13 and 2.14 for details) were stained with haematoxylin and eosin as follows: firstly, they were washed with 2 ml PBS for 15 minutes, fixed in PBS containing 4% PFA for 45 minutes at room temperature, and washed again in PBS (at this point samples can be stored at 4°C in 3 ml PBS). Secondly, tubules were harvested from collagen (see the paragraph 2.13 for details on this manoeuvre), submerged in 3 ml of haematoxylin (05-M06012; Bio-Optica, Milan, Italy) diluted 1:6 in distilled water for 5 minutes, washed abundantly in distilled water and then

soaked in 3 ml of eosin (05-M10002; Bio-optica) diluted 1:9 in distilled water for 1 minute. After washing, samples were placed on Polysine® slides, completely covered with Ready-to-use Dako Faramount Aqueous Mounting Medium, and observed by light microscopy.

All digital images were acquired and analysed using AxioImager Z2 microscope and AxioVision 4.8 imaging software (Carl Zeiss), respectively.

2.11 Kidney tubule immunofluorescence staining

For immunofluorescence analysis, tubules were harvested from the scaffolds, fixed in PBS containing 4% PFA as described in the paragraph 2.10, washed in PBS for 10 minutes, and permeabilised in 100% ice-cold methanol (414814; Carlo Erba Reagents, Cornaredo, Milan, Italy) for 10 minutes. Next, samples were washed again and incubated with the following primary antibodies diluted in PBS: mouse anti-E-cadherin (610182; BD Biosciences, CA, USA; 1:100), rabbit anti-podocalyxin (NB110-41503; Novus Biologicals, Littleton, CO, USA; 1:80), rabbit anti-PKC-ζ (C-20) (sc-216; Santa Cruz; 1:100) and rabbit anti-cleaved caspase-3 (D175-5A1E; Cell Signaling Technology, MA, USA; 1:200) overnight at 4°C. After washing, tubules were incubated with the appropriate secondary antibodies diluted in PBS: Cy™3-conjugated AffiniPure Donkey Anti-Mouse IgG (715-165-151; 1:50), Cy™5-conjugated AffiniPure F(ab')$_2$ Fragment Donkey Anti-Mouse IgG (715-176-151; 1:50), Cy™3-conjugated AffiniPure Donkey Anti-Rabbit IgG (711-165-152; 1:50) and Fluorescein (FITC)-conjugated AffiniPure Donkey Anti-Rabbit IgG (711-095-152; 1:50) overnight at 4°C in the dark. All secondary antibodies were purchased from Jackson ImmunoResearch Labs, PA, USA. After washing, samples were soaked in DAPI for 10 minutes to label cell nuclei, washed again, placed on 24x60 mm coverslips (Knittel Gleaser, Germany), and completely covered with Dako Fluorescence

Mounting Medium (S3023; DAKO Corporation).

For the immunostaining of 3-μm cross-sections, sample sections were permeabilised with PBS containing 0.3% Triton X-100 for 5 minutes, washed, blocked with 1% BSA solution in PBS for 30 minutes, washed again, and incubated overnight at 4°C with the indicated primary antibodies. After washing, sections were incubated with the appropriate secondary antibodies (Jackson ImmunoResearch Labs; 1:50) for 2 hours at room temperature in the dark, followed by washing and nuclear staining with DAPI for 10 minutes. Negative controls were obtained by omitting primary antibodies on adjacent sections on the same slide. Finally, slides were mounted with Dako Fluorescence Mounting Medium and examined.

In some cases, samples were further labelled with wheat germ agglutinin-lectin (WGA-lectin) (FL-1021; Vector Labs, Burlingame, CA, USA; 1:400) for 15 minutes or peanut agglutinin-lectin (PNA-lectin) (RL-1072; Vector Labs; 1:80) for 1 hour and 30 minutes, both diluted in PBS. Digital images were acquired using the LSM 510 Meta inverted confocal laser scanning microscope and LSM Image browser (Carl Zeiss). All images were analysed using the free open-source image processing ImageJ software (1.49v, National Institutes of Health).

2.12 Functional studies

After 2 days of culture in PDMS scaffolds, engineered tubules were harvested, transferred in transparent plastic tubes with screw cap, washed with 1 ml of PBS for 10 minutes, and then soaked in 500 μl of PBS containing 25 mg/ml 10-KDa FITC-conjugated dextran (FD10S; Sigma-Aldrich) or 2 mM 6-Carboxyfluorescein (6CF) (C0662; Sigma-Aldrich) alone or in combination with 2 mM probenecid (P8761; Sigma-Aldrich) for 1 hour at 37°C in the dark. Subsequently, tubules were washed 4-5 times with ice-cold PBS, were fixed

with PBS containing 4% PFA for 10 minutes, and processed for immunofluorescence analysis as described in the paragraph 2.11.

2.13 Cyst formation and drug testing in 3D culture system

After 2 days of culture, MDCK cell-derived tubules were harvested from PDMS microscaffold cavities through gentle suction with a 200 μl micropipette (Gilson), washed in PBS for 10 minutes, embedded within 200 μl of 2.4 mg/ml rat-tail collagen type I, and finally transferred onto polyester Transwell membranes (0.4 μm pore size) in 12-well plates (CC3460; Corning-Costar, MA, USA). Following collagen polymerisation (35-40 minutes at 37°C), 1.5 ml of culture medium, composed of MEM supplemented with 10% FBS, 1% L-glutamine and 1% Pen Strep, was added. To induce cyst formation, samples were cultured in culture medium supplemented with 10 μM forskolin (F6886; Sigma-Aldrich) for 7 days. Next, 'polycystic' tubules were cultured in the presence of 10^{2} μM Octreotide acetate (OCTR) (0239950; Toronto Research Chemicals, Brisbane Rd, North York, Canada), 10^{2} μM Pasireotide diaspartate (PAS) (kind gift from Novartis Farma S.p.A., Varese, Italy), 10^{4} μM 2-Deoxy-D-glucose (2DG) (D6134; Sigma-Aldrich), 10 μg/ml berberine chloride (B3251; Sigma-Aldrich), 0.5 μM Rapamycin (R0395; Sigma-Aldrich), or with 10^{-2} μM Arginine Vasopressin (AVP) (V9879; Sigma-Aldrich) alone or in combination with 10^{-2} μM Tolvaptan (T7455; Sigma-Aldrich) for another 7 days. Control samples were maintained in culture medium alone for all 14 days. In each culture condition, culture medium was changed every 2 days. After fixing, tubules were harvested by gently cutting the surrounding collagen gel with insulin-needles under a stereomicroscope, and were processed for immunofluorescence and histological analysis as described in the paragraphs 2.10 and 2.11. The number of cysts was quantified in different fields of haematoxylin and eosin-stained tubules using ImageJ software. Haematoxylin and

eosin staining images were acquired with AxioImager Z2 microscope (Carl Zeiss). The area of each field was calculated using AxioVision 4.8 software (Carl Zeiss). Data are expressed as number of cysts/mm^2. Two independent scientists performed quantification analyses in blind. According to the manufacturer's indications, both forskolin, rapamycin, Tolvaptan and berberine were reconstituted in DMSO; OCTR and PAS were reconstituted in sterile saline solution; and AVP and 2DG were resuspended in sterile distilled water. Once in solution, compounds were diluted in culture medium to achieve the desired final concentration. The final DMSO concentration in the culture media never exceeded 0.1%.

2.14 3D culture experiments for human developmental studies

Fragments of about 0.6 mm in width x 4.0 mm in length of 2-day cultured hiPSC-derived macrotubules were transferred to polyester Transwell membranes as described in the paragraph 2.13. To obtain fragments of the appropriate size, tubules harvested from PDMS scaffolds were manually cut using insulin-needles. E13.5 CD1 mouse kidneys were freshly isolated as previously described (Xinaris *et al.*, 2012, 2016). For 3D co-culture experiments, four E13.5 kidneys were placed within collagen in close proximity to each tubule and, after collagen polymerisation, culture medium [Advanced DMEM (12491023; Invitrogen) supplemented with 2% embryonic stem cell FBS (16141079; Invitrogen), 1% L-glutamine and 1% Pen-Strep] was added. Other samples were cultured in Advanced DMEM supplemented with 1 μg/ml heparin (VERACER, Medic Italia S.r.l., Roma, Italy) and with different combinations of the following growth factors: 40 ng/ml HGF, 100 ng/ml GDNF, 200 ng/ml FGF1 (100-17A; PeproTech) and 100 ng/ml FGF7 (100-19; PeproTech). Both heparin and growth factors were reconstituted and stored following the manufacturer's instructions, and diluted in culture medium to achieve the desired final concentration indicated above. Cultures were monitored by light microscopy for up to 2

days without changing the medium, and eventually fixed and processed for immunofluorescence analysis as described in the paragraph 2.11. Bright-field images of tubules cultured in the different aforementioned conditions were acquired with Primo Vert inverted microscope (Carl Zeiss). The total budding events of the human UB-like tubules were quantified using ImageJ software. Two independent scientists performed quantification analyses in blind. Data are expressed as percentage of ramified buds over total buds that emerged from human tubules.

The IRCCS - Istituto di Ricerche Farmacologiche 'Mario Negri' adheres to the principles set out in the following laws, regulations, and policies governing the care and use of laboratory animals: Italian Governing Law (D.lgs 26/2014; Authorisation n.19/2008-A issued March 6, 2008 by Ministry of Health); Mario Negri Institutional Regulations and Policies providing internal authorisation for persons conducting animal experiments (Quality Management System Certificate - UNI EN ISO 9001:2008 - Reg. N° 6121); the NIH Guide for the Care and Use of Laboratory Animals (2011 edition) and EU directives and guidelines (EEC Council Directive 2010/63/UE). The Statement of Compliance (Assurance) with the Public Health Service (PHS) Policy on Human Care and Use of Laboratory Animals has been recently reviewed (9/9/2014) and will expire on September 30, 2019 (Animal Welfare Assurance #A5023-01).

2.15 Statistical analyses

Samples were randomly allocated in every experimental groups/conditions and no inclusion/exclusion criteria were used. Statistical analysis was performed using GraphPad Prism software, version 7 (GraphPad, San Diego, CA, USA). When two conditions were compared, two-tailed Student's t-test was used. When more than two conditions were compared, one-way ANOVA with the Tukey's multiple comparisons test

(for cyst quantification) and with the Holm-Sidak's multiple comparisons test (for ramified over total buds quantification) was used. Differences were considered to be significant when $P < 0.05$. Data are expressed as means ± s.e.m. See figure legends for details on number of replicates and *n* values used.

Catalogue number	Gene symbol	Description
Hs00742896_s1	*OCT4*	*H. sapiens* POU class 5 homeobox 1
Hs00602736_s1	*SOX2*	*H. sapiens* SRY (sex determining region Y)-box 2
Hs02387400_g1	*NANOG*	*H. sapiens* NANOG homeobox
Hs00610080_ml	*T*	*H. sapiens* T, brachyury homolog
Hs00232144_m1	*LHX1*	*H. sapiens* LIM homeobox 1
Hs01057416_m1	*PAX2*	*H. sapiens* paired box 2
Hs00231122_m1	*GATA3*	*H. sapiens* GATA binding protein 3
Hs04187556_m1	*HOXB7*	*H. sapiens* homeobox B7
Hs99999909_m1	*HPRT1*	*H. sapiens* hypoxanthine phosphoribosyltransferase 1
Hs02758991_g1	*GAPDH*	*H. sapiens* glyceraldehyde-3-phosphate dehydrogenase

Table 1. List of TaqMan probes used in qRT-PCR experiments

CHAPTER 3 - RESULTS

3.1 Design and fabrication of 3D-printed PDMS scaffolds

In collaboration with NanoMed Labs (University of Genova, Italy) and relying on the physiological structure of the UB tree during early kidney development (Lin *et al.*, 2003; Watanabe and Costantini, 2004; Lindström *et al.*, 2015), we designed three basic patterns shaped to resemble some UB segments. These patterns consisted of: a straight line **(Supplementary Figure 1a)** for UB trunks, a terminal 80° bifid branch **(Supplementary Figure 1b)** and asymmetric lateral 30° branches **(Supplementary Figure 1c)**, both for UB ramifications. To mimic advanced stages of UB branching morphogenesis, we merged the 80° and 30° basic schemes into a ramified pattern **(Supplementary Figure 1d)**. Moreover, to quickly and routinely design fractal-like ramifications similar to those observed in early kidney development (Lin *et al.*, 2003), we developed a 'golden fractal tree' (GFT) formula **(Supplementary Figure 1e)**. Unlike the previously described GFTs with a constant amplitude (Taylor, 2007; Pons, 2013), our formula allows progressive narrowing of bifurcations for an infinite number of times, preventing branch overlapping **(Supplementary Figure 1f).** Finally, with the aim of engineering numerous individual tubules at the same time, we designed a linear multichannel pattern **(Supplementary Figure 1g)**. Thereafter, we converted the custom-designed patterns into plastic masters through rapid prototyping technologies and 3D printing, and used them as moulds to produce polydimethylsiloxane (PDMS) replicas **(Figure 5a)**. PDMS is a silicon-based organic polymer with numerous desirable properties that make it suitable for cell biology studies. In particular, PDMS is biocompatible, non-toxic to cells, chemically inert, gas permeable, and optically transparent for imaging applications (Briganti *et al.*, 2006; Adler *et al.*, 2010; Young and Beebe, 2010; Markov *et al.*, 2014).

Given their distinct geometries, we refer to the replicas with bigger, linear and ramified cavities as 'macro-scaffolds', and those with multiple micro-patterned linear cavities as

'micro-scaffolds'. Differently from typical PDMS devices made for cell cultures, which are pre-treated to possess hydrophilic properties and adhesive surfaces (Halldorsson *et al.*, 2015), our scaffolds were kept hydrophobic to facilitate detachment of engineered tissues without compromising cell-ECM seeding, and to enable standard sterilisation processes so that the scaffolds could be reused.

3.2 Engineering kidney tubular structures with different geometries by seeding epithelial cell suspensions into PDMS scaffolds

To develop and optimise our system for tubule engineering, we used the MDCK epithelial cell line, which is composed of both distal tubule and collecting duct cells (Rindler *et al.*, 1979; Herzlinger *et al.*, 1982), and has been widely used in studies examining cyst and tubule formation. Collagen type I was chosen as ECM-mimicking gel in which to resuspend the cells as it is the most abundant ECM component, can store and support diffusion of nutrients and growth factors, permits 3D intercellular interactions, and provides structural support for cell movement and organisation into tissues (Davies, 2001). With the aim of engineering epithelial kidney tubules, a range of 0.7-6.5x10^5 MDCK cells/µl collagen were seeded into PDMS scaffold cavities, and cultured for up to 2 days **(Figure 5b)**. In accordance with previous studies, tubulogenesis was induced by supplementing culture medium with 40 ng/ml hepatocyte growth factor (HGF), a molecule capable of strongly inducing *in vitro* branching tubulogenesis (Montesano *et al.*, 1991b, 1991a; Sakurai *et al.*, 1997; Pollack *et al.*, 1998; Liu *et al.*, 2007). The seeding conditions with the highest rate of tubule formation (94% of total seeded scaffolds) were 1.2x10^5 and 2x10^5 cells/µl collagen for macro- and micro-scaffolds, respectively **(Figure 5c-e and f)**. It is important to know that, in the remaining cell concentrations tested, only cell clustering

was observed within the scaffolds' cavities and no tubules developed **(Supplementary Figure 2a and b)**.

Under the aforementioned conditions, three hours post-seeding, dispersed cells organised to give rise to tubular structures with analogous size and shape to the scaffold's cavity **(Supplementary Figure 2c)**. At day 1, single and branched structures noticeably shrank and began detaching from the moulds **(Figure 5c)**. At day 2, the shrinkage increased and whole intact branches emerged autonomously from the cavity. Strikingly, at bifid branching points, a presumptive luminal space was observed through bright-field microscopy and appeared as a translucent region delimited by darker edges. This suggested that a common cavity between tubular structures was forming **(Figure 5c)**. Using PDMS scaffolds with more complex geometries, we successfully applied our method to engineer increasingly branched and tree-like tubular structures **(Figure 5d and e)**. By seeding cells into multichannel scaffolds with micro-patterned linear cavities, we concomitantly obtained multiple individual linear microtubules within 2 days of culture **(Figure 5f)**, thus demonstrating the applicability of our system on a micro-scale.

Depending on scaffold size, we refer to the tubular structures generated and depicted in **Figure 5c-e** and **Figure 5f** as 'macrotubules' (both single and in networks) and 'microtubules', respectively.

3.3 Engineered tubules undergo rapid lumen formation and epithelial polarisation

Development of mature epithelial tubules involves cell rearrangements that lead to the formation of a lumen enclosed by an epithelium with appropriate polarisation (Andrew and Ewald, 2010). Kidney tubules consist of aligned epithelial cells, which adhere by means of specialised intercellular junctions and lie on a basement membrane, giving rise to a monolayered epithelium enclosing a central lumen. This configuration entails that cells

acquire a well-established apical-basal polarity, with apical membranes facing the lumen, and lateral and basal membranes in contact with neighbouring cells and basement membrane, respectively (Bryant and Mostov, 2008; Andrew and Ewald, 2010).

To examine the presence of a lumen and evaluate the establishment of a polarised epithelium, we immunostained the engineered microtubules and analysed them from the surface to the inner region through confocal Z-stack imaging. Remarkably, this analysis revealed the presence of a single lumen surrounded by a monolayer of epithelial cells positive for E-cadherin **(Figure 6a)**. This transmembrane glycoprotein is abundantly expressed in distal tubule, collecting duct and most medullary segments, where it plays an important role in the establishment of intercellular adherens junctions and renal epithelial polarity (Prozialeck *et al.*, 2004). Identically to microtubules, branches from macrotubular systems possessed well-established epithelial structures with a coalesced lumen. In particular, the lumen was lined by tubular walls consisting of a monolayer of cells showing aligned nuclei, positivity for E-cadherin in the lateral membranes and wheat germ agglutinin (WGA)-lectin in the basement membranes, **(Figure 6b)**. Some cells of the tubular walls were positive for peanut agglutinin (PNA)-lectin - a known MDCK cell luminal surface marker (Schumacher *et al.*, 2008) - and podocalyxin - an integral membrane protein expressed in the apical domain of terminally polarised MDCK cells – in the apical membranes (Meder *et al.*, 2005) **(Supplementary Figure 3a)**.

Overall, these findings proved that we were successful in engineering tubules consisting of a properly apical-basal polarised monolayered epithelium lining a continous lumen.

Apoptosis is one crucial step underlying lumen formation during tubulogenesis. In tubule primordia, cells that are not in direct contact with ECM undergo programmed cell death generating an empty space, namely the lumen. Hence, this process gives rise to a tubule. Considering the timely occurrence of this phenomenon, engineered tubules were examined

at an earlier stage of development, providing insight into the mechanism of lumen formation in our system. Haematoxylin staining of cross-sectioned 1-day macrotubules showed that these had a major lumen enclosed by a peripheral layer of cells with nuclei aligned along the tubular walls. In macrotubules, centrally located cells featured chromatin condensation and immunoreactivity for cleaved caspase 3 (**Supplementary Figure 3b and c respectively**), both clear signs of apoptosis. By contrast, peripheral cells constituting tubular walls revealed normal cell morphology and no signs of apoptosis **(Supplementary Figure 3c)**. These findings implied that, in our system, cells in the central region of the tubular aggregate die by apoptosis, creating a hollow, eventually giving rise to the lumen by a process known as cavitation (Schumacher *et al.*, 2008; Sigurbjörnsdóttir *et al.*, 2014). In control experiments, in which cells were cultured in the absence of HGF, phenotypically compact tubules did indeed form, but could not develop a lumen **(Supplementary Figure 3d)**.

3.4 Engineered tubules exhibit macromolecule absorption and organic anion transport capacities

The mature renal tubular epithelia reabsorb macromolecules, and control the excretion of endogenous compounds, xenobiotics and organic anions. It has been previously described that both medullary and cortical collecting duct cells are capable of dextran macromolecule internalisation from their basolateral surfaces (Schwartz and Al-Awqati, 1985; Raghavan *et al.*, 2014). Organic anion transepithelial transport and excretion into the lumen are mediated by specific organic anion transporters (OATs) widely distributed across kidney tubules. Specifically, these localise to both the basolateral and apical membranes of proximal tubule as well as collecting duct epithelial cells (Kojima *et al.*, 2002; Sweet *et al.*, 2006; Yokoyama *et al.*, 2008; Burckhardt, 2012).

Therefore, to test whether the engineered microtubules possessed such functional properties, we soaked them in solutions containing either fluorescein isothiocyanate-conjugated (FITC)-dextran (molecular weight 10 kDa) or the tracer anion 6-carboxyfluorescein (6CF) (Sweet *et al*., 2006). The latter has better kinetic properties than fluorescein for investigating cellular OAT-mediated transport, due to its additional negative charge that, in comparison, causes increased cell retention (De Clerck *et al.*, 1994).

Immunofluorescence analysis showed that dextran was internalised abundantly in the central areas of the microtubules **(Figure 6c)** and in the cytoplasm of cells of the tubular surface **(Figure 6c, inset)**. With regards to 6CF, it was transported through the tubular epithelium and then secreted into the peripheral regions of the lumen **(Figure 6d)**. Moreover, some E-cadherin-positive cells confined to the tubules' wall, internalised 6CF and retained it within their cytoplasm **(Figure 6d, inset)**. When we soaked tubules in the presence of both 6CF and probenecid - a potent and broad inhibitor of the OAT system (Nagle *et al.*, 2011; Nigam *et al.*, 2015) - fluorescent signal was no longer detectable, neither in the cells nor in the lumen **(Figure 6e)**. These findings demonstrated that engineered tubules displayed absorption and transport characteristics typical of collecting duct epithelia, as they appear capable of macromolecule internalisation and organic anion transport through the OAT-mediated process.

3.5 Using engineered tubules as a tool to model polycystic kidney disease (PKD)

PKD is one of the most frequent genetic disorders (the fourth leading cause of CKD resulting in ESRD in the USA), affecting about 7 million people worldwide and accounting for 7%-15% of patients on RRT (Akoh, 2015; Saigusa and Bell, 2015). It is characterised by the development of fluid-filled epithelial cysts within kidney tubules in a cAMP-

dependent fashion. Unfortunately, at present, there is no effective therapy for PKD (Ong *et al.*, 2015).

When cultured in a 3D ECM environment in the presence of cAMP elevating agents, MDCK cells can form individual epithelial cysts (Mangoo-Karim *et al.*, 1989; Li *et al.*, 2004), as the *in vivo* models of PKD (Gattone *et al.*, 2003; Torres *et al.*, 2004; Wang *et al.*, 2005). For these reasons, they have been extensively used to model PKD and explore the effects of drugs on cyst development. However, *in vitro* cultures of individual cysts do not replicate the gradual expansion of cysts that occurs in PKD, and substantially differ from the physical and biochemical conditions of the tightly packed cysts within the polycystic tubules.

We decided to test whether our system, allowing the engineering of kidney epithelial tubules, could provide an efficient tool to generate polycystic tubules that better replicate pathological tissue phenotype *in vitro*. To this aim, we transferred microtubules to a 3D collagen culture system and stimulated them with forskolin for 7 days. Forskolin is a compound that has previously been shown to increase intracellular cAMP levels and induce cyst development *in vitro* and *in vivo* (Balkovetz, 1998; Sullivan *et al.*, 1998; Li *et al.*, 2004) **(Figure 7a)**. At day 14, both macroscopic and histological examination showed that forskolin-treated tubules developed numerous translucent spheroidal cysts along the whole length of the tubule **(Figure 7b)**. Immunofluorescence analysis confirmed that numerous round-shaped cysts formed homogeneously throughout the tubule **(Figure 7c)**. Cysts were circumscribed by a monolayer of cells positive for E-cadherin in the basolateral membranes, and podocalyxin in the apical membranes, demonstrating the presence of polarised cysts within tubules **(Figure 7d)**. Remarkably, cyst formation disrupted tubular epithelial organisation and caused lumen loss. Overall, these features appear similar to *in*

vivo PKD pathophysiology (Martinez and Grantham, 1995; Grantham, 1996; Torres and Harris, 2006), indicating that engineered tubules efficiently model PKD.

3.6 Using engineered polycystic tubules for drug testing and discovery studies

One major aspiration in designing this system was to provide a novel tool for drug testing and discovery studies *in vitro*. To this purpose, we examined whether forskolin-stimulated tubules would respond to pharmacological treatment to inhibit cyst formation by comparing the effect of compounds with different mechanisms of action on cyst regression.

We, therefore, treated forskolin-stimulated tubules for 7 days with: *(i)* rapamycin - an inhibitor of the mammalian target of rapamycin (mTOR) pathway, which is aberrantly activated in cystic epithelia leading to cystic cell hyperproliferation and marked cystogenesis (Shillingford *et al.*, 2006; Serra *et al.*, 2010); *(ii)* tolvaptan - a highly selective arginine vasopressin (AVP) V2 receptor antagonist, which inhibits the overactivated AVP signalling for intracellular cAMP production, cell proliferation, transepithelial fluid secretion, and cyst growth in PKD collecting ducts and distal nephrons (Reif *et al.*, 2011; Blair and Keating, 2015); *(iii)* octreotide (OCTR) and pasireotide (PAS) - somatostatin analogues that reduce intracellular cAMP levels, cell proliferation and cystogenesis in *in vitro* and *in vivo* experimental models, with different specificity and binding affinity to somatostatin receptors (Masyuk *et al.*, 2007, 2013); *(iv)* 2-deoxy-D-glucose (2DG) - a glucose analogue that ameliorates disease progression *in vivo* by competing with glucose thereby blocking aerobic glycolysis in PKD cells (Rowe *et al.*, 2013; Priolo and Henske, 2013; Chiaravalli *et al.*, 2016); and *(v)* berberine - an isoquinoline quaternary alkaloid isolated from Chinese medicinal herbs, with anti-proliferative effect, mainly linked to cell cycle arrest at G_0/G_1 phase (Bonon *et al.*, 2013), and able to inhibit the mitochondrial

oxidative phosphorylation resulting in ATP depletion (Fan *et al.*, 2013). This compound has never been studied in a PKD model.

We performed immunofluorescence staining to evaluate the effect of tested compounds on cyst regression; in parallel, we carried out cyst quantification on haematoxylin and eosin stained tubules. These analyses demonstrated that rapamycin treatment had no significant effect on reducing cyst number compared to forskolin-stimulated tubules (controls) **(Figure 7e and k)**. To test the effect of Tolvaptan, we treated forskolin-stimulated tubules with AVP alone, or in combination with Tolvaptan (Reif *et al.*, 2011). As expected, treatment with AVP alone increased cyst number, while administration of AVP in combination with Tolvaptan significantly decreased cyst size and number (63%) **(Figure 7f and l)** (Reif *et al.*, 2011). Moreover, cyst number significantly diminished when tubules were treated with OCTR (58%) **(Figure 7g and k)** and PAS (43%) **(Figure 7h and k)** compared to controls. Notably, 2DG and berberine were the most effective compounds for cyst regression, reducing the number of cysts by 71% and 72%, respectively **(Figure 7i-k)**, and limiting cysts to the peripheral areas of tubules. An outstanding difference observed between the treatments was the drugs' ability to restore both the tubular central lumen and epithelial organisation. Indeed, only 2DG and berberine possessed this ability **(Figure 7i and j)**, whereas Tolvaptan, OCTR and PAS did not, even though they reduced cyst numbers to various extents, **(Figure 7f-h)**. Together these data demonstrate that engineered 'polycystic' tubules responded to drug treatments in a quantifiable manner, making this system a valuable tool for drug testing and discovery studies. Furthermore, we revealed the anti-cystogenic properties of berberine in polycystic kidney tissue, making it a promising new drug with therapeutic potential for PKD treatment.

3.7 Engineering functional human epithelial tubules starting with hiPSC-derived UB-like progenitor cells

The next goal was to test our system's ability to efficiently engineer human tubules, using hiPSCs previously generated in our laboratory through lentiviral-mediated reprogramming of somatic cells (Imberti *et al.*, 2015). First, we directed the differentiation of the hiPSCs into UB-committed renal progenitor cells through 4-day exposure to chemically defined media as previously described by Belmonte group (Xia *et al.*, 2013). This differentiation protocol consists of a first step of mesoderm commitment and a second step of UB fate induction (Xia *et al.*, 2014). As expected, differentiating cells displayed a temporal gene expression pattern similar to that obtained by Xia and colleagues, which corresponded to mesoderm and IM commitment, and eventually UB-like progenitor cell differentiation **(Supplementary Figure 4)**. Once the differentiation protocol had been optimised, we resuspended cells obtained from 2 to 4 days of differentiation in collagen, and seeded them into PDMS scaffolds according to the 3D culture settings and tubulogenic conditions established for MDCK cells **(Figure 8a)**. Although 3- and 4-day differentiated cells generated compact tubular structures, the exposure to HGF alone was not sufficient to induce formation of monolayered epithelia surrounding a single lumen **(Supplementary Figure 5a)**. To overcome this problem, we modified culture conditions by enriching the medium with glial cell-derived neurotrophic factor (GDNF), a molecule secreted by the MM that is essential for UB formation, growth and branching during kidney development (Shakya *et al.*, 2005). After 2 days in these culture conditions, immunofluorescence analysis of tubules derived from 3- and 4-day differentiated hiPSCs showed the formation of a continous lumen **(Figure 8b and c)** delimited by a monolayer of cells positive for WGA-lectin and E-cadherin in the basolateral membranes **(Figure 8b)**. A fraction of the cells expressed the apical epithelial marker protein kinase C-ζ (PKC-ζ) (Yang *et al.*, 2013)

in the apical membranes **(Supplementary Figure 5b)**. Neither undifferentiated hiPSCs, used as controls, nor 2-day differentiated cells were able to form tubular structures **(Supplementary Figure 5c and d)**.

Finally, to test whether this maturation degree would reflect UB-associated functions, we soaked engineered human microtubules in a solution containing FITC-dextran or 6CF. Confocal microscopy analysis revealed massive dextran internalisation throughout the tubular lumen **(Figure 8d)** and 6CF transport visible as a patchy signal in the cytoplasm of peripheral cells **(Figure 8e)**, both functional features typical of *in vitro*-cultured UB.

Similarly to MDCK tubules, at day 1, human tubules had many apoptotic cells, positive for cleaved caspase 3 and displaying condensed chromatin, at the centre of cross-sectioned macrotubules, confirming that cavitation is the mechanism of tubular lumen formation **(Supplementary Figure 5e and f)**.

To assess the reproducibility of our system, we engineered tubules from a hiPSC line obtained in our laboratory through a different technology, the Sendai virus-mediated expression of reprogramming factors in healthy donor-derived peripheral blood mononuclear cells (Ciampi *et al.*, 2016). Both hiPSC differentiation towards UB progenitor-like cells and UB-like tubule engineering were successful **(Supplementary Figure 6)**. Altogether, these data demonstrate that our innovative system is strongly robust and reproducible in that it allows successful production of human UB-like tubules from several hiPSC lines.

3.8 Using human tubules as a tool for studying UB developmental processes and defects

One of the greatest limitations in studying the developmental processes and disorders of human kidney is the scarcity of human embryonic samples and the lack of methods for

engineering kidney tissue or units from patients with genetic mutations. In virtue of our establishing a technology able to provide human UB-like tubules, we decided to investigate first whether they exhibited developmental capacities. Next, we evaluated the possibility of using the engineered tubules to examine both human UB morphogenetic mechanisms and possible developmental anomalies associated with genetic disorders.

3.8.1 Engineered human tubules recapitulate early steps of UB morphogenesis following mouse embryonic kidney induction or by exposure to selected growth factors

During the early developmental stages, the UB undergoes rapid budding and branching events, which mainly consist of iterative lateral ramifications and terminal bifid bifurcations (al-Awqati and Goldberg, 1998; Shah *et al.*, 2004; Nigam and Shah, 2009; Costantini and Kopan, 2010). Although during kidney development the MM is involved in inducing and regulating UB branching pattern through direct contact, the ability to elongate and branch is intrinsic to the UB epithelium. Indeed, these processes can also take place without direct contact with MM, in the presence of soluble growth factors and ECM components (Qiao *et al.*, 1999a).

Thus, we tested whether engineered human tubules possessed UB developmental properties and would respond to kidney developmental cues. Firstly, we co-cultured macrotubules into a 3D collagen culture system with mouse embryonic kidneys as sources of soluble factors to stimulate UB morphogenesis **(Figure 9a)**. At day 1, bright-field microscopy showed primary buds emerging from the main body of the tubule. At day 2, lateral ramifications emerged from elongated primary buds, leading to the formation of secondary buds **(Figure 9b)**. Immunofluorescence analysis revealed that these buds consisted of multicellular cords of epithelial cells with aligned nuclei and expressing E-

cadherin **(Figure 9c)**. This configuration represents an early step of tubulogenesis *in vitro* (Sakurai *et al.*, 1997).

Secondly, we assessed the effect of different combinations of selected growth factors known to be involved in rodent UB morphogenesis (Qiao *et al.*, 1999a, 1999b, 2001; Shakya *et al.*, 2005) on inducing human tubule budding. The basal culture condition with HGF and GDNF induced 35.05 ± 1.02% of ramified buds in the total budding events **(Figure 9d)**. Addition of FGF1 - a strong inducer of UB branching and stalk formation (Qiao *et al.*, 2001) - or FGF7 - a stimulator of UB survival and growth *in vitro* (Qiao *et al.*, 1999b, 2001) - to the basal culture condition did not significantly increase the percentage of ramified buds (41.11 ± 10.60% and 52.38 ± 6.24%, respectively) **(Figure 9d)**. Conversely, when all growth factors were used together, the number of ramified buds markedly increased (71.96 ± 3.22%) **(Figure 9d-f)** and was comparable to that observed in co-culture with mouse embryonic kidneys (74.81 ± 4.12%) **(Figure 9b and d)**. Remarkably, when all growth factors were added in combination, a fraction of ramified buds displayed terminal bifid bifurcations **(Figure 9e)**.

Overall, these data indicate that engineered human tubules are capable of recapitulating early steps of UB morphogenesis, thus providing a valuable tool for studying the mechanisms of human UB development.

3.8.2 Investigating UB developmental defects in tubules engineered using hiPSCs derived from a patient with a heterozygous PAX2 mutation

Taking advantage of engineered human tubules' developmental capacities, we next applied our system to study possible defects in UB morphogenesis using Paired box 2 (*PAX2*) mutated cells. *PAX2* gene is highly expressed during early kidney developmental stages in both condensing MM and branching UB (Dressler *et al.*, 1990; Eccles *et al.*, 1995; Dressler

and Woolf, 1999). It has been previously described that heterozygous *PAX2* mutations cause reductions in UB branching and nephron number *in vivo* (Harshman and Brophy, 2012), indicating that a direct relationship exists between UB branching and nephron induction.

We therefore derived hiPSCs from a patient with a heterozygous *PAX2* mutation (Barua *et al.*, 2014) through Sendai virus-mediated reprogramming of somatic cells **(Supplementary Figure 7)**. Pluripotency was confirmed by evaluating the expression of pluripotency transcription factors (OCT4, NANOG and SOX2) and hESC surface markers (SSEA-3, SSEA4, TRA-1-60 and TRA-1-81), and the specification into the three germ layers **(Supplementary Figure 7a-c)**. Moreover, reprogrammed cells showed a normal karyotype of 46,XY **(Supplementary Fig. 7d)**. Having confirmed the pluripotent state, we successfully differentiated patient-derived hiPSCs towards UB progenitor-like cells, and engineered patient-derived UB-like macrotubules **(Supplementary Figure 8)**. The latter were cultured in the presence of all selected growth factors as mentioned above **(Figure 9h and i)**, and alongside healthy donor-derived tubules, used as controls **(Figure 9e and f)**. Strikingly, under these culture conditions, patient-derived tubules were capable of developing almost exclusively primary buds **(Figure 9h)**, as opposed to the numerous ramified buds seen in healthy donor-derived tubules **(Figure 9e)**. It is also worth noting that quantification analysis disclosed a marked decrease in ramified buds in these tubules compared with controls **(Figure 9g)**. These results are in agreement with previous *in vivo* data indicating that heterozygous mutation in the *PAX2* gene caused paucity in UB growth and significant reduction in UB branching (Porteous *et al.*, 2000; Eccles *et al.*, 2002). Overall, this proves the effectiveness of our system for studying developmental defects in tubules derived from patients carrying genetic mutations.

CHAPTER 4 - DISCUSSION

In the present study, we have developed a novel technology for engineering functional custom-made complex kidney epithelial tubules by 3D-printed PDMS scaffolds using different cell types. We first began by creating tubules of varying sizes and shapes with the MDCK cell line, which is derived from adult distal tubule/collecting duct epithelia. The engineered tubules were endowed with a single lumen enclosed by a monolayer of oriented and polarised cells exhibiting transport properties typical of mature renal tubular epithelia. We successfully employed engineered tubules to model PKD and screen for several anticystogenic drugs. Then, we refined our system in order to engineer functional hiPSC-derived UB-like tubules and used them as a tool for investigating human kidney developmental mechanisms and patient-specific defects.

Previous studies documented the development of engineering systems that, by exploiting the renal progenitor cells' self-assembly potential *in vitro*, were able to yield 3D tubular structures. However, these systems have important limitations that made them inappropriate to generate kidney tubular units suitable for engineering a functional and anatomically correct kidney tissue. Relying on cell-driven assembly, these technologies lack control over the tubular structure formation, as tubulogenesis occurred through chaotic and geometrically uncontrolled cell organisation in 3D ECM-based cell cultures (Barros *et al.*, 1995; Sakurai *et al.*, 1997; Yuri *et al.*, 2017). Consequently, instead of developing with precise architectural frameworks, engineered tubules were highly heterogeneous in size and shape.

Other kidney tubule engineering systems were based on cell seeding into 3D-printed scaffolds with pre-defined geometries (MacKay *et al.*, 1998; Humes *et al.*, 1999; Schumacher *et al.*, 2008; Shen *et al.*, 2013, 2015, Jansen *et al.*, 2015, 2016; Homan *et al.*, 2016). In particular, tubule formation arose from cell seeding into hollow cylindrical-shaped scaffolds with pre-coated inner surfaces to which cells adhered and grew up to form

a confluent monolayer. Thus, no cell self-assembly into tubular epithelia took place (MacKay *et al.*, 1998; Humes *et al.*, 1999; Schumacher *et al.*, 2008; Shen *et al.*, 2013, 2015, Jansen *et al.*, 2015, 2016; Homan *et al.*, 2016), as instead occurs *in vivo* when cells are embedded in a 3D ECM environment in the presence of tubulogenic conditions. In spite of their unnatural formation, these bio-artificial renal tubules were still exploited for functional and toxicological studies (MacKay *et al.*, 1998; Humes *et al.*, 1999; Shen *et al.*, 2013, 2015, Jansen *et al.*, 2015, 2016; Homan *et al.*, 2016). The shared inability in reproducing the *in vivo* epithelial tubulogenesis is a limitation we have overcome by developing a system that, relying on cell self-assembly into epithelial tubules, yields renal tissues more fitting for functional and pharmacological investigations.

Most of these systems share an additional drawback: the epithelial tubular structures cannot be physically removed from the surrounding ECM or from the pre-formed 3D-printed scaffolds in which they formed. This prevents tubules from being used for further investigations, such as morphogenetic studies and kidney tissue engineering experiments.

On the other hand, our technology allows engineering tubules with lumen, predefined geometries, resembling foetal UB/collecting duct epithelia's architecture and functions, which can be easily removed from the scaffolds. We engineered kidney tubular units in a controlled fashion by seeding cells, which were previously resuspended in collagen gel, into the 3D-printed PDMS scaffolds' cavities and exposing them to appropriate tubulogenic stimuli. Under these conditions, similar to those *in vivo*, cells are directed to self-assemble into geometrically defined epithelial tubules within a 3D ECM-mimicking environment. The fact that our engineered tubules can be harvested, handled and transferred to different experimental conditions makes our system a valuable platform for several applications, such as kidney disease modelling, drug testing and discovery, as well as developmental studies.

In tissue engineering, the nature of the biomaterials' surface and the biostructures' complexity play a pivotal role for establishing realistic diagnostic and therapeutic solutions. In our system, we decided to fabricate hydrophobic PDMS scaffolds. This technical expedient was key to enable the development of complex tubular structures. Indeed, the scaffold cavities' hydrophobicity allowed cell-collagen mixture gathering and immobilisation, thus limiting the risk of cell and ECM dispersal, and precluded irreversible cell adhesion and collagen attachment. Hence, PDMS hydrophobicity indirectly endorsed cell movement and spatial organisation in order to generate functional complex kidney tubules for studying development, modelling disease and investigating therapeutic approaches.

To rapidly prototype more complex structures with truly biomimetic features (Díaz Lantada *et al.*, 2013) we developed a mathematical model that can provide fractal-like geometries. This 'Golden Fractal Tree' model maximised the amount of matter that can suit a limited surface, such as that of the scaffolds' cavities, and allow progressive narrowing of bifurcations an infinite number of times. This avoids branch overlapping, a clear advantage for the serial production of reproducible complex tissues. Furthermore, our PDMS scaffolds can be reused upon conventional sterilisation techniques without requiring any other kind of treatment, thus providing an additional technical advantage.

Since kidney tubulogenesis is a biological process modulated by interactions between epithelial cells, soluble factors and the surrounding ECM components (Santos and Nigam, 1993), we first determined the precise ECM concentration that will allow for cell viability, growth, movement, establishment of cell-ECM and cell-cell adhesion, and organisation into tissue. Based on data published by Hauser *et al.*, (Hauser *et al.*, 2016) we selected the collagen type I concentration of 2.4 mg/ml. This concentration was described as the most efficient for tubule formation compared to lower ones, whereas higher concentrations

caused collagen gel to become too much rigid, thus preventing cell organisation and, concomitantly, tubulogenesis. Even in our system, the use of collagen at a concentration of 2.4 mg/ml has proved to be effective for tubule engineering; hence, we adopted this condition for our protocol.

Although tubular structures seemingly formed at a given cell number per collagen volume, a polarised epithelium and lumen were established only in the presence of HGF, a growth factor previously used to modulate cell growth and motility, and induce kidney morphogenetic processes in various epithelial cell lines (Santos and Nigam, 1993; Nakamura *et al.*, 1997; Maeshima *et al.*, 2000). Unlike previous methods that require long-term cultures - often ranging from 7 to 15 days (Sakurai *et al.*, 1997; Schumacher *et al.*, 2008; Hauser *et al.*, 2016) - our highly efficient method produced epithelial tubules with lumen and predetermined geometries in only 2 days of culture.

Engineered tubules displayed functional characteristic of kidney tubules (Meyer *et al.*, 2004; Sweet *et al.*, 2006; Lawrence *et al.*, 2015), such as internalisation of the synthetic macromolecule dextran and transporter-mediated organic anion tracer transport. These functional properties may be exploited in studies focussing on the mechanisms of active and passive trafficking of endogenous substrates and metabolites across renal tubular epithelial membranes, as well as transporter-mediated absorption, distribution, and elimination of drugs and other xenobiotics. In particular, the organic anion and cation transporters are broadly involved in transporting steroids, hormones and neurotransmitters, as well as excreting antivirals, antibiotics, chemotherapeutics and statins (Roth *et al.*, 2012). These transporters are, therefore, able to influence the pharmacokinetics of their specific drug substrates, thus playing crucial roles in the effectiveness of pharmacological therapies and removal of toxicants. Hence, our engineered tubules may potentially

constitute a powerful tool for experimental nephrology, pharmacokinetic and toxicology studies.

By optimising our protocol, we successfully engineered hiPSCs-derived-UB-like tubules that replicated the kidney tubular epithelial architecture and functions as described above and, when co-cultured with mouse embryonic kidneys, underwent budding morphogenesis. The latter phenomenon indicated that human tubules could respond to kidney developmental cues in the form of soluble factors, a key aspect that made them suitable for elucidating mechanisms of human UB early morphogenesis. Indeed, we used the engineered human tubules to identify a novel combination of growth factors that is capable of inducing human UB-like tubules budding and ramification.

Finally, we applied our system to investigate how budding morphogenesis is affected by a heterozygous mutation in the *PAX2* gene through the generation of UB-like tubules from patient-derived hiPSCs.

To the best of our knowledge, no other existing technology is able to engineer custom-made, complex and functional kidney tubules with different cell sources, such as renal cell lines and *in vitro*-differentiated hiPSCs. It is also remarkable that, in our tissue engineering system, kidney tubules develop into patterned and polarised epithelia enclosing a lumen through cell spatial organisation in response to tubulogenic cues, as occurs *in vivo*. For these reasons, and since the engineered tubules can be transferred to different experimental conditions, we used them to model PKD, test drugs, and study human development.

PKD is characterised by the gradual formation of plenty fluid-filled cysts in the kidney. Unfortunately, there are currently no approved therapies, causing this disease to remain incurable; the existing treatments can only help manage the wide range of problems associated with this condition. PKD is an inherited disorder linked to the disturbance of multiple intracellular pathways and cell functions, and affecting, with varying incidences,

both children and adults (Grantham *et al.*, 2011; Sun *et al.*, 2011; Sweeney and Avner, 2011; Wallace, 2011; Willey *et al.*, 2017). Most of children and adult patients are destined to experience ESRD, thus eventually requiring RRT. In PKD, the development and enlargement of spheroidal epithelial cysts are the consequence of aberrant cell proliferation in the renal tubular epithelia, accompanied by transepithelial fluid secretion into the cystic luminal space. The over-stimulated cell proliferation is due to increased intracellular cAMP levels, a second messenger that is responsible for up-regulating B-Raf/MEK/ERK signalling in both animal models and patients. Hence, decreasing intracellular cAMP levels is considered one of the most appealing approaches for ameliorating PKD outcome.

Given the severity of the disease, the absence of *in vitro* and *in vivo* models able to faithfully mimic human PKD and the lack of effective therapies, it is imperative to develop more realistic PKD modelling systems suitable for drug screening. To begin to address this issue, we decided to use our collecting duct-like tubules engineered with the MDCK cells. These cells are known to form individual fluid-filled cysts when cultured in 3D ECM environments and stimulated with pharmacological agents capable of elevating intracellular cAMP levels. For this reason, their use in modelling PKD and exploring drugs' efficacy on renal cyst regression has been extensive (Mangoo-Karim *et al.*, 1989; Li *et al.*, 2004; Gao *et al.*, 2011). Nonetheless, conventional PKD models present one major drawback, namely the production of individual cysts, which cannot recapitulate the gradual cyst expansion into the tubular lumen as occurs in PKD *in vivo*. This precluded the possibility of modelling lumen obstruction and perturbations in both tissue architecture and epithelial polarisation, as well as the induction of mechanical stress and hypoxic conditions typical of PKD tubules. No other *in vitro* models can recapitulate PKD appropriately enough to constitute a valid alternative to conventional 3D cell cultures. Therefore, we decided to verify whether our engineered collecting duct-like tubules could provide a tool

to more realistically model PKD and perform drug testing and discovery studies. When we transferred the engineered collecting duct-like tubules to a 3D collagen culture system and stimulated them with the diterpene forskolin - a compound that induces cAMP production by activating several adenylyl cyclases - they developed many polarised cysts closely packed along the whole length of the tubules, causing lumen loss and disrupting the overall epithelial organisation. These features resembled *bona fide* those of diseased tubules *in vivo* and indicated that our engineered tubules can be used to model PKD *in vitro*.

When we added Tolvaptan, OCTR, PAS, 2DG or berberine to the culture medium, cyst density within tubules decreased to different extents. This indicated that engineered tubules could be an efficient tool for quantifying the effects of different known pharmacological agents and novel compounds on cyst regression.

The AVP V2 receptor antagonist Tolvaptan has been shown able to inhibit distal tubule and collecting duct cyst progression in both humans (Torres *et al.*, 2012) and PKD rodent model (Gattone *et al.*, 2003; Torres *et al.*, 2004) by decreasing intracellular cAMP levels. According to these observations, concomitant administration of AVP - the V2 receptor's ligand and the major cAMP agonist in the collecting duct (Yasuda and Jeffries, 1998; Wallace *et al.*, 2001) - and Tolvaptan, following forskolin stimulation, significantly decreased cyst density within our tubules, when compared to the sole AVP stimulation. This confirmed that our PKD modelling system was applicable and reliable for drug screening purposes.

The synthetic somatostatin analogues OCTR and PAS, which possess longer half-lives than somatostatin and inhibit cAMP production, have been tested in preclinical and clinical trials. It has been previously reported that OCTR, which binds to somatostatin receptor 2 (SSTR2) and SSTR3, counteracts renal cyst growth in rodent models (Masyuk *et al.*, 2007) and humans (Ruggenenti *et al.*, 2005; Hogan *et al.*, 2010; Caroli *et al.*, 2013), whereas

PAS, which has high affinity to SSTR1, SSTR2, SSTR3 and SSTR5, was more effective than OCTR in mouse and rat PKD models (Masyuk *et al.*, 2013). Conversely, in our system, we observed that OCTR was more effective than PAS in reducing cyst density, but the difference was not statistically significant. This inconsistency may be due to the condition in which the authors evaluated and quantified the effects of the two compounds on cyst growth. Since they adopted *in vivo* models and kept into consideration the whole renal parenchyma, they did not exclusively regard the kidney tubular compartment. We have instead investigated the drugs' effects *in vitro* and solely on the engineered 'polycystic' collecting duct-like tubules.

Although *in vivo* studies demonstrated that treatments with Tolvaptan and somatostatin analogues slow PKD progression by decreasing cell proliferation and inducing cyst regression, severe adverse effects are associated with these pharmacological treatments (Riella *et al.*, 2014). This makes the identification of novel effective therapeutic compounds with better tolerance an imperative need, so that many research groups are currently performing intense research to achieve this goal.

Working in this direction, in the present study we showed that 2DG - a glucose analogue that cannot be metabolised - and berberine - a compound approved for clinical trials in some diseases but that has never been tested in PKD - had a robust effect on cyst regression and completely restored both the central lumen and tubular epithelium integrity.

The marked cyst regression in our 'polycystic' tubules following 2DG treatment is in line with data from recent studies conducted *in vitro* and in *in vivo* models of both aggressive (Rowe *et al.*, 2013) and slowly progressive (Chiaravalli *et al.*, 2016) PKD. Rowe *et al.* demonstrated that PKD cells and mice displayed enhanced glycolysis, whereas glucose deprivation decreased PKD cell proliferation *in vitro*, and 2DG treatment ameliorated kidney volume, cystic index, but also reduced cell proliferation rate *in vivo* (Rowe *et al.*,

2013). When Chiaravalli *et al.* treated PKD mouse models with 2DG, slower disease progression with both kidney/body weight and tubular and collecting duct cyst number reduction was observed in the absence of obvious signs of toxicity (Chiaravalli *et al.*, 2016). These studies indicate that, like cancer cells, PKD cells require high levels of glucose - the principal source of energy of the cells - and reprogram their metabolism to use aerobic glycolysis (known as the Warburg effect) for energy production. This metabolic switch leads to enhanced glucose metabolism and uncontrolled cell proliferation. Considering the slow progression of PKD in humans and the late onset of therapeutic treatments, the proven enhanced effect of 2DG in slowly progressive murine PKD model (Chiaravalli *et al.*, 2016) makes this compound a compelling therapeutic agent, even though it is not currently approved for treating any human condition. Hence, our results, together with existing evidence from *in vivo* studies, confirm 2DG clinical potential in the treatment of PKD and encourage its use and efficacy evaluation in clinical trials.

Previous investigations indicate that berberine exerts anti-proliferative effects in different cancer cell lines (Iizuka *et al.*, 2000) and PKD cells (Bonon *et al.*, 2013).

Iizuka *et al.* reported that berberine causes cancer cell accumulation in G_0/G_1 phase and a relative reduction of the S phase (Iizuka *et al.*, 2000). Bonon *et al.* demonstrated that berberine treatment of human and mouse PKD cystic cell lines reduces cell proliferation by increasing G_0/G_1 phase and inhibiting both phosphorylation of the extracellular signal-regulated kinase (ERK) - which stimulates cell proliferation (Yamaguchi *et al.*, 2003) - and activity of p70-S6 kinase, a downstream effector of mTOR (Bonon *et al.*, 2013).

Moreover, berberine is able to increase intracellular levels of reactive oxygen species by altering mitochondrial membrane potential, leading to mitochondrial collapse and compromising oxidative phosphorylation process. Being able to interact with the adenine nucleotide translocator, berberine causes ATP depletion in cancer cells (Diogo *et al.*,

2011). Moreover, because of its chemical structure that resembles that of intercalating agents, berberine can directly bind to DNA (Krey and Hahn, 1969), eliciting double-strand breaks, eventually leading to cell death for apoptosis (Zhu *et al.*, 2014). Overall, these properties may justify the effects of berberine in our system. By demonstrating the potent effect of this compound on cyst regression, as well as on tubular lumen and epithelial architecture restoration, we highlighted the hitherto unknown therapeutic potential of berberine for the treatment of PKD.

Important issues affect the study of the mechanisms of renal epithelial tubulogenesis and UB branching in human tissues. The first is the scarcity of suitable human embryonic material. The second is the lack of systems that, starting from single cells, allow engineering UB capable of recapitulating morphogenetic events occurring during early organogenesis. These problems are also present when studying human developmental disorders, as there is lack of methods for engineering *in vitro* kidney tissue from patients carrying genetic mutations.

To deal with these problems, we tested our engineering system for its ability to efficiently provide human kidney tubules from hiPSCs. To this end, we differentiated hiPSCs into UB-committed renal progenitor-like cells using a robust protocol based on brief exposure to defined growth factors (Xia *et al.*, 2013), and then directed them to grow within PDMS scaffolds under tubulogenic conditions, as we did with MDCK cells. Like MDCK cells, human cells generated seemingly compact tubular structures, but HGF stimulation alone was not enough to induce the formation of a monolayered epithelium surrounding a continuous lumen. To achieve such architectural arrangement it was necessary to add GDNF to the medium, which indicates that GDNF exerts an essential signalling role in the maturation of hiPSC-derived UB tubular structures. This reflects the utmost importance of the GDNF for UB formation and growth during early kidney development *in vivo*. Hence,

we successfully engineered human UB-like branched tubular structures endowed with a single lumen bounded by a monolayered epithelium. The engineered human tubules were capable of synthetic macromolecule internalisation and OAT-mediated anion tracer transport, both maturation features typical of *in vitro* cultured UBs (Sweet *et al.*, 2006; Meyer *et al.*, 2004; Lawrence *et al.*, 2015). Of note, these findings are unprecedented in stem cell-derived kidney tissues.

When engineered human tubules were co-cultured with mouse embryonic kidneys in a 3D collagen culture system, they responded to kidney developmental cues by forming primary and secondary buds. These findings clearly demonstrate that our UB-like tubules are able to recapitulate early steps of UB morphogenesis and highlight the usefulness of our system for studying mechanisms of human kidney development.

Previous *in vitro* tubulogenesis systems using rodent kidney cell lines or isolated UBs, revealed that distinct growth factors are indispensable for regulating UB growth and branching morphogenesis within a 3D ECM environment (Qiao *et al.*, 1999a, 1999b, 2001; Sakurai *et al.*, 1997; Steer and Nigam, 2004). In our 3D collagen culture system, we identified a novel combination of growth factors that allows the engineered human UB-like tubules to undergo budding morphogenesis to an extent akin to that obtained with mouse embryonic kidney co-culture.

Although a higher degree of tubule maturation needs to be reached and a number of UB functions must be still tested, our data suggest that the engineered human tubules can be employed for studying human development and modelling diseases arising from or affecting the collecting duct system.

In a similar set of experiments, we used the system to disclose and quantify possible morphogenetic defects in tubules engineered with hiPSCs derived from a patient carrying a heterozygous *PAX2* mutation, and previously diagnosed with focal segmental

glomerulosclerosis (FSGS) (Barua *et al.*, 2014). In developing kidney, *PAX2* gene is expressed in branching UB, collecting duct epithelia and early nephrons (Dressler *et al.*, 1990; Dressler and Woolf, 1999). FSGS is a rare CKD that affects glomeruli. This condition arises when podocytes are targeted by cellular stresses to which they respond through cytoskeletal reorganisation, leading to foot-processes effacement. In case of long-lasting harmful stressors, podocytes reach critical injury levels causing their irreversible detachment from the GBM and the underlying glomerular capillaries' sclerosis due to plentiful matrix accumulation (D'Agati *et al.*, 2011). Therefore, pivotal in the FSGS pathogenesis is podocyte damage and loss (D'Agati *et al.*, 2011).

However, our findings suggest that the podocytes' attrition typical of FSGS may occur secondary to kidney developmental anomalies associated with UB morphogenesis. We observed that the patient-derived UB-like tubules' budding ability was significantly lower than that of healthy donor-derived tubules. This suggests that *PAX2* mutations, such as the one we studied here, may be contributing to the defective UB arborisation and, ultimately, to a reduction in nephron number. This is supported by data from heterozygous *Pax2* mutant mice showing diminished UB branching during fetal kidney development, associated with a marked decrease in nephron number at birth (Dziarmaga *et al.*, 2006). As the amount of UB branching events determines the definitive number of nephrons (Nigam and Shah, 2009; Nagalakshmi and Yu, 2015), the patient's kidneys may have had a reduced UB arborisation during early developmental stages, which led to suboptimal nephron endowment. It is also conceivable that the patient's pathological lesions may have arisen as a consequence of haemodynamic stresses, which accelerated podocyte impairment by acting on nephrons reduced in number.

Although additional studies are necessary to validate these hypotheses, our findings provide new insights in understanding the pathogenesis of FSGS and confirm the

usefulness of our system to investigate individual patient's genetic disorders, for which no models currently exist.

By directing hPSC *in vitro* differentiation, other groups created rudimental 3D human kidney organoids in a dish (Taguchi *et al.*, 2014; Morizane *et al.*, 2015; Freedman *et al.*, 2015; Takasato *et al.*, 2015). Yet, the complete lack of UB (Taguchi *et al.*, 2014; Freedman *et al.*, 2015; Morizane *et al.*, 2015) or otherwise its formation as multiple, individual small ducts (Takasato *et al.*, 2015; Xinaris *et al.*, 2016) impeded establishment of the proper kidney tissue patterning and cortical-medullary orientation, which would normally be imposed by a single collecting duct tree. These developmental insufficiencies may probably account for severe anatomical malformations within the organoids, that is the establishment of nephron-nephron connections and multi-branched nephrons (Freedman *et al.*, 2015; Morizane *et al.*, 2015; Takasato *et al.*, 2015). Overall, these anomalies indicate that such approaches cannot accurately replicate kidney organogenesis *in vitro*.

In terms of kidney organoid function, there would also be a serious limitation arising from the above-mentioned developmental insufficiencies. Indeed, as the urine produced by nephrons should be drained away via a single collecting duct tree, the absence of UB or the lack of connections among the multitude of collecting ducts would impede the accomplishment of this vital function.

Our innovative technology may prove extremely useful to overcome all these problems, as it allows engineering hiPSC-derived UB-like tubular units with developmental capacities, which could be physically combined and reciprocally interact with hiPSC-derived MM cell aggregates, giving rise to functional human kidney organoids arranged organotypically around a single collecting duct tree. Constructing functional organoids from hiPSCs, which can be directly derived from patients' own somatic cells, will facilitate the establishment of systems for *in vitro* disease modelling, personalised therapies, toxicology and

developmental studies, and may offer solid foundation for regenerative medicine applications.

To summarise, we have developed a 3D culture system that produces functional epithelial tubules of predetermined geometries starting from dispersed epithelial cells. Tubules engineered using the renal epithelial cell line are able to accurately replicate the PKD phenotype and respond to pharmacological treatments in a quantifiable manner. It demonstrates that these tissues can provide a pioneering tool for studying renal pathophysiology *in vitro* and conducting pharmacological studies. Importantly, our system can efficiently produce human UB-like tubules able to exert kidney-specific functions, endowed with developmental capacities, and suitable to investigate mechanisms of normal kidney development as well as possible aetiological roles of genetic alterations in UB morphogenesis and disease.

Although culture conditions for other cell types have yet to be defined, our technology is applicable and can be ideally adapted, with only minor modifications, to engineer different kinds of tissue, such as branched endothelial and lung epithelia. These may in turn be used to study human vascular and pulmonary developmental and pathophysiological mechanisms, respectively.

Overall, this controlled experimental system provides an accurate, rapid, cost-effective and reproducible methodology with which to model kidney disease, screen drugs and study development. It may represent an attractive and promising platform from which the spatially and geometrically controlled engineering of human kidney tissue with realistic anatomies and functions can be optimised and applied for regenerative medicine purposes.

CHAPTER 5 – FIGURES AND LEGENDS

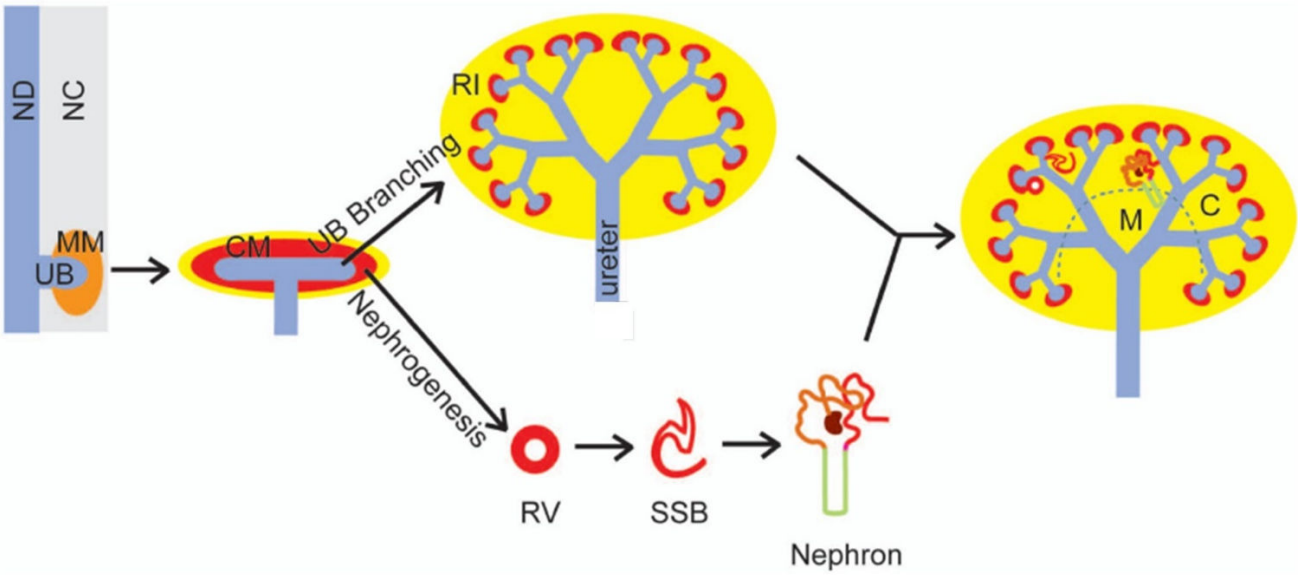
ND
NC
MM
UB
CM
UB Branching
Nephrogenesis
RI
ureter
M
C
RV
SSB
Nephron

Figure 1

Figure 1. Schematic diagram of kidney development and nephron formation. Metanephric kidney development begins when ureteric bud (UB) emerges as a swelling of the caudal nephric duct (ND) and invades the metanephric mesenchyme (MM) of the posterior nephric cord (NC). Reciprocal autocrine and paracrine interactions between UB and MM induce the UB to first undergo bifurcated branching to form a T-shaped bud consisting of two tips and a stalk. Hereafter, each UB tip undergoes multiple rounds of bifurcation (branching morphogenesis) giving rise to the tree-like collecting duct system, whereas the elongated UB stalk forms the ureter. In turn, the branching UB epithelium induces nephrogenesis by promoting condensation of a subset of nephron progenitor cells within the MM around each UB tip. Condensed cells form the cap mesenchyme (CM), which epithelialise to form the renal vesicle (RV), the first epithelial structure of the nephron. The RV further grows and progressively forms comma- and S-shaped bodies (SSB), which eventually develop into mature nephrons. The distal end of the SSB fuses with a UB tip to form a continous lumen, giving rise to the distal tubule of the nephron. The MM contains another cell population, the renal interstitial (RI) cells - also known as renal stromal cells. These cells support nephrogenesis and UB branching, and are the precursors of renal interstitial fibroblasts, vascular smooth muscle cells, pericytes and mesangial cells. Kidneys are subdivided into two main regions: the cortex (C) and the medulla (M), each containing different segments of nephron and UB/collecting duct tubular epithelia. Adapted from (Nagalakshmi and Yu, 2015). Copyright 2015 by the John Wiley & Sons, Inc. Reused with permission.

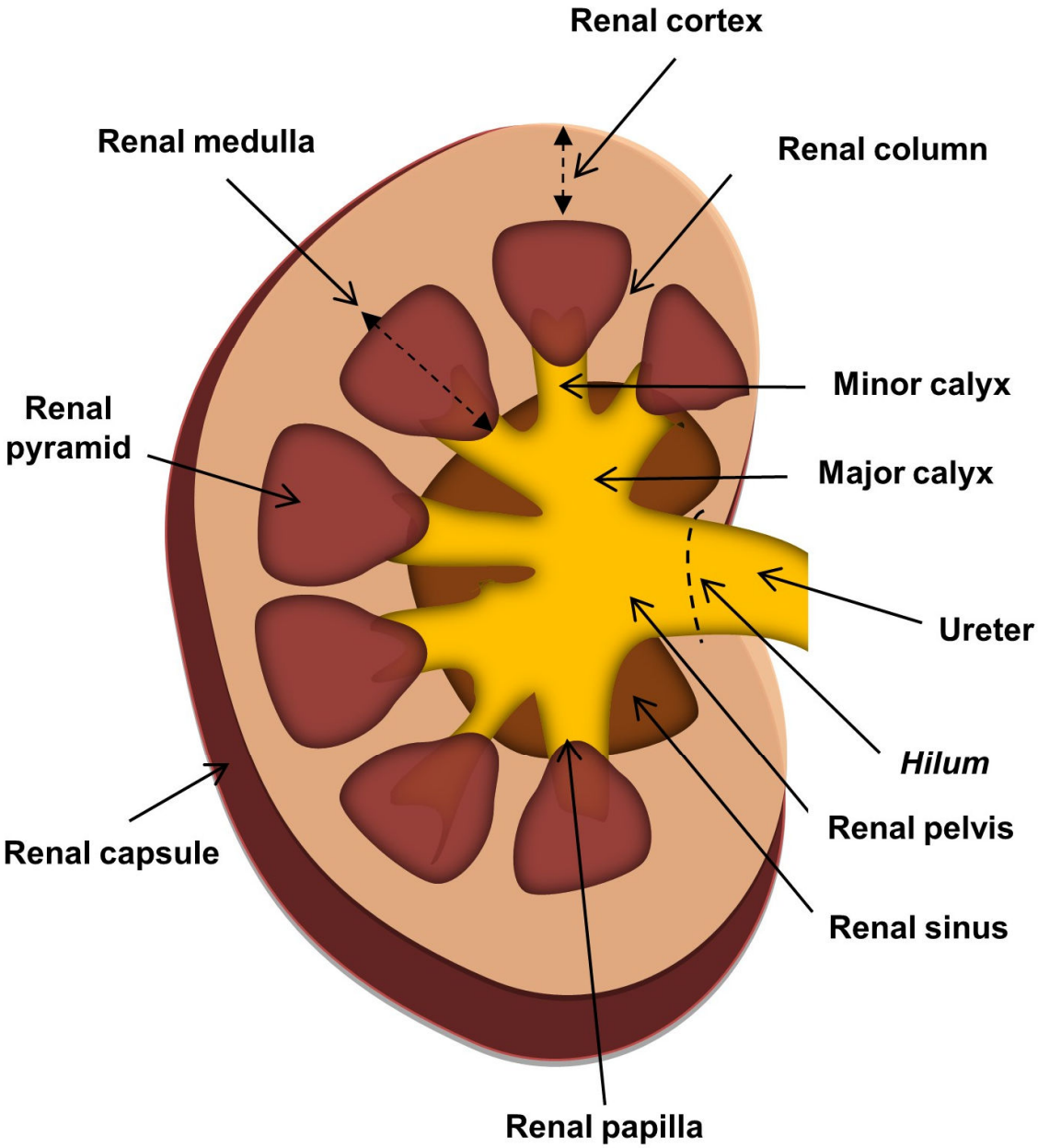
Renal cortex
Renal medulla
Renal column
Minor calyx
Renal pyramid
Major calyx
Ureter
Hilum
Renal pelvis
Renal capsule
Renal sinus
Renal papilla

Figure 2

Figure 2. Kidney anatomy. Schematic cross section of the kidney showing the overall internal structure and the main anatomical components of the organ. Adapted from (Rodrigues-Díez *et al.*, 2017).

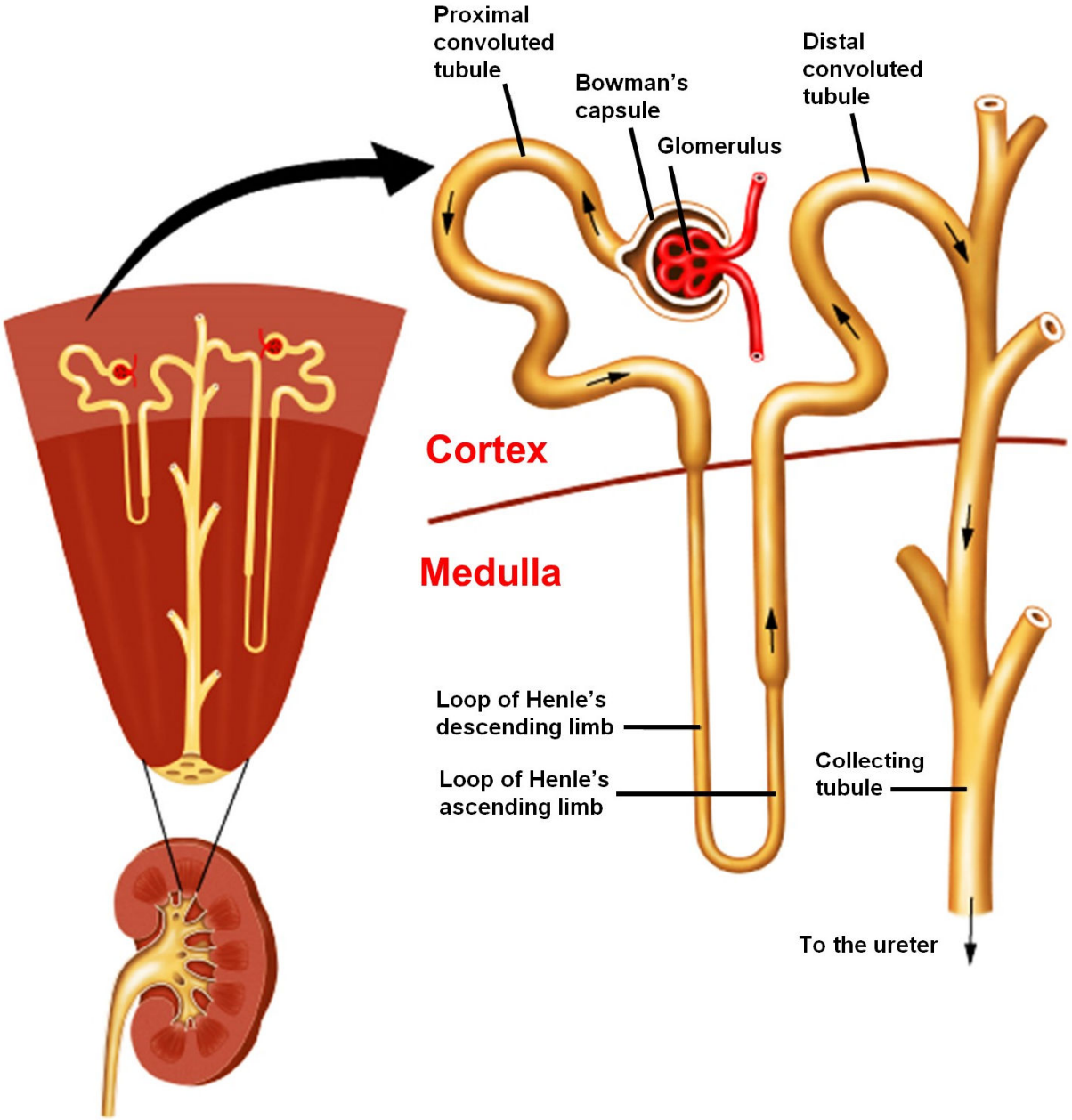
Proximal convoluted tubule
Bowman's capsule
Glomerulus
Distal convoluted tubule
Cortex
Medulla
Loop of Henle's descending limb
Loop of Henle's ascending limb
Collecting tubule
To the ureter

Figure 3

Figure 3. Nephron anatomy and collecting duct cortical-medullary orientation. Schematic illustration of a nephron and spatial distribution of mature glomerulus and renal epithelial tubular structures (proximal convoluted tubule, loop of Henle, distal convoluted tubule and collecting tubule) along the kidney cortical-medullary axis. Note the clear distinction between cortical and medullary regions. Arrows indicate the ultrafiltrate (urine) flow direction. Adapted from *Beltina.org - Encyclopedia of Health (2011)*. Source: http://www.beltina.org/health-dictionary/nephron-function-kidney-definition.html. Image in the public domain.

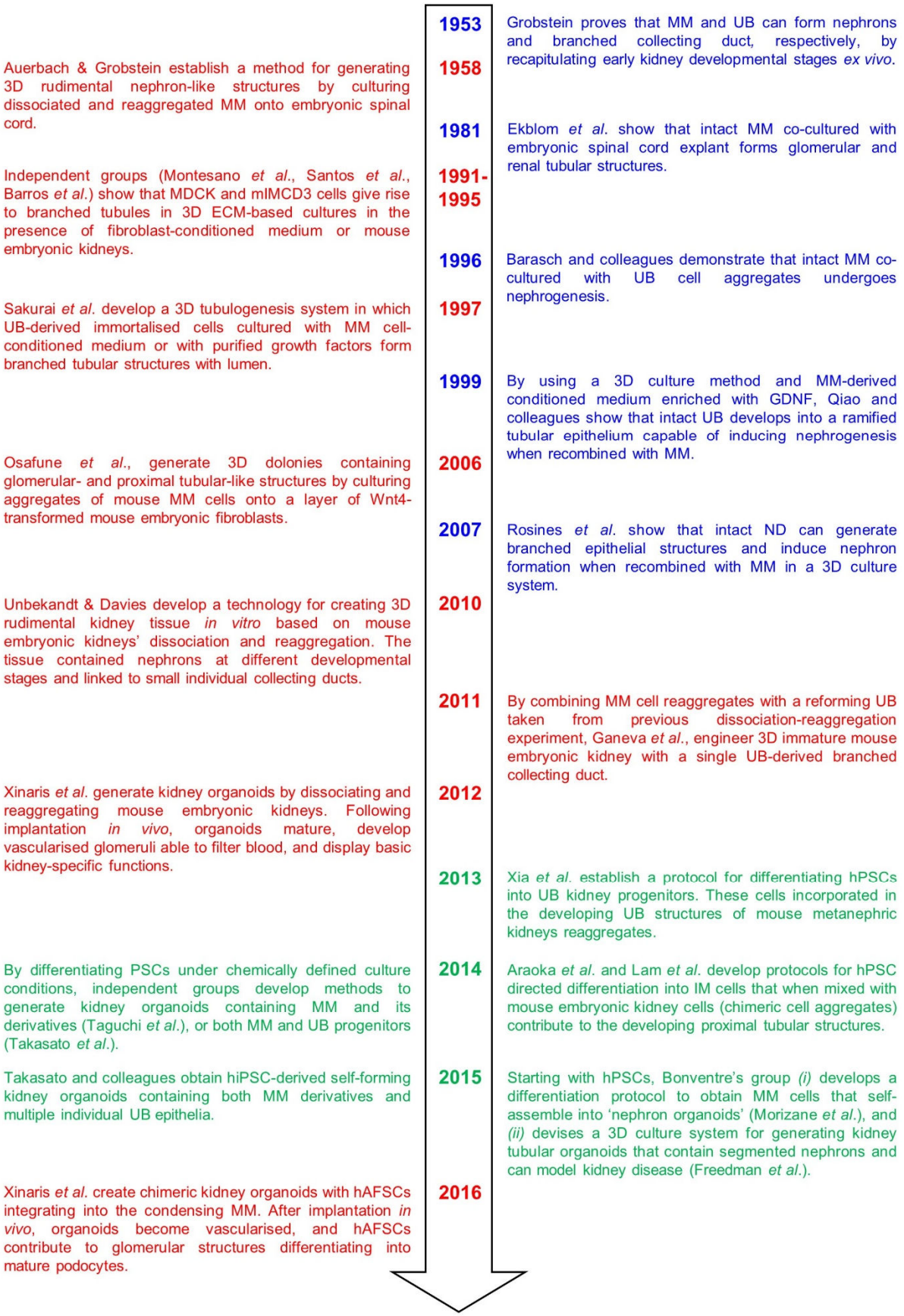
1953
Grobstein proves that MM and UB can form nephrons and branched collecting duct, respectively, by recapitulating early kidney developmental stages ex vivo.
1958
Auerbach & Grobstein establish a method for generating 3D rudimental nephron-like structures by culturing dissociated and reaggregated MM onto embryonic spinal cord.
1981
Ekblom et al. show that intact MM co-cultured with embryonic spinal cord explant forms glomerular and renal tubular structures.
1991-1995
Independent groups (Montesano et al., Santos et al., Barros et al.) show that MDCK and mIMCD3 cells give rise to branched tubules in 3D ECM-based cultures in the presence of fibroblast-conditioned medium or mouse embryonic kidneys.
1996
Barasch and colleagues demonstrate that intact MM co-cultured with UB cell aggregates undergoes nephrogenesis.
1997
Sakurai et al. develop a 3D tubulogenesis system in which UB-derived immortalised cells cultured with MM cell-conditioned medium or with purified growth factors form branched tubular structures with lumen.
1999
By using a 3D culture method and MM-derived conditioned medium enriched with GDNF, Qiao and colleagues show that intact UB develops into a ramified tubular epithelium capable of inducing nephrogenesis when recombined with MM.
2006
Osafune et al., generate 3D dolonies containing glomerular- and proximal tubular-like structures by culturing aggregates of mouse MM cells onto a layer of Wnt4-transformed mouse embryonic fibroblasts.
2007
Rosines et al. show that intact ND can generate branched epithelial structures and induce nephron formation when recombined with MM in a 3D culture system.
2010
Unbekandt & Davies develop a technology for creating 3D rudimental kidney tissue in vitro based on mouse embryonic kidneys' dissociation and reaggregation. The tissue contained nephrons at different developmental stages and linked to small individual collecting ducts.
2011
By combining MM cell reaggregates with a reforming UB taken from previous dissociation-reaggregation experiment, Ganeva et al., engineer 3D immature mouse embryonic kidney with a single UB-derived branched collecting duct.
2012
Xinaris et al. generate kidney organoids by dissociating and reaggregating mouse embryonic kidneys. Following implantation in vivo, organoids mature, develop vascularised glomeruli able to filter blood, and display basic kidney-specific functions.
2013
Xia et al. establish a protocol for differentiating hPSCs into UB kidney progenitors. These cells incorporated in the developing UB structures of mouse metanephric kidneys reaggregates.
2014
By differentiating PSCs under chemically defined culture conditions, independent groups develop methods to generate kidney organoids containing MM and its derivatives (Taguchi et al.), or both MM and UB progenitors (Takasato et al.).
Araoka et al. and Lam et al. develop protocols for hPSC directed differentiation into IM cells that when mixed with mouse embryonic kidney cells (chimeric cell aggregates) contribute to the developing proximal tubular structures.
2015
Takasato and colleagues obtain hiPSC-derived self-forming kidney organoids containing both MM derivatives and multiple individual UB epithelia.
Starting with hPSCs, Bonventre's group (i) develops a differentiation protocol to obtain MM cells that self-assemble into 'nephron organoids' (Morizane et al.), and (ii) devises a 3D culture system for generating kidney tubular organoids that contain segmented nephrons and can model kidney disease (Freedman et al.).
2016
Xinaris et al. create chimeric kidney organoids with hAFSCs integrating into the condensing MM. After implantation in vivo, organoids become vascularised, and hAFSCs contribute to glomerular structures differentiating into mature podocytes.

Figure 4

Figure 4. Historical summary of 3D kidney tissue engineering approaches. The main themes and technologies concerning kidney organ generation are listed in chronological order. Tissue-based approaches (blue); embryonic kidney cell- and cell line-based approaches (red); hPSC-based approaches (green).

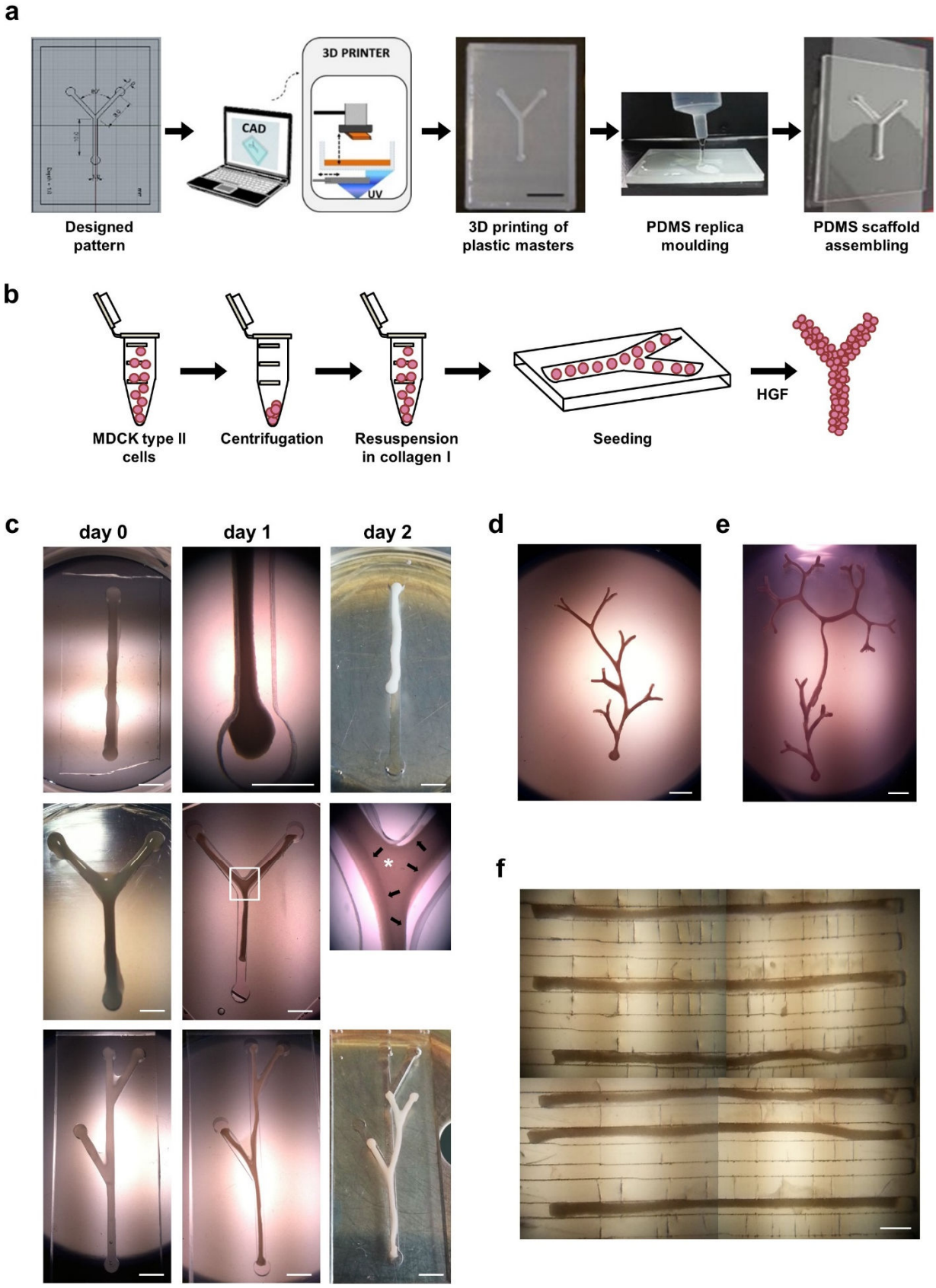
a
3D PRINTER
CAD
UV
Designed pattern
3D printing of plastic masters
PDMS replica moulding
PDMS scaffold assembling
b
MDCK type II cells
Centrifugation
Resuspension in collagen I
Seeding
HGF
c
day 0
day 1
day 2
d
e
f

Figure 5

Figure 5. Engineering tubular structures starting from MDCK cell suspensions. (a) Schematic workflow for PDMS scaffold fabrication. Based on the custom-designed patterns, plastic masters are 3D-printed using rapid prototyping technologies and then utilised to produce the scaffolds through PDMS replica moulding and polymerisation. **(b)** Experimental design: MDCK cells are centrifuged, resuspended in collagen I, seeded into the PDMS scaffold cavity and cultured in the presence of HGF for up to 2 days. **(c)** Immediately after seeding (day 0), the mixture of collagen and cells completely fills the scaffold cavity. At day 1, cells organise to form tubular aggregates corresponding to the shape of the cavity and showing marked shrinkage. At day 2, branches of the shrunk tubular structures emerge from the cavities, and a translucent area (middle panel, asterisk) delimited by darker edges (middle panel, arrows) is visible through bright-field microscopy. **(d)** Ramified and **(e)** tree-like tubular structures after 2 days of culture. **(f)** A multichannel scaffold containing epithelial microtubules after 2 days of culture. Scale bars: 2 mm **(b-d)**, 500 μm **(e)**.

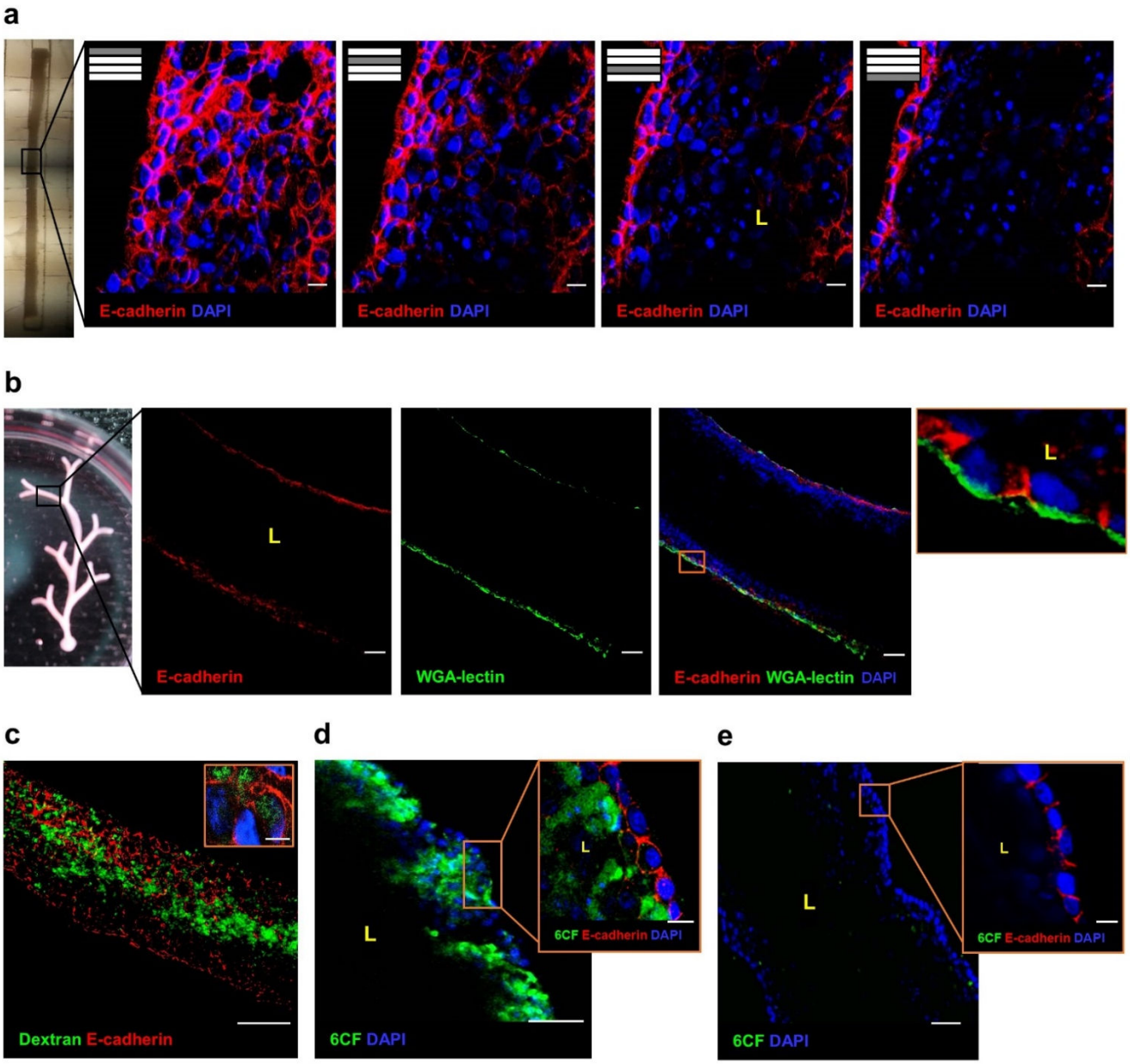
a
E-cadherin DAPI
E-cadherin DAPI
L
E-cadherin DAPI
E-cadherin DAPI
b
L
E-cadherin
WGA-lectin
E-cadherin WGA-lectin DAPI
L
c
Dextran E-cadherin
d
L
6CF DAPI
L
6CF E-cadherin DAPI
e
L
6CF DAPI
L
6CF E-cadherin DAPI

Figure 6

Figure 6. Engineered tubules display lumen formation, epithelial absorption of molecules and transport of ions at 2 days. (a) Confocal Z-stack imaging from the surface to the inner region of a microtubule demonstrates the formation of a continous lumen (L) in the central region. E-cadherin (red) is expressed by peripheral cells of the microtubule. **(b)** A branch from a macrotubular system showing an extended lumen (L) enclosed by a monolayered epithelium of cells with aligned nuclei and expressing E-cadherin (red) and WGA-lectin (green) in the lateral and basal membranes, respectively (inset). **(c-e)** Microtubules displaying **(c)** dextran (green) internalisation and **(d)** 6CF (green) anion transport in the absence or **(e)** presence of the organic anion transporter inhibitor probenecid. WGA-lectin, wheat-germ agglutinin-lectin; 6CF, 6-carboxyfluorescein; DAPI, blue-stained nuclei. Scale bars: 10 μm **(a, c-e insets)**, 100 μm **(b, c)**, 50 μm **(d, e)**.

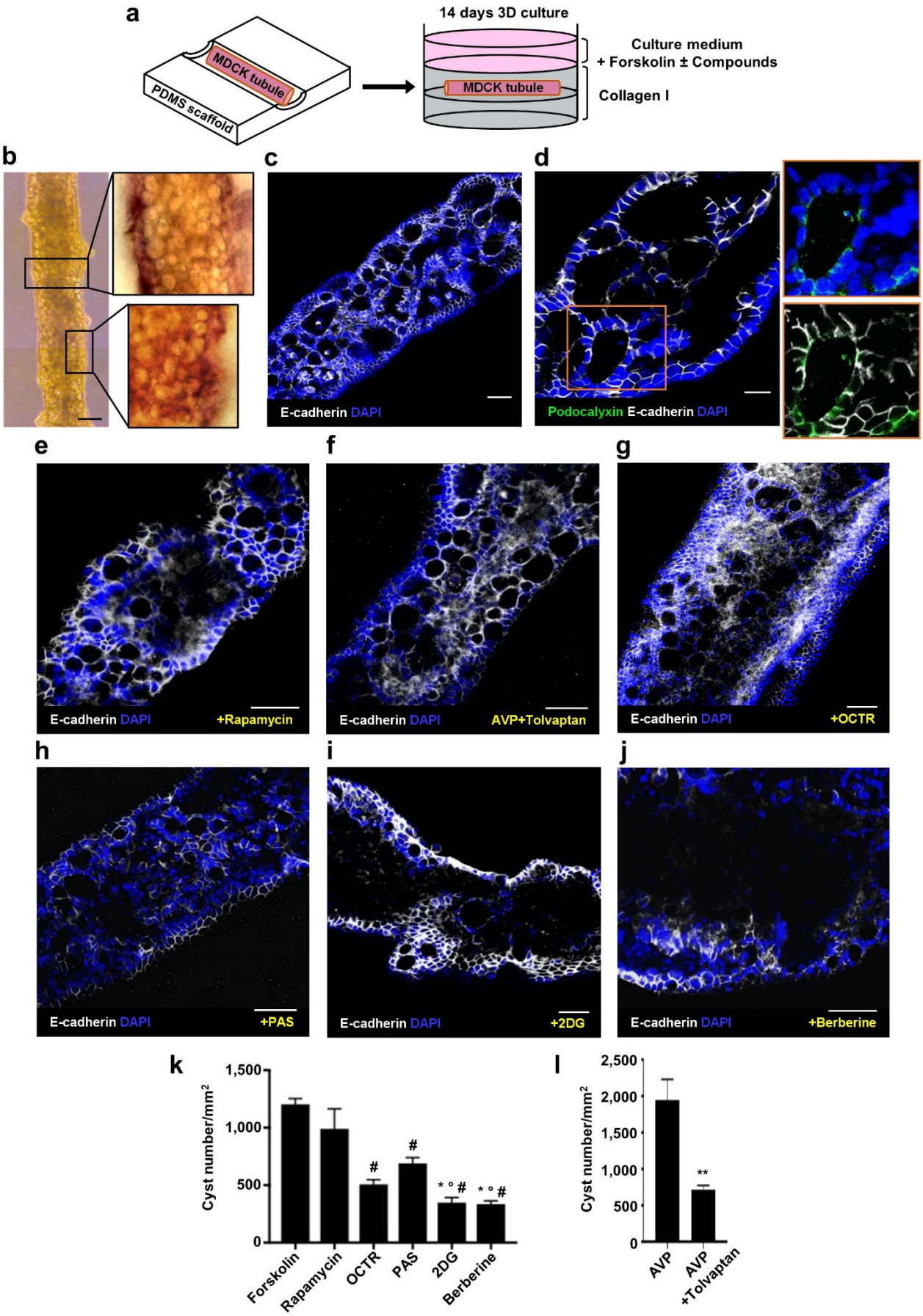
a
14 days 3D culture
MDCK tubule
PDMS scaffold
MDCK tubule
Culture medium
+ Forskolin ± Compounds
Collagen I
b
c
E-cadherin DAPI
d
Podocalyxin E-cadherin DAPI
e
E-cadherin DAPI
+Rapamycin
f
E-cadherin DAPI
AVP+Tolvaptan
g
E-cadherin DAPI
+OCTR
h
E-cadherin DAPI
+PAS
i
E-cadherin DAPI
+2DG
j
E-cadherin DAPI
+Berberine
k
Cyst number/mm²
1,500
1,000
500
0
Forskolin
Rapamycin
OCTR
PAS
2DG
Berberine
l
Cyst number/mm²
2,500
2,000
1,500
1,000
500
0
AVP
AVP +Tolvaptan

Figure 7

Figure 7. MDCK-derived tubules model PKD and respond to the treatment with different compounds. (a) Schematic representation of 3D collagen culture system. After 2 days of culture, engineered microtubules are harvested from the scaffold, embedded in collagen I, stimulated with forskolin for 7 days to induce cyst formation and then treated with different compounds to evaluate cyst regression. **(b)** Bright-field image of a forskolin-stimulated microtubule showing many large spheroidal cysts stained with hematoxylin and eosin (insets). **(c, d)** Cysts are delimited by a monolayered epithelium of cells positive for E-cadherin (white) in the basolateral membranes and **(d)** podocalyxin (green) in the apical membranes (insets). The tubular lumen is lost. **(e-j)** Forskolin-stimulated tubules after a 7-day treatment with **(e)** rapamycin, **(f)** Tolvaptan in combination with AVP, **(g)** OCTR, **(h)** PAS, **(i)** 2DG or **(j)** berberine. **(i, j)** 2DG and berberine treatments restore tubular lumen. **(k, l)** Quantification of cyst number/mm^2: No treatment (forskolin; 1205 ± 48.81); rapamycin (990 ± 174.5); OCTR (508.5 ± 39.52); PAS (688.9 ± 52.1); 2DG (348.1 ± 44.15); berberine (335.8 ± 27.93); AVP (1948 ± 283.4); AVP+Tolvaptan (716.4 ± 57). Data are expressed as means ± s.e.m. from three independent experiments. **(k)** Number of fields analysed: n=18 for forskolin, n=6 for rapamycin, n=6 for OCTR, n=7 for PAS, n=8 for 2DG, n=11 for berberine. *P<0.05 versus PAS, °P<0.0001 versus rapamycin, #P<0.0001 versus forskolin by one-way ANOVA with Tukey's multiple comparisons test. **(l)** Number of fields analysed: n=4 for AVP, n=9 for Tolvaptan in combination with AVP. **P<0.0001 by two-tailed Student's t-test. DAPI, blue-stained nuclei; AVP, arginine vasopressin; OCTR, octreotide; PAS, pasireotide; 2DG, 2-deoxy-D-glucose. Scale bars: 100 μm **(b)**, 50 μm **(c, e-j)**, 20 μm **(d)**.

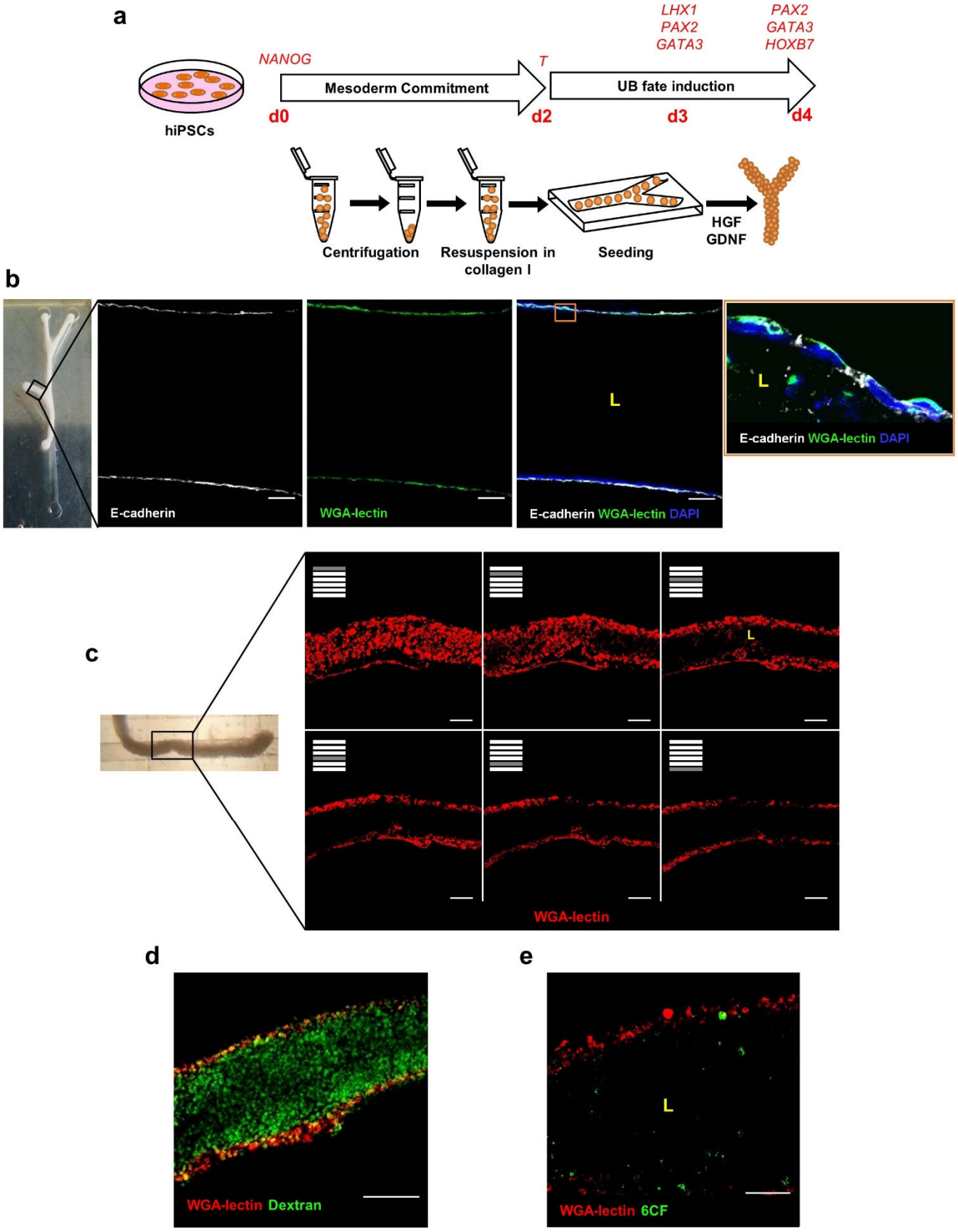
a
LHX1
PAX2
GATA3
PAX2
GATA3
HOXB7
NANOG
T
Mesoderm Commitment
UB fate induction
hiPSCs
d0
d2
d3
d4
Centrifugation
Resuspension in collagen I
Seeding
HGF
GDNF
b
E-cadherin
WGA-lectin
E-cadherin WGA-lectin DAPI
L
E-cadherin WGA-lectin DAPI
c
L
WGA-lectin
d
WGA-lectin Dextran
e
L
WGA-lectin 6CF

Figure 8

Figure 8. Engineering functional human UB-like tubules using iPSCs. (a) Experimental design. Human iPSCs are differentiated toward UB-like progenitor cells. Cells from differentiation days 3 and 4 are pelleted and then re-suspended in collagen I, seeded into the PDMS scaffold cavity, and cultured in the presence of HGF and GDNF for 2 days. **(b)** A branch from a macrotubule engineered with cells from differentiation day 3 displaying a continous lumen (L) enclosed by a monolayer of E-cadherin (white) and WGA-lectin (green) positive cells. Inset: cells of the tubular wall show aligned nuclei (blue), and E-cadherin (white) and WGA-lectin (green) in the basolateral membranes. **(c)** Z-stack images of a microtubule engineered with cells from differentiation day 4 show the presence of a single central lumen (L) lined by a WGA-lectin-positive (red) epithelium. **(d, e)** Microtubules showing **(d)** dextran (green) internalisation and **(e)** 6CF (green) transport. UB, ureteric bud; d, day; WGA-lectin, wheat germ agglutinin-lectin; DAPI, blue-stained nuclei; 6CF, 6-carboxyfluorescein. Scale bars: 100 μm **(b-d)**, 50 μm **(e)**.

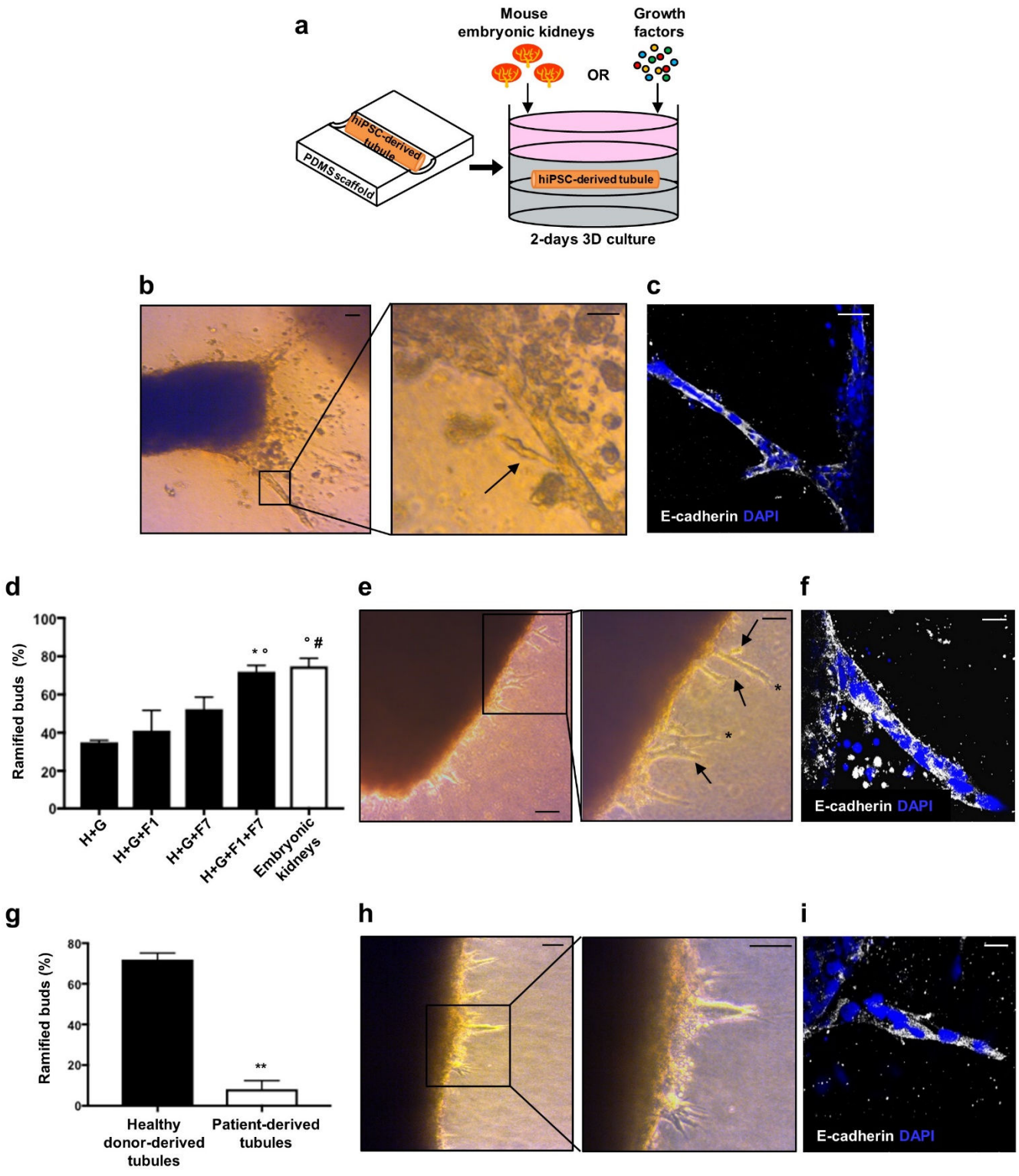
a
Mouse embryonic kidneys
Growth factors
OR
hiPSC-derived tubule
PDMS scaffold
hiPSC-derived tubule
2-days 3D culture
b
c
E-cadherin DAPI
d
Ramified buds (%)
100
80
60
40
20
0
* °
° #
H+G
H+G+F1
H+G+F7
H+G+F1+F7
Embryonic kidneys
e
f
E-cadherin DAPI
g
Ramified buds (%)
80
60
40
20
0
**
Healthy donor-derived tubules
Patient-derived tubules
h
i
E-cadherin DAPI

Figure 9

Figure 9. Engineered tubules as a tool for studying human UB developmental processes and defects. (a) Experimental design. Fragments of hiPSC-derived macrotubules are transferred from the PDMS scaffold to the 3D collagen culture system and cultured with mouse embryonic kidneys or in the presence of different combinations of growth factors for up to 2 days. **(b, c)** Healthy donor-derived tubule co-cultured with mouse embryonic kidneys. **(b)** At day 1, long primary buds emerge (left panel). At day 2, a lateral ramification (arrow) arises from the primary bud. **(c)** A ramified bud consists of aligned E-cadherin-positive cells with linearly oriented nuclei. **(d)** Percentage of the ramified buds in the total buds emerged from healthy donor-derived tubules. Data are expressed as means ± s.e.m. from three independent experiments. Number of fields analysed: n=48 for H+G, n=30 for H+G+F1 and H+G+F7, n=22 for H+G+F1+F7, n=21 for mouse embryonic kidneys. *P<0.05 versus H+G, °P<0.05 versus H+G+F1, #P<0.01 versus H+G by one-way ANOVA with Holm-Sidak's multiple comparisons test. **(e, f)** A healthy donor-derived tubule cultured with the complete combination of growth factors displays primary and secondary buds (arrows) some of which showing terminal bifid branching (asterisks). **(f)** A primary bud arising from healthy donor-derived tubule cultured as that in **(e)**. **(g)** Percentage of the ramified buds in the total buds emerged in healthy donor- and patient-derived tubules cultured with all growth factors. Data are expressed as means ± s.e.m. from three independent experiments. Number of fields analysed: n=22 for healthy donor- and n=27 for patient-derived tubules. **P<0.0005 by two-tailed Student's t-test. **(h, i)** Patient-derived tubule cultured with all growth factors develops mainly primary buds. **(i)** A primary bud arising from patient-derived tubule cultured as that in **(h)**. DAPI, blue-stained nuclei; H, HGF; G, GDNF; F1, FGF1; F7, FGF7. Scale bars: 100 μm **(b, left panel; e, left panel)**, 50 μm **(e, right panel; h)**, 20 μm **(b, right panel; c, f, i)**.

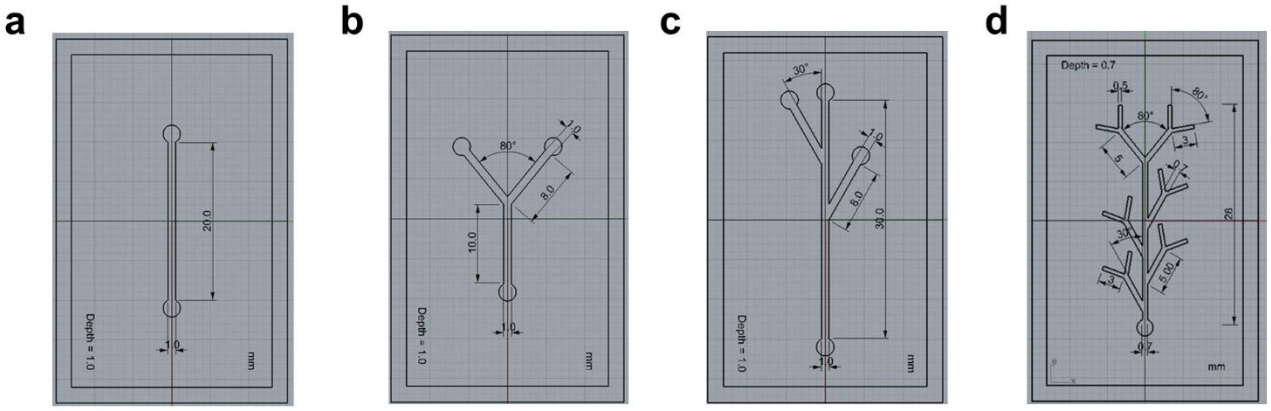

e

$$\begin{cases} \alpha_0 = 160° \\ \alpha_1 = 130° \\ \alpha_n = \dfrac{\alpha_{n-2}}{\varphi} \end{cases} \quad n = 2,3,\ldots \qquad \begin{cases} L_0 = \dfrac{1}{\varphi} L \\ L_n = \dfrac{1}{\varphi} L_{n-1} \quad n = 1,3,5,\ldots \\ L_n = L_{n-1} \quad n = 2,4,6,\ldots \end{cases}$$

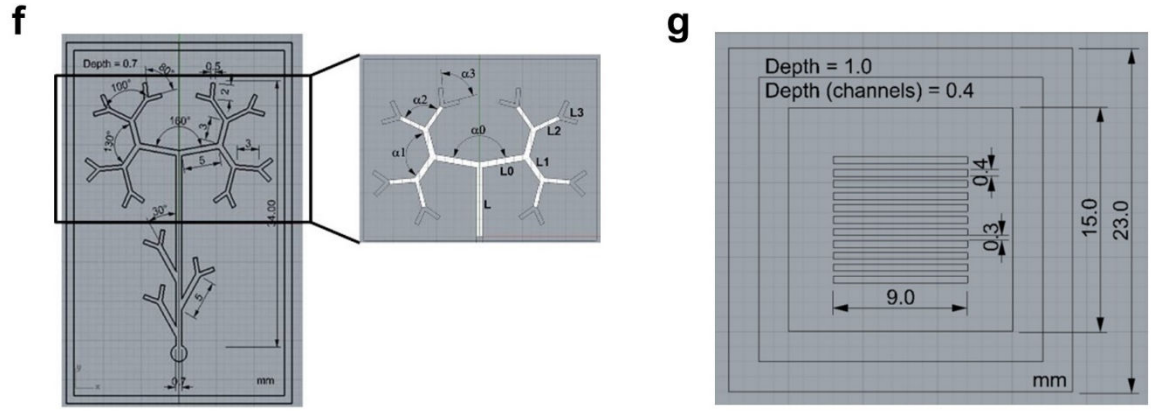

Supplementary Figure 1

Supplementary Figure 1. PDMS scaffold design and fabrication. (a-d) Patterns designed for PDMS scaffold fabrication. Related lengths, depths, widths and angles are indicated for each pattern. Designed geometries: **(a)** linear, **(b)** bifurcated with an 80° terminal bifid branch, **(c)** asymmetrical with two 30° lateral branches arising from the central channel, and **(d)** ramified. **(e)** The 'golden fractal tree' formula. α_0 and α_1 represent the amplitude of first and second branching generation, respectively; L refers to central trunk length; n is the order of branching generation, and φ=1.618 is the 'golden ratio'. **(f)** The tree-like pattern consisting of fractal-like planar ramifications with different lengths and branching angles calculated by setting α_0=160° and α_1=130° and n=3. **(g)** Linear multichannel pattern for engineering multiple independent tubules at the same time.

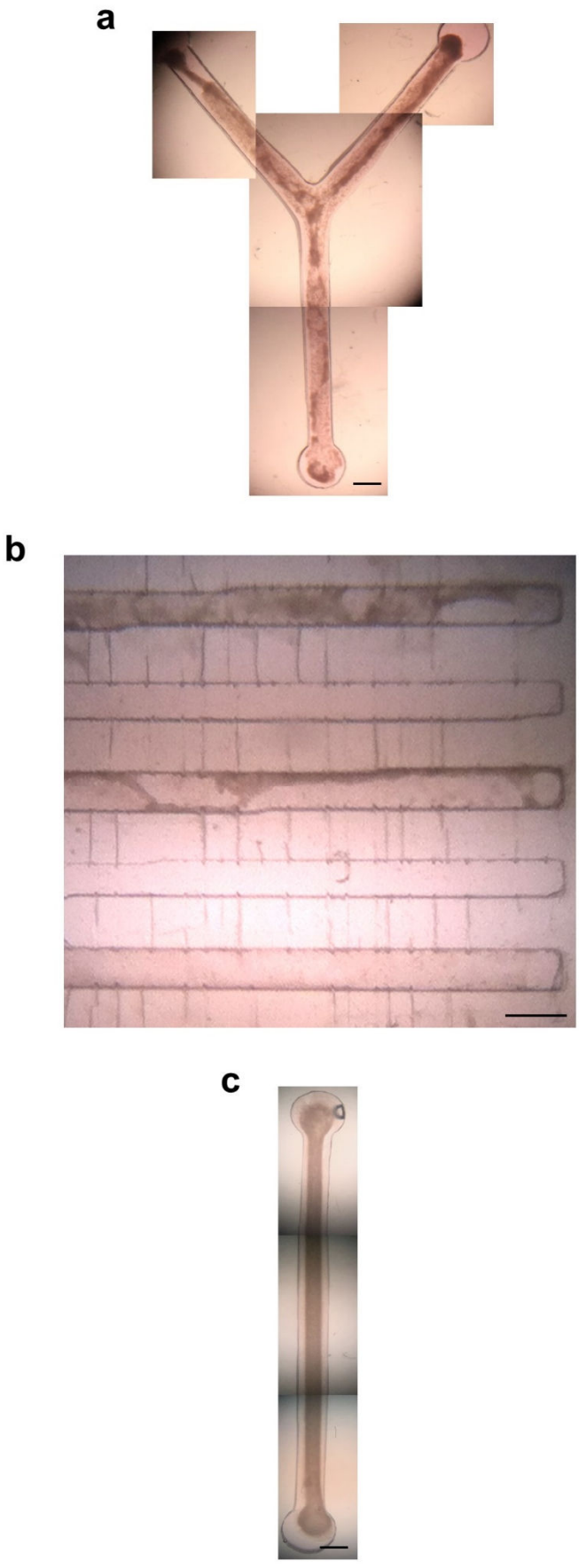

Supplementary Figure 2

Supplementary Figure 2. Effect of cell densities on tubule formation. (a, b) Cell concentrations lower than those established as optimal completely prevent tubular structure formation both **(a)** in macro- and **(b)** in micro-scaffolds. **(c)** Three hours after seeding at the optimal cell concentration, MDCK cells organise to form a tube-shaped aggregate. Scale bars: 1 mm **(a, c)**, 500 μm **(b)**.

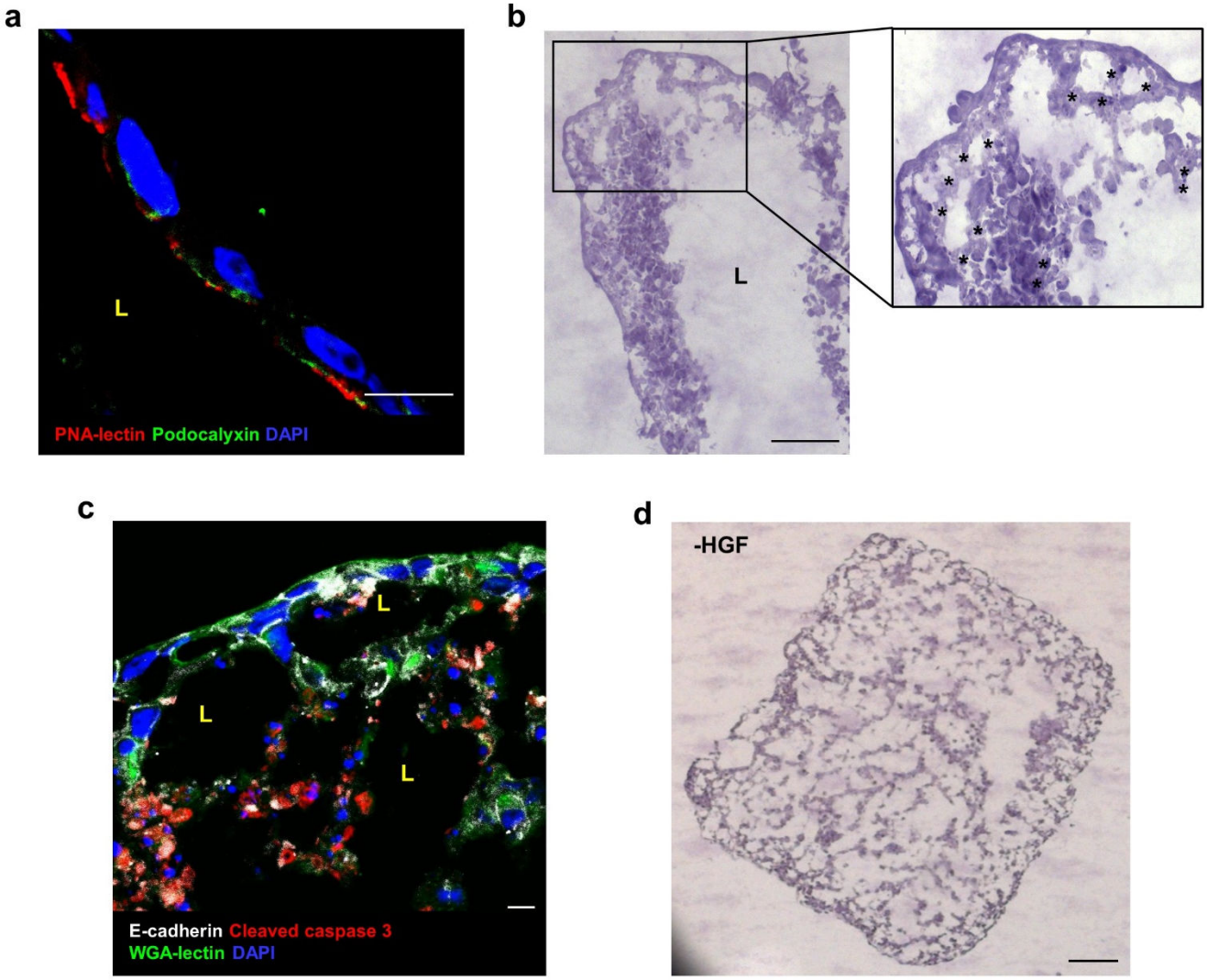

Supplementary Figure 3

Supplementary Figure 3. MDCK cell-derived tubules display polarised epithelium establishment and apoptosis during lumen formation. (a) At day 2, the monolayered epithelium forming the tubular wall is double positive for PNA-lectin (red) and podocalyxin (green) in the apical domains. **(b)** At day 1, macrotubules develop a major luminal space (L) bounded by aggregates of cells with condensed chromatin (inset, asterisks). **(c)** Cells forming the aggregates in the central areas of tubule display nuclear fragmentation and are positive for the apoptotic marker cleaved caspase 3 (red). **(d)** At day 2, tubular structures formed in the absence of HGF do not develop a single central lumen. PNA-lectin, peanut agglutinin-lectin; WGA-lectin, wheat germ agglutinin-lectin; DAPI, blue-stained nuclei. Scale bars: 10 μm **(a, c)**, 100 μm **(b, d)**.

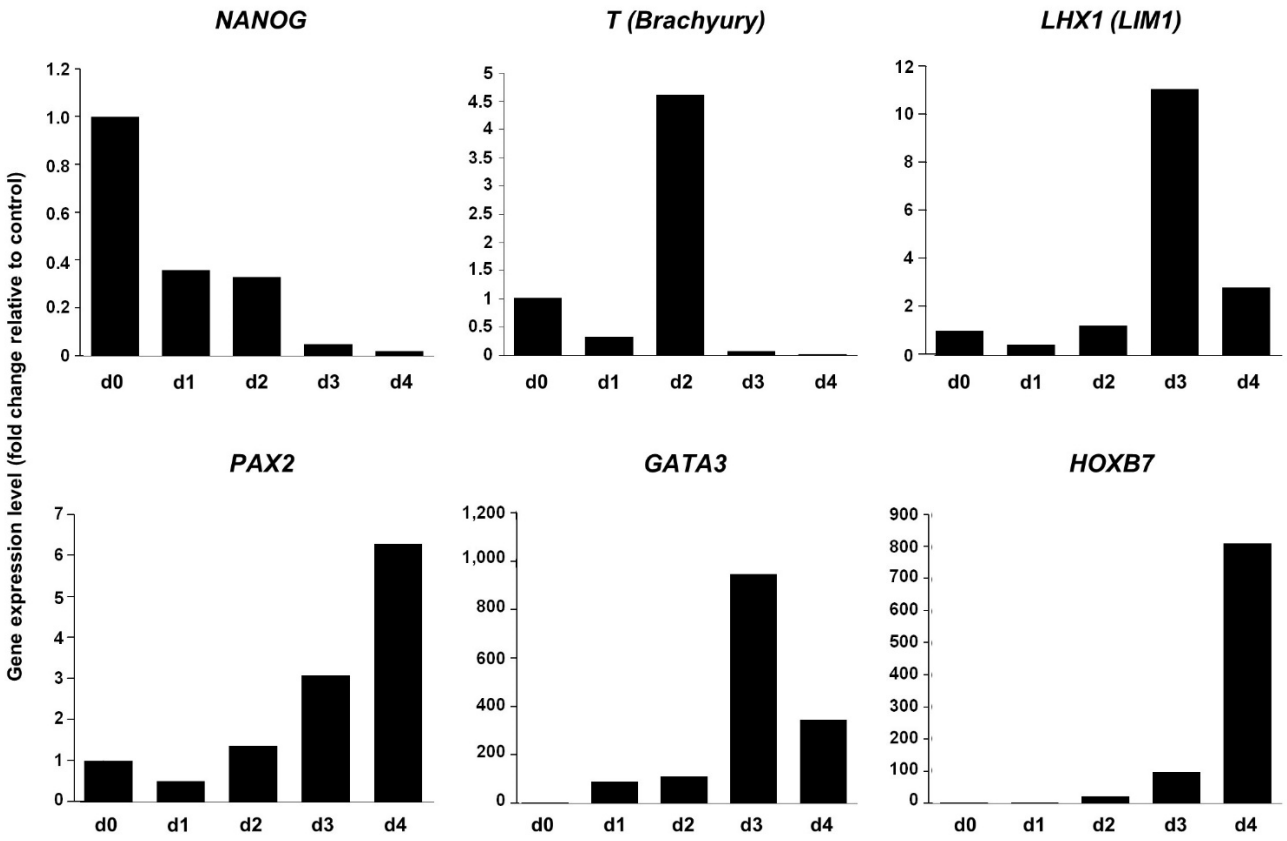

Supplementary Figure 4

Supplementary Figure 4. Gene expression profile of human iPSCs during differentiation into UB-like progenitor cells. *NANOG* (pluripotency marker) expression decreases progressively. *T* (*Brachyury*) (mesendoderm marker) expression peaks at d2, while *LHX1 (LIM1)* (intermediate mesoderm marker) and *GATA3* (ureteric epithelium marker) peak at d3. *PAX2* (nephric lineage marker) and *HOXB7* (UB-related transcription factor) expression levels increase progressively up to d4. Values are relative to the housekeeping gene glyceraldehyde-3-phosphate dehydrogenase (*GAPDH*). Data shown are from one representative experiment of three independent experiments. d, day; *NANOG*, Nanog homeobox; *T*, brachyury transcription factor; *LHX1*, LIM homeobox 1; *GATA3*, GATA binding protein 3; *PAX2*, paired box 2; *HOXB7*, homeobox B7.

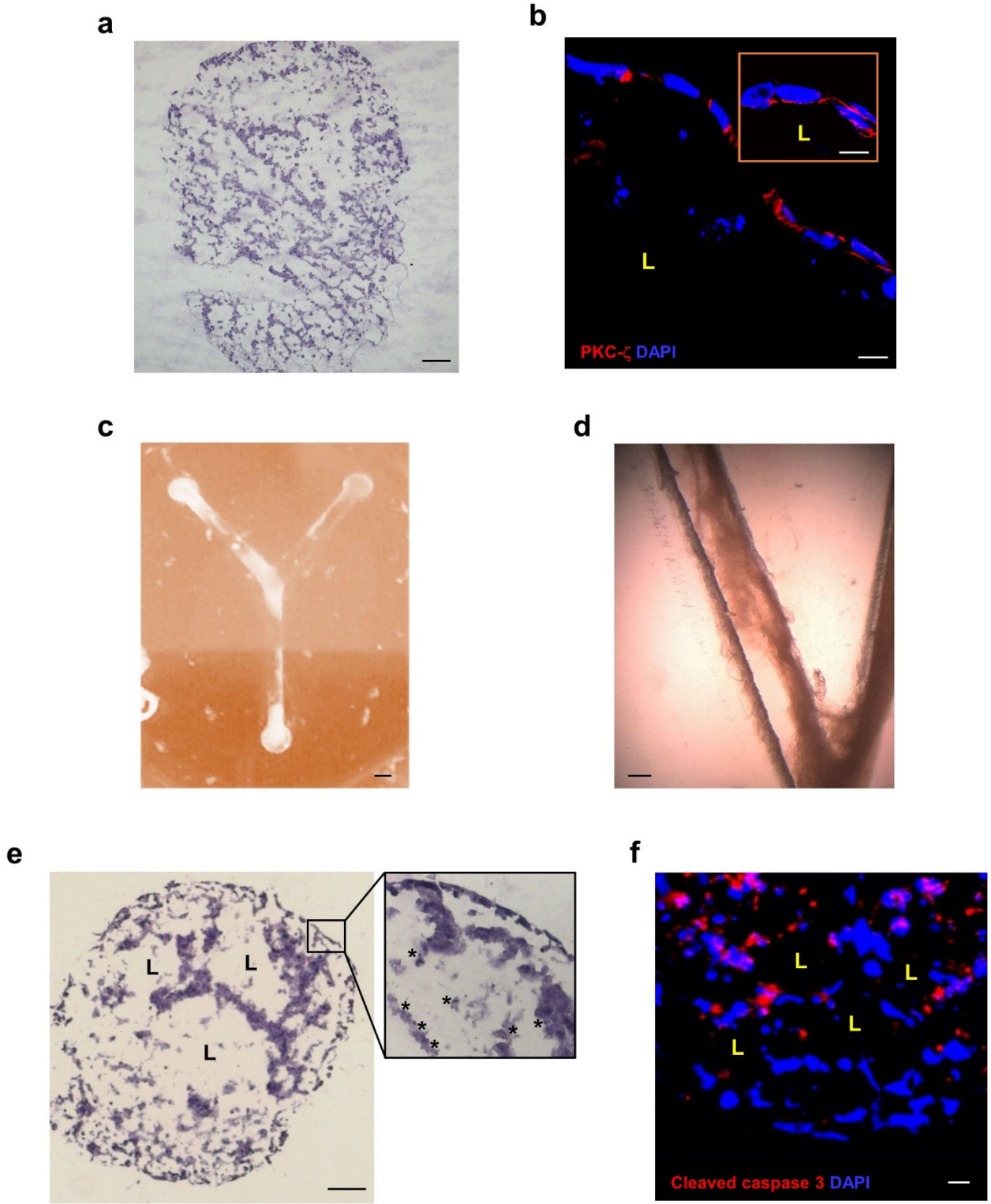

Supplementary Figure 5

Supplementary Figure 5. GDNF is indispensable for lumen formation in human UB-like tubules engineered with 3- and 4-day differentiated iPSCs. (a) Tubular structure engineered using 3-day differentiated hiPSCs cultured for 2 days in the presence of HGF alone fails to develop a single lumen. **(b)** Tubular structure engineered using 3-day differentiated hiPSCs exposed to both HGF and GDNF displays a lumen (L) and some cells in the tubular wall positive for PKC-ζ (red) in the apical domains, indicating the establishment of epithelial polarisation. **(c)** Undifferentiated hiPSCs proliferate massively within the scaffold cavity and appear scattered throughout the culture medium. **(d)** hiPSCs from differentiation day 2 form large and filamentous cell aggregates that detach from the mould and fail to form tubules. **(e)** At day 1, a macrotubule cultured in the presence of HGF and GDNF displays multiple lumens (L) surrounded by apoptotic cells with condensed chromatin (inset, asterisks). **(f)** The same cells that show chromatin condensation also express the apoptosis marker cleaved caspase 3 (red) and display nuclear fragmentation. PKC-ζ, protein kinase C isoform-zeta; DAPI, blue-stained nuclei. Scale bars: 100 mm **(a, e)**, 10 mm **(b, f)**, 1 mm **(c)**, 500 mm **(d)**.

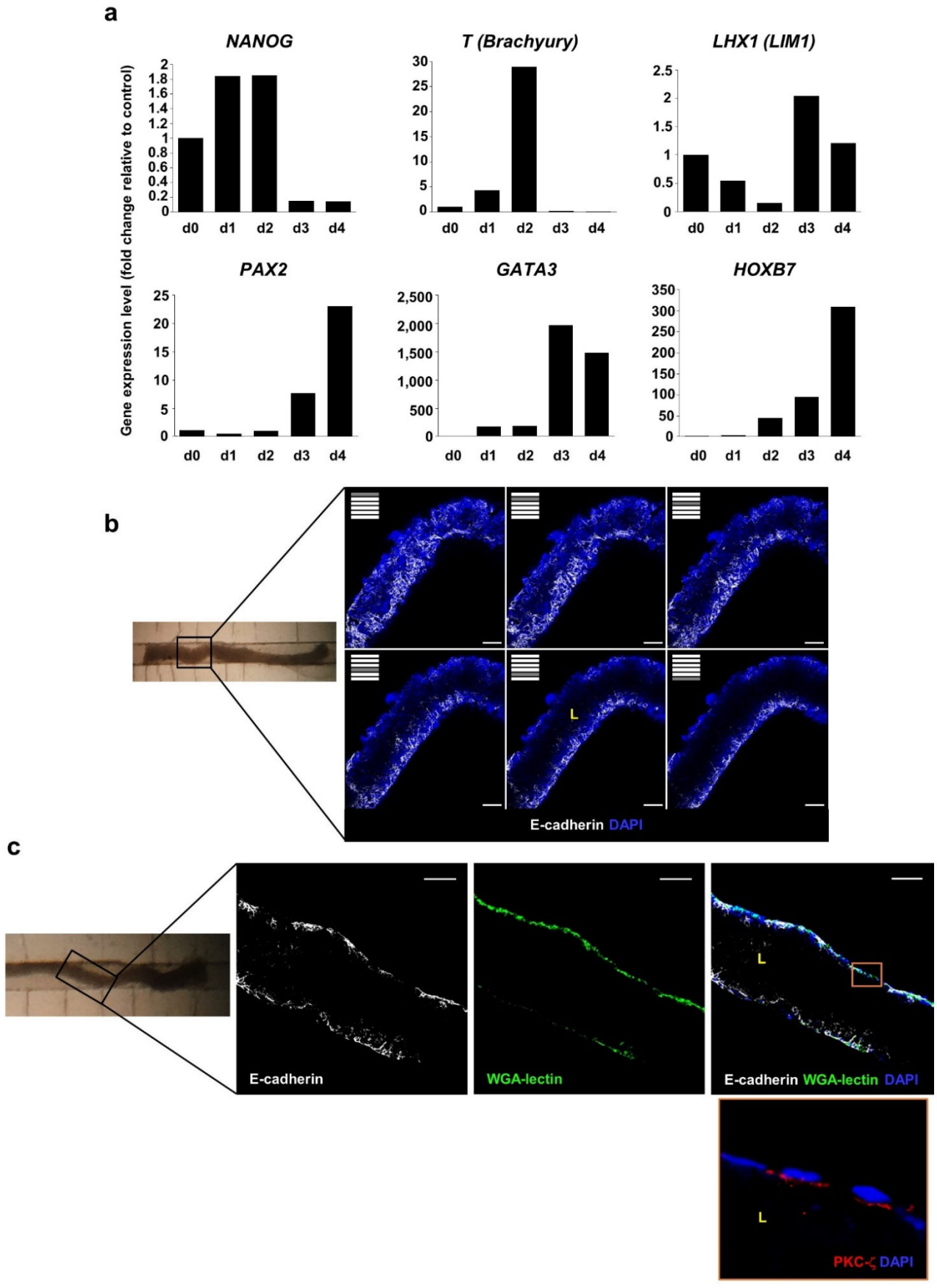

Supplementary Figure 6

Supplementary Fig. 6. Differentiation of healthy donor-derived iPSCs toward UB-like progenitor cells and tubule engineering. (a) Gene expression profile of healthy donor-derived iPSCs during differentiation. *NANOG* expression decreases up to d4, while *T* (*Brachyury*) peaks at d2. *LHX1* (*LIM1*) and *GATA3* peak at d3, while *PAX2* and *HOXB7* expression levels increase up to d4. Values are relative to the housekeeping gene glyceraldehyde-3-phosphate dehydrogenase (*GAPDH*). Data shown are from one representative experiment of three independent experiments. **(b)** Z-stack images of healthy donor-derived microtubule display formation of a single lumen (L) in the tubular central region. **(c)** Healthy donor-derived microtubule showing a continous lumen (L) lined by a monolayered epithelium positive for **(c, inset)** PKC-ζ (red) in the apical membranes. d, day; *NANOG*, Nanog homeobox; *T*, brachyury transcription factor; *LHX1*, LIM homeobox 1; *PAX2*, paired box 2; *GATA3*, GATA binding protein 3; *HOXB7*, homeobox B7; WGA-lectin, wheat-germ agglutinin lectin; PKC-ζ, protein kinase C isoform-zeta; DAPI, blue-stained nuclei. Scale bars: 100 μm **(b, c)**.

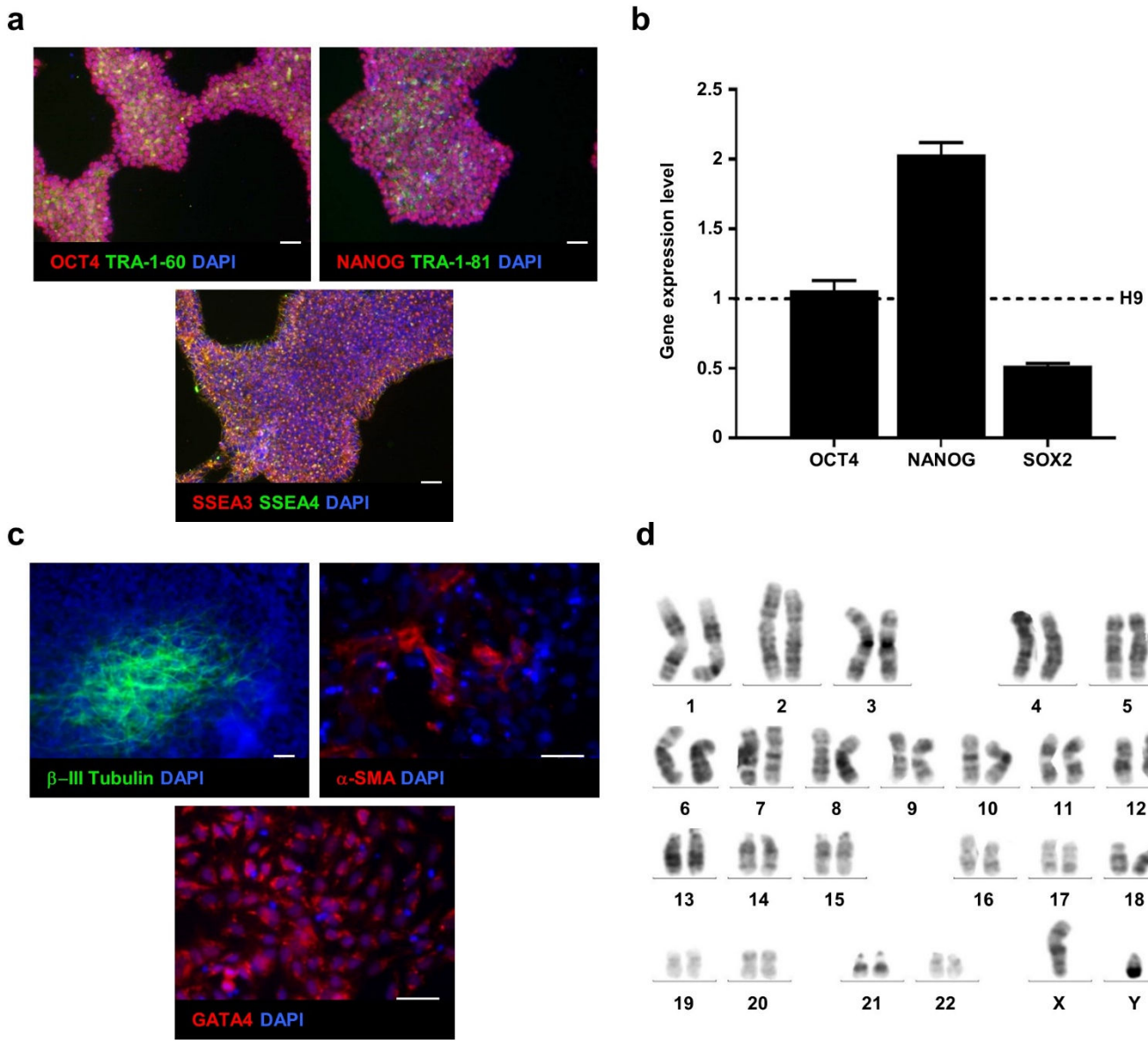

Supplementary Figure 7

Supplementary Figure 7. Characterisation of patient-derived iPSCs. (a) Patient-derived iPSCs are positive for the pluripotency markers OCT4, TRA-1-60, NANOG, TRA-1-81, SSEA3 and SSEA4. **(b)** The pluripotency genes' expression level in patient-derived iPSCs is similar to that in human embryonic stem cell line H9, used as control. Data are expressed as means ± s.e.m. from three independent experiments. **(c)** Patient-derived iPSC *in vitro* differentiation into all three germ layers through EBs formation: β-Tubulin III (ectoderm marker), α-SMA (mesoderm marker) and GATA4 (endoderm marker). **(d)** Karyotype analysis revealing normal 46,XY chromosomal number and structure. TRA-1-60, Tumour-related antigen-1-60; NANOG, Nanog homeobox; TRA-1-81, Tumour-related antigen-1-81; SSEA3, Stage-specific embryonic antigen 3; SSEA4, Stage-specific embryonic antigen 4; SOX2, SRY-box2: α-SMA, alpha-smooth muscle actin; GATA4, GATA binding protein 4; EBs, Embryoid bodies; DAPI, blue-stained nuclei. Scale bars: 50 μm **(a, c)**.

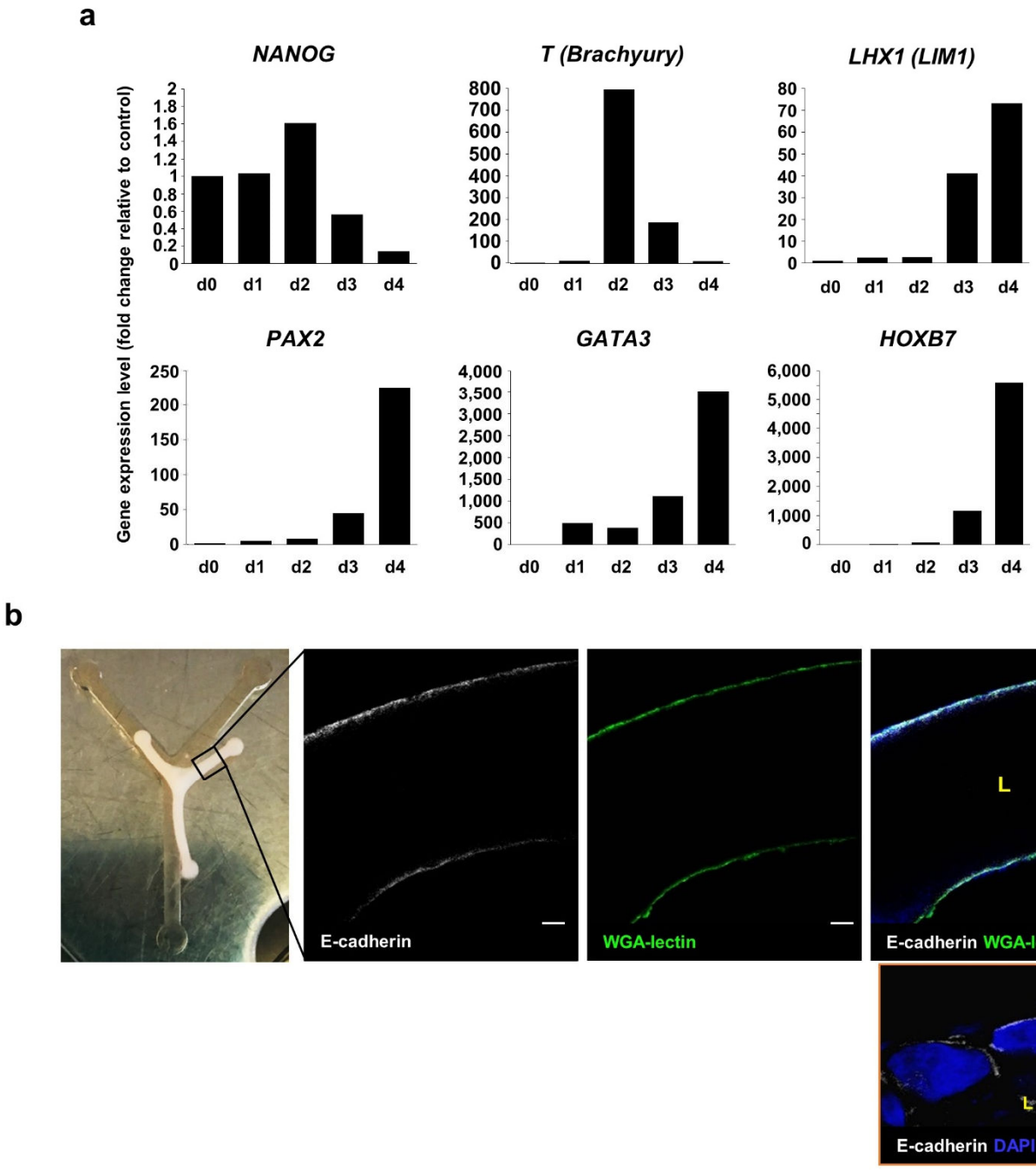

Supplementary Figure 8

Supplementary Figure 8. Differentiation of patient-derived iPSCs toward UB-like progenitor cells and tubule engineering. (a) Gene expression profile of patient-derived iPSCs during differentiation. *NANOG* expression decreases up to d4, while *T* (*Brachyury*) peaks at d2. *LHX1 (LIM1)*, *PAX2*, *GATA3* and *HOXB7* expression levels increase up to d4. Values are relative to the housekeeping gene glyceraldehyde-3-phosphate dehydrogenase (*GAPDH*). Data shown are from one representative experiment of three independent experiments. **(b)** Patient-derived macrotubule after 2 days of culture shows marked shrinkage and develops a continuous lumen (L) lined by a monolayered epithelium of aligned cells positive for E-cadherin in the basolateral membranes (inset). d, day; *NANOG*, Nanog homeobox; *T*, brachyury transcription factor; *LHX1*, LIM homeobox 1; *PAX2*, paired box 2; *GATA3*, GATA binding protein 3; *HOXB7*, homeobox B7; WGA-lectin, wheat-germ agglutinin lectin; DAPI, blue-stained nuclei. Scale bars: 100 μm **(b)**.

CHAPTER 6 - BIBLIOGRAPHY

Bibliography

Adler, M., Polinkovsky, M., Gutierrez, E., Groisman, A., 2010. Generation of oxygen gradients with arbitrary shapes in a microfluidic device. Lab. Chip 10, 388–391. https://doi.org/10.1039/b920401f

Akoh, J.A., 2015. Current management of autosomal dominant polycystic kidney disease. World J. Nephrol. 4, 468–479. https://doi.org/10.5527/wjn.v4.i4.468

al-Awqati, Q., Goldberg, M.R., 1998. Architectural patterns in branching morphogenesis in the kidney. Kidney Int. 54, 1832–1842. https://doi.org/10.1046/j.1523-1755.1998.00196.x

Al-Awqati, Q., Oliver, J.A., 2002. Stem cells in the kidney. Kidney Int. 61, 387–395. https://doi.org/10.1046/j.1523-1755.2002.00164.x

Andrew, D.J., Ewald, A.J., 2010. Morphogenesis of epithelial tubes: Insights into tube formation, elongation, and elaboration. Dev. Biol. 341, 34–55. https://doi.org/10.1016/j.ydbio.2009.09.024

Angeli, E., Volpe, A., Fanzio, P., Repetto, L., Firpo, G., Guida, P., Lo Savio, R., Wanunu, M., Valbusa, U., 2015. Simultaneous Electro-Optical Tracking for Nanoparticle Recognition and Counting. Nano Lett. 15, 5696–5701. https://doi.org/10.1021/acs.nanolett.5b01243

Araoka, T., Mae, S., Kurose, Y., Uesugi, M., Ohta, A., Yamanaka, S., Osafune, K., 2014. Efficient and rapid induction of human iPSCs/ESCs into nephrogenic intermediate mesoderm using small molecule-based differentiation methods. PloS One 9, e84881. https://doi.org/10.1371/journal.pone.0084881

Auerbach, R., Grobstein, C., 1958. Inductive interaction of embryonic tissues after dissociation and reaggregation. Exp. Cell Res. 15, 384–397.

Bachmann, S., Le Hir, M., Eckardt, K.U., 1993. Co-localization of erythropoietin mRNA and ecto-5'-nucleotidase immunoreactivity in peritubular cells of rat renal cortex indicates that fibroblasts produce erythropoietin. J. Histochem. Cytochem. 41, 335–341. https://doi.org/10.1177/41.3.8429197

Balkovetz, D.F., 1998. Hepatocyte growth factor and Madin-Darby canine kidney cells: in vitro models of epithelial cell movement and morphogenesis. Microsc. Res. Tech. 43, 456–463. https://doi.org/10.1002/(SICI)1097-0029(19981201)43:5<456::AID-JEMT11>3.0.CO;2-2

Barak, H., Huh, S.-H., Chen, S., Jeanpierre, C., Martinovic, J., Parisot, M., Bole-Feysot, C., Nitschké, P., Salomon, R., Antignac, C., Ornitz, D.M., Kopan, R., 2012. FGF9 and FGF20 maintain the stemness of nephron progenitors in mice and man. Dev. Cell 22, 1191–1207. https://doi.org/10.1016/j.devcel.2012.04.018

Barasch, J., Pressler, L., Connor, J., Malik, A., 1996. A ureteric bud cell line induces nephrogenesis in two steps by two distinct signals. Am. J. Physiol. 271, F50-61.

Bard, J.B., Gordon, A., Sharp, L., Sellers, W.I., 2001. Early nephron formation in the developing mouse kidney. J. Anat. 199, 385–392.

Barros, E.J., Santos, O.F., Matsumoto, K., Nakamura, T., Nigam, S.K., 1995. Differential tubulogenic and branching morphogenetic activities of growth factors: implications for epithelial tissue development. Proc. Natl. Acad. Sci. U. S. A. 92, 4412–4416.

Barua, M., Stellacci, E., Stella, L., Weins, A., Genovese, G., Muto, V., Caputo, V., Toka, H.R., Charoonratana, V.T., Tartaglia, M., Pollak, M.R., 2014. Mutations in PAX2 associate with adult-onset FSGS. J. Am. Soc. Nephrol. JASN 25, 1942–1953. https://doi.org/10.1681/ASN.2013070686

Benedetti*, V., Brizi*, V., Xinaris, C., 2016. Generation of Functional Kidney Organoids In Vivo Starting from a Single-Cell Suspension. Humana Press, Totowa, NJ.

Blair, H.A., Keating, G.M., 2015. Tolvaptan: A Review in Autosomal Dominant Polycystic Kidney Disease. Drugs 75, 1797–1806. https://doi.org/10.1007/s40265-015-0475-x

Bonon, A., Mangolini, A., Pinton, P., Del Senno, L., Aguiari, G., 2013. Berberine slows cell growth in autosomal dominant polycystic kidney disease cells. Biochem. Biophys. Res. Commun. 441, 668–674. https://doi.org/10.1016/j.bbrc.2013.10.076

Briganti, E., Losi, P., Raffi, A., Scoccianti, M., Munaò, A., Soldani, G., 2006. Silicone based polyurethane materials: a promising biocompatible elastomeric formulation

for cardiovascular applications. J. Mater. Sci. Mater. Med. 17, 259–266. https://doi.org/10.1007/s10856-006-7312-4

Brunelli, S., Blanchette, C., Claxton, A., Roy, D., Rossetti, S., Gutierrez, B., 2015. End-stage renal disease in autosomal dominant polycystic kidney disease: a comparison of dialysis-related utilization and costs with other chronic kidney diseases. Clin. Outcomes Res. 65. https://doi.org/10.2147/CEOR.S76269

Bryant, D.M., Datta, A., Rodríguez-Fraticelli, A.E., Peränen, J., Martín-Belmonte, F., Mostov, K.E., 2010. A molecular network for de novo generation of the apical surface and lumen. Nat. Cell Biol. 12, 1035–1045. https://doi.org/10.1038/ncb2106

Bryant, D.M., Mostov, K.E., 2008. From cells to organs: building polarized tissue. Nat. Rev. Mol. Cell Biol. 9, 887–901. https://doi.org/10.1038/nrm2523

Burckhardt, G., 2012. Drug transport by Organic Anion Transporters (OATs). Pharmacol. Ther. 136, 106–130. https://doi.org/10.1016/j.pharmthera.2012.07.010

Caroli, A., Perico, N., Perna, A., Antiga, L., Brambilla, P., Pisani, A., Visciano, B., Imbriaco, M., Messa, P., Cerutti, R., Dugo, M., Cancian, L., Buongiorno, E., De Pascalis, A., Gaspari, F., Carrara, F., Rubis, N., Prandini, S., Remuzzi, A., Remuzzi, G., Ruggenenti, P., ALADIN study group, 2013. Effect of longacting somatostatin analogue on kidney and cyst growth in autosomal dominant polycystic kidney disease (ALADIN): a randomised, placebo-controlled, multicentre trial. Lancet Lond. Engl. 382, 1485–1495. https://doi.org/10.1016/S0140-6736(13)61407-5

Chi, X., Hadjantonakis, A.-K., Wu, Z., Hyink, D., Costantini, F., 2009. A transgenic mouse that reveals cell shape and arrangement during ureteric bud branching. genesis 47, 61–66. https://doi.org/10.1002/dvg.20452

Chiaravalli, M., Rowe, I., Mannella, V., Quilici, G., Canu, T., Bianchi, V., Gurgone, A., Antunes, S., D'Adamo, P., Esposito, A., Musco, G., Boletta, A., 2016. 2-Deoxy-d-Glucose Ameliorates PKD Progression. J. Am. Soc. Nephrol. JASN 27, 1958–1969. https://doi.org/10.1681/ASN.2015030231

Ciampi, O., Iacone, R., Longaretti, L., Benedetti, V., Graf, M., Magnone, M.C., Patsch, C., Xinaris, C., Remuzzi, G., Benigni, A., Tomasoni, S., 2016. Generation of functional podocytes from human induced pluripotent stem cells. Stem Cell Res. 17, 130–139. https://doi.org/10.1016/j.scr.2016.06.001

Costantini, F., Kopan, R., 2010. Patterning a complex organ: branching morphogenesis and nephron segmentation in kidney development. Dev. Cell 18, 698–712. https://doi.org/10.1016/j.devcel.2010.04.008

Cullen-McEwen, L.A., Caruana, G., Bertram, J.F., 2005. The Where, What and Why of the Developing Renal Stroma. Nephron Exp. Nephrol. 99, e1–e8. https://doi.org/10.1159/000081792

D'Agati, V.D., 2012. Growing New Kidneys from Embryonic Cell Suspensions: Fantasy or Reality? J. Am. Soc. Nephrol. 23, 1763–1766. https://doi.org/10.1681/ASN.2012090888

D'Agati, V.D., Kaskel, F.J., Falk, R.J., 2011. Focal segmental glomerulosclerosis. N. Engl. J. Med. 365, 2398–2411. https://doi.org/10.1056/NEJMra1106556

Davidson, A.J., 2008. Mouse kidney development, in: StemBook. Harvard Stem Cell Institute, Cambridge (MA).

Davies, J.A., 2001. Extracellular Matrix, in: Encyclopedia of Life Sciences. Nature Publishing Group, pp. 1–7.

De Clerck, L.S., Bridts, C.H., Mertens, A.M., Moens, M.M., Stevens, W.J., 1994. Use of fluorescent dyes in the determination of adherence of human leucocytes to endothelial cells and the effect of fluorochromes on cellular function. J. Immunol. Methods 172, 115–124.

Díaz Lantada, A., Pareja Sánchez, B., Gómez Murillo, C., Urbieta Sotillo, J., 2013. Fractals in tissue engineering: toward biomimetic cell-culture matrices, microsystems and microstructured implants. Expert Rev. Med. Devices 10, 629–648. https://doi.org/10.1586/17434440.2013.827506

Diogo, C.V., Machado, N.G., Barbosa, I.A., Serafim, T.L., Burgeiro, A., Oliveira, P.J., 2011. Berberine as a promising safe anti-cancer agent - is there a role for mitochondria? Curr. Drug Targets 12, 850–859.

Dressler, G.R., 2006. The cellular basis of kidney development. Annu. Rev. Cell Dev. Biol. 22, 509–529. https://doi.org/10.1146/annurev.cellbio.22.010305.104340

Dressler, G.R., Deutsch, U., Chowdhury, K., Nornes, H.O., Gruss, P., 1990. Pax2, a new murine paired-box-containing gene and its expression in the developing excretory system. Dev. Camb. Engl. 109, 787–795.

Dressler, G.R., Woolf, A.S., 1999. Pax2 in development and renal disease. Int. J. Dev. Biol. 43, 463–468.

Dziarmaga, A., Eccles, M., Goodyer, P., 2006. Suppression of ureteric bud apoptosis rescues nephron endowment and adult renal function in Pax2 mutant mice. J. Am. Soc. Nephrol. JASN 17, 1568–1575. https://doi.org/10.1681/ASN.2005101074

Eccles, M.R., He, S., Legge, M., Kumar, R., Fox, J., Zhou, C., French, M., Tsai, R.W.S., 2002. PAX genes in development and disease: the role of PAX2 in urogenital tract development. Int. J. Dev. Biol. 46, 535–544.

Eccles, M.R., Yun, K., Reeve, A.E., Fidler, A.E., 1995. Comparative in situ hybridization analysis of PAX2, PAX8, and WT1 gene transcription in human fetal kidney and Wilms' tumors. Am. J. Pathol. 146, 40–45.

Ekblom, P., Miettinen, A., Virtanen, I., Wahlström, T., Dawnay, A., Saxén, L., 1981. In vitro segregation of the metanephric nephron. Dev. Biol. 84, 88–95.

Eyre, J., Ioannou, K., Grubb, B.D., Saleem, M.A., Mathieson, P.W., Brunskill, N.J., Christensen, E.I., Topham, P.S., 2007. Statin-sensitive endocytosis of albumin by glomerular podocytes. Am. J. Physiol. Renal Physiol. 292, F674-681. https://doi.org/10.1152/ajprenal.00272.2006

Fan, L., Liu, C., Gao, A., Zhou, Y., Li, J., 2013. Berberine combined with 2-deoxy-d-glucose synergistically enhances cancer cell proliferation inhibition via energy depletion and unfolded protein response disruption. Biochim. Biophys. Acta 1830, 5175–5183. https://doi.org/10.1016/j.bbagen.2013.07.010

Freedman, B.S., Brooks, C.R., Lam, A.Q., Fu, H., Morizane, R., Agrawal, V., Saad, A.F., Li, M.K., Hughes, M.R., Werff, R.V., Peters, D.T., Lu, J., Baccei, A., Siedlecki, A.M., Valerius, M.T., Musunuru, K., McNagny, K.M., Steinman, T.I., Zhou, J., Lerou, P.H., Bonventre, J.V., 2015. Modelling kidney disease with CRISPR-mutant kidney organoids derived from human pluripotent epiblast spheroids. Nat. Commun. 6, 8715. https://doi.org/10.1038/ncomms9715

Freundlich, M., Quiroz, Y., Zhang, Z., Zhang, Y., Bravo, Y., Weisinger, J.R., Li, Y.C., Rodriguez-Iturbe, B., 2008. Suppression of renin–angiotensin gene expression in the kidney by paricalcitol. Kidney Int. 74, 1394–1402. https://doi.org/10.1038/ki.2008.408

Gagliardini, E., Conti, S., Benigni, A., Remuzzi, G., Remuzzi, A., 2010. Imaging of the Porous Ultrastructure of the Glomerular Epithelial Filtration Slit. J. Am. Soc. Nephrol. 21, 2081–2089. https://doi.org/10.1681/ASN.2010020199

Ganeva, V., Unbekandt, M., Davies, J.A., 2011. An improved kidney dissociation and reaggregation culture system results in nephrons arranged organotypically around a single collecting duct system. Organogenesis 7, 83–87. https://doi.org/10.4161/org.7.2.14881

Gao, J., Zhou, H., Lei, T., Zhou, L., Li, W., Li, X., Yang, B., 2011. Curcumin inhibits renal cyst formation and enlargement in vitro by regulating intracellular signaling pathways. Eur. J. Pharmacol. 654, 92–99. https://doi.org/10.1016/j.ejphar.2010.12.008

Gattone, V.H., Wang, X., Harris, P.C., Torres, V.E., 2003. Inhibition of renal cystic disease development and progression by a vasopressin V2 receptor antagonist. Nat. Med. 9, 1323–1326. https://doi.org/10.1038/nm935

Grantham, J.J., 1996. The etiology, pathogenesis, and treatment of autosomal dominant polycystic kidney disease: Recent advances. Am. J. Kidney Dis. 28, 788–803. https://doi.org/10.1016/S0272-6386(96)90378-9

Grantham, J.J., Mulamalla, S., Swenson-Fields, K.I., 2011. Why kidneys fail in autosomal dominant polycystic kidney disease. Nat. Rev. Nephrol. 7, 556–566. https://doi.org/10.1038/nrneph.2011.109

Grobstein, C., 1955. Inductive interaction in the development of the mouse metanephros. J. Exp. Zool. 130, 319–339. https://doi.org/10.1002/jez.1401300207

Grobstein, C., 1953. Inductive epitheliomesenchymal interaction in cultured organ rudiments of the mouse. Science 118, 52–55.

Guan, F., Villegas, G., Teichman, J., Mundel, P., Tufro, A., 2006. Autocrine VEGF-A system in podocytes regulates podocin and its interaction with CD2AP. Am. J.

Physiol. Renal Physiol. 291, F422-428. https://doi.org/10.1152/ajprenal.00448.2005

Halldorsson, S., Lucumi, E., Gómez-Sjöberg, R., Fleming, R.M.T., 2015. Advantages and challenges of microfluidic cell culture in polydimethylsiloxane devices. Biosens. Bioelectron. 63, 218–231. https://doi.org/10.1016/j.bios.2014.07.029

Haraldsson, B., Nystrom, J., Deen, W.M., 2008. Properties of the Glomerular Barrier and Mechanisms of Proteinuria. Physiol. Rev. 88, 451–487. https://doi.org/10.1152/physrev.00055.2006

Harshman, L.A., Brophy, P.D., 2012. PAX2 in human kidney malformations and disease. Pediatr. Nephrol. Berl. Ger. 27, 1265–1275. https://doi.org/10.1007/s00467-011-2053-0

Hatini, V., Huh, S.O., Herzlinger, D., Soares, V.C., Lai, E., 1996. Essential role of stromal mesenchyme in kidney morphogenesis revealed by targeted disruption of Winged Helix transcription factor BF-2. Genes Dev. 10, 1467–1478.

Hauser, P.V., Nishikawa, M., Kimura, H., Fujii, T., Yanagawa, N., 2016. Controlled tubulogenesis from dispersed ureteric bud-derived cells using a micropatterned gel. J. Tissue Eng. Regen. Med. 10, 762–771. https://doi.org/10.1002/term.1871

Hendry, C., Rumballe, B., Moritz, K., Little, M.H., 2011. Defining and redefining the nephron progenitor population. Pediatr. Nephrol. 26, 1395–1406. https://doi.org/10.1007/s00467-010-1750-4

Herrmann, B.G., Labeit, S., Poustka, A., King, T.R., Lehrach, H., 1990. Cloning of the T gene required in mesoderm formation in the mouse. Nature 343, 617–622. https://doi.org/10.1038/343617a0

Herzlinger, D.A., Easton, T.G., Ojakian, G.K., 1982. The MDCK epithelial cell line expresses a cell surface antigen of the kidney distal tubule. J. Cell Biol. 93, 269–277.

Hill, N.R., Fatoba, S.T., Oke, J.L., Hirst, J.A., O'Callaghan, C.A., Lasserson, D.S., Hobbs, F.D.R., 2016. Global Prevalence of Chronic Kidney Disease – A Systematic Review and Meta-Analysis. PLOS ONE 11, e0158765. https://doi.org/10.1371/journal.pone.0158765

Hogan, M.C., Masyuk, T.V., Page, L.J., Kubly, V.J., Bergstralh, E.J., Li, X., Kim, B., King, B.F., Glockner, J., Holmes, D.R., Rossetti, S., Harris, P.C., LaRusso, N.F., Torres, V.E., 2010. Randomized clinical trial of long-acting somatostatin for autosomal dominant polycystic kidney and liver disease. J. Am. Soc. Nephrol. JASN 21, 1052–1061. https://doi.org/10.1681/ASN.2009121291

Homan, K.A., Kolesky, D.B., Skylar-Scott, M.A., Herrmann, J., Obuobi, H., Moisan, A., Lewis, J.A., 2016. Bioprinting of 3D Convoluted Renal Proximal Tubules on Perfusable Chips. Sci. Rep. 6, 34845. https://doi.org/10.1038/srep34845

Humes, H.D., MacKay, S.M., Funke, A.J., Buffington, D.A., 1999. Tissue engineering of a bioartificial renal tubule assist device: in vitro transport and metabolic

characteristics. Kidney Int. 55, 2502–2514. https://doi.org/10.1046/j.1523-1755.1999.00486.x

Humphreys, B.D., Lin, S.-L., Kobayashi, A., Hudson, T.E., Nowlin, B.T., Bonventre, J.V., Valerius, M.T., McMahon, A.P., Duffield, J.S., 2010. Fate Tracing Reveals the Pericyte and Not Epithelial Origin of Myofibroblasts in Kidney Fibrosis. Am. J. Pathol. 176, 85–97. https://doi.org/10.2353/ajpath.2010.090517

Iizuka, N., Miyamoto, K., Okita, K., Tangoku, A., Hayashi, H., Yosino, S., Abe, T., Morioka, T., Hazama, S., Oka, M., 2000. Inhibitory effect of Coptidis Rhizoma and berberine on the proliferation of human esophageal cancer cell lines. Cancer Lett. 148, 19–25.

Imberti, B., Tomasoni, S., Ciampi, O., Pezzotta, A., Derosas, M., Xinaris, C., Rizzo, P., Papadimou, E., Novelli, R., Benigni, A., Remuzzi, G., Morigi, M., 2015. Renal progenitors derived from human iPSCs engraft and restore function in a mouse model of acute kidney injury. Sci. Rep. 5, 8826. https://doi.org/10.1038/srep08826

Jansen, J., De Napoli, I.E., Fedecostante, M., Schophuizen, C.M.S., Chevtchik, N.V., Wilmer, M.J., van Asbeck, A.H., Croes, H.J., Pertijs, J.C., Wetzels, J.F.M., Hilbrands, L.B., van den Heuvel, L.P., Hoenderop, J.G., Stamatialis, D., Masereeuw, R., 2015. Human proximal tubule epithelial cells cultured on hollow fibers: living membranes that actively transport organic cations. Sci. Rep. 5, 16702. https://doi.org/10.1038/srep16702

Jansen, J., Fedecostante, M., Wilmer, M.J., Peters, J.G., Kreuser, U.M., van den Broek, P.H., Mensink, R.A., Boltje, T.J., Stamatialis, D., Wetzels, J.F., van den Heuvel, L.P., Hoenderop, J.G., Masereeuw, R., 2016. Bioengineered kidney tubules efficiently excrete uremic toxins. Sci. Rep. 6, 26715. https://doi.org/10.1038/srep26715

Jeffrey, H., Miner D.R.A., 2012. Molecular and cellular mechanism of glomerular capillary development, in: The Kidney: Physiology & Pathophysiology. Elsevier Health Sciences.

Junttila, S., Saarela, U., Halt, K., Manninen, A., Parssinen, H., Lecca, M.R., Brandli, A.W., Sims-Lucas, S., Skovorodkin, I., Vainio, S.J., 2015. Functional Genetic Targeting of Embryonic Kidney Progenitor Cells Ex Vivo. J. Am. Soc. Nephrol. 26, 1126–1137. https://doi.org/10.1681/ASN.2013060584

Kispert, A., Vainio, S., McMahon, A.P., 1998. Wnt-4 is a mesenchymal signal for epithelial transformation of metanephric mesenchyme in the developing kidney. Dev. Camb. Engl. 125, 4225–4234.

Kitamoto, Y., Tokunaga, H., Miyamoto, K., Tomita, K., 2002. VEGF is an essential molecule for glomerular structuring. Nephrol. Dial. Transplant. Off. Publ. Eur. Dial. Transpl. Assoc. - Eur. Ren. Assoc. 17 Suppl 9, 25–27.

Kitamoto, Y., Tokunaga, H., Tomita, K., 1997. Vascular endothelial growth factor is an essential molecule for mouse kidney development: glomerulogenesis and nephrogenesis. J. Clin. Invest. 99, 2351–2357. https://doi.org/10.1172/JCI119416

Kojima, R., Sekine, T., Kawachi, M., Cha, S.H., Suzuki, Y., Endou, H., 2002. Immunolocalization of multispecific organic anion transporters, OAT1, OAT2, and OAT3, in rat kidney. J. Am. Soc. Nephrol. JASN 13, 848–857.

Koseki, C., Herzlinger, D., al-Awqati, Q., 1992. Apoptosis in metanephric development. J. Cell Biol. 119, 1327–1333.

Krause, M., Rak-Raszewska, A., Pietilä, I., Quaggin, S., Vainio, S., 2015. Signaling during Kidney Development. Cells 4, 112–132. https://doi.org/10.3390/cells4020112

Krey, A.K., Hahn, F.E., 1969. Berberine: complex with DNA. Science 166, 755–757.

Lam, A.Q., Freedman, B.S., Morizane, R., Lerou, P.H., Valerius, M.T., Bonventre, J.V., 2014. Rapid and efficient differentiation of human pluripotent stem cells into intermediate mesoderm that forms tubules expressing kidney proximal tubular markers. J. Am. Soc. Nephrol. JASN 25, 1211–1225. https://doi.org/10.1681/ASN.2013080831

Lawrence, M.L., Chang, C.-H., Davies, J.A., 2015. Transport of organic anions and cations in murine embryonic kidney development and in serially-reaggregated engineered kidneys. Sci. Rep. 5, 9092. https://doi.org/10.1038/srep09092

Li, H., Findlay, I.A., Sheppard, D.N., 2004. The relationship between cell proliferation, Cl- secretion, and renal cyst growth: a study using CFTR inhibitors. Kidney Int. 66, 1926–1938. https://doi.org/10.1111/j.1523-1755.2004.00967.x

Li, W., Hartwig, S., Rosenblum, N.D., 2014. Developmental origins and functions of stromal cells in the normal and diseased mammalian kidney: Origins and Functions of Kidney Stromal Cells. Dev. Dyn. 243, 853–863. https://doi.org/10.1002/dvdy.24134

Lin, Y., Zhang, S., Tuukkanen, J., Peltoketo, H., Pihlajaniemi, T., Vainio, S., 2003. Patterning parameters associated with the branching of the ureteric bud regulated by epithelial-mesenchymal interactions. Int. J. Dev. Biol. 47, 3–13.

Lindström, N.O., Chang, C.-H., Valerius, M.T., Hohenstein, P., Davies, J.A., 2015. Node retraction during patterning of the urinary collecting duct system. J. Anat. 226, 13–21. https://doi.org/10.1111/joa.12239

Little, M.H., Combes, A.N., Takasato, M., 2016. Understanding kidney morphogenesis to guide renal tissue regeneration. Nat. Rev. Nephrol. 12, 624–635. https://doi.org/10.1038/nrneph.2016.126

Liu, Z., Greco, A.J., Hellman, N.E., Spector, J., Robinson, J., Tang, O.T., Lipschutz, J.H., 2007. Intracellular signaling via ERK/MAPK completes the pathway for tubulogenic fibronectin in MDCK cells. Biochem. Biophys. Res. Commun. 353, 793–798. https://doi.org/10.1016/j.bbrc.2006.12.106

Lubarsky, B., Krasnow, M.A., 2003. Tube morphogenesis: making and shaping biological tubes. Cell 112, 19–28.

Machiguchi, T., Nakamura, T., 2013. Cellular interactions via conditioned media induce in vivo nephron generation from tubular epithelial cells or mesenchymal stem cells. Biochem. Biophys. Res. Commun. 435, 327–333. https://doi.org/10.1016/j.bbrc.2013.04.050

MacKay, S.M., Funke, A.J., Buffington, D.A., Humes, H.D., 1998. Tissue engineering of a bioartificial renal tubule. ASAIO J. Am. Soc. Artif. Intern. Organs 1992 44, 179–183.

Mae, S.-I., Shono, A., Shiota, F., Yasuno, T., Kajiwara, M., Gotoda-Nishimura, N., Arai, S., Sato-Otubo, A., Toyoda, T., Takahashi, K., Nakayama, N., Cowan, C.A., Aoi, T., Ogawa, S., McMahon, A.P., Yamanaka, S., Osafune, K., 2013. Monitoring and robust induction of nephrogenic intermediate mesoderm from human pluripotent stem cells. Nat. Commun. 4, 1367. https://doi.org/10.1038/ncomms2378

Maeshima, A., Zhang, Y.Q., Furukawa, M., Naruse, T., Kojima, I., 2000. Hepatocyte growth factor induces branching tubulogenesis in MDCK cells by modulating the activin-follistatin system. Kidney Int. 58, 1511–1522. https://doi.org/10.1046/j.1523-1755.2000.00313.x

Mangoo-Karim, R., Uchic, M., Lechene, C., Grantham, J.J., 1989. Renal epithelial cyst formation and enlargement in vitro: dependence on cAMP. Proc. Natl. Acad. Sci. U. S. A. 86, 6007–6011.

Mao, Z., Chong, J., Ong, A.C.M., 2016. Autosomal dominant polycystic kidney disease: recent advances in clinical management. F1000Research 5, 2029. https://doi.org/10.12688/f1000research.9045.1

Markov, D.A., Lillie, E.M., Garbett, S.P., McCawley, L.J., 2014. Variation in diffusion of gases through PDMS due to plasma surface treatment and storage conditions. Biomed. Microdevices 16, 91–96. https://doi.org/10.1007/s10544-013-9808-2

Martinez, J.R., Grantham, J.J., 1995. Polycystic kidney disease: etiology, pathogenesis, and treatment. Dis.--Mon. DM 41, 693–765.

Masyuk, T.V., Masyuk, A.I., Torres, V.E., Harris, P.C., Larusso, N.F., 2007. Octreotide inhibits hepatic cystogenesis in a rodent model of polycystic liver disease by reducing cholangiocyte adenosine 3',5'-cyclic monophosphate. Gastroenterology 132, 1104–1116. https://doi.org/10.1053/j.gastro.2006.12.039

Masyuk, T.V., Radtke, B.N., Stroope, A.J., Banales, J.M., Gradilone, S.A., Huang, B., Masyuk, A.I., Hogan, M.C., Torres, V.E., Larusso, N.F., 2013. Pasireotide is more effective than octreotide in reducing hepatorenal cystogenesis in rodents with polycystic kidney and liver diseases. Hepatol. Baltim. Md 58, 409–421. https://doi.org/10.1002/hep.26140

Maxwell, P.H., Osmond, M.K., Pugh, C.W., Heryet, A., Nicholls, L.G., Tan, C.C., Doe, B.G., Ferguson, D.J., Johnson, M.H., Ratcliffe, P.J., 1993. Identification of the renal erythropoietin-producing cells using transgenic mice. Kidney Int. 44, 1149–1162.

Meder, D., Shevchenko, A., Simons, K., Füllekrug, J., 2005. Gp135/podocalyxin and NHERF-2 participate in the formation of a preapical domain during polarization of MDCK cells. J. Cell Biol. 168, 303–313. https://doi.org/10.1083/jcb.200407072

Meyer, T.N., Schwesinger, C., Bush, K.T., Stuart, R.O., Rose, D.W., Shah, M.M., Vaughn, D.A., Steer, D.L., Nigam, S.K., 2004. Spatiotemporal regulation of morphogenetic molecules during in vitro branching of the isolated ureteric bud: toward a model of branching through budding in the developing kidney. Dev. Biol. 275, 44–67. https://doi.org/10.1016/j.ydbio.2004.07.022

Montesano, R., Matsumoto, K., Nakamura, T., Orci, L., 1991a. Identification of a fibroblast-derived epithelial morphogen as hepatocyte growth factor. Cell 67, 901–908.

Montesano, R., Schaller, G., Orci, L., 1991b. Induction of epithelial tubular morphogenesis in vitro by fibroblast-derived soluble factors. Cell 66, 697–711.

Morizane, R., Lam, A.Q., Freedman, B.S., Kishi, S., Valerius, M.T., Bonventre, J.V., 2015. Nephron organoids derived from human pluripotent stem cells model kidney development and injury. Nat. Biotechnol. 33, 1193–1200. https://doi.org/10.1038/nbt.3392

Nagalakshmi, V.K., Yu, J., 2015. The ureteric bud epithelium: morphogenesis and roles in metanephric kidney patterning. Mol. Reprod. Dev. 82, 151–166. https://doi.org/10.1002/mrd.22462

Nagle, M.A., Truong, D.M., Dnyanmote, A.V., Ahn, S.-Y., Eraly, S.A., Wu, W., Nigam, S.K., 2011. Analysis of three-dimensional systems for developing and mature kidneys clarifies the role of OAT1 and OAT3 in antiviral handling. J. Biol. Chem. 286, 243–251. https://doi.org/10.1074/jbc.M110.139949

Nakamura, T., Matsumoto, K., Kiritoshi, A., Tano, Y., Nakamura, T., 1997. Induction of hepatocyte growth factor in fibroblasts by tumor-derived factors affects invasive growth of tumor cells: in vitro analysis of tumor-stromal interactions. Cancer Res. 57, 3305–3313.

Nigam, S.K., Bush, K.T., Martovetsky, G., Ahn, S.-Y., Liu, H.C., Richard, E., Bhatnagar, V., Wu, W., 2015. The organic anion transporter (OAT) family: a systems biology perspective. Physiol. Rev. 95, 83–123. https://doi.org/10.1152/physrev.00025.2013

Nigam, S.K., Shah, M.M., 2009. How does the ureteric bud branch? J. Am. Soc. Nephrol. JASN 20, 1465–1469. https://doi.org/10.1681/ASN.2008020132

Nishinakamura, R., Matsumoto, Y., Nakao, K., Nakamura, K., Sato, A., Copeland, N.G., Gilbert, D.J., Jenkins, N.A., Scully, S., Lacey, D.L., Katsuki, M., Asashima, M., Yokota, T., 2001. Murine homolog of SALL1 is essential for ureteric bud invasion in kidney development. Dev. Camb. Engl. 128, 3105–3115.

Ong, A.C.M., Devuyst, O., Knebelmann, B., Walz, G., 2015. Autosomal dominant polycystic kidney disease: the changing face of clinical management. The Lancet 385, 1993–2002. https://doi.org/10.1016/S0140-6736(15)60907-2

Osafune, K., Takasato, M., Kispert, A., Asashima, M., Nishinakamura, R., 2006. Identification of multipotent progenitors in the embryonic mouse kidney by a novel colony-forming assay. Dev. Camb. Engl. 133, 151–161. https://doi.org/10.1242/dev.02174

Papadimou, E., Morigi, M., Iatropoulos, P., Xinaris, C., Tomasoni, S., Benedetti, V., Longaretti, L., Rota, C., Todeschini, M., Rizzo, P., Introna, M., Grazia de Simoni, M., Remuzzi, G., Goligorsky, M.S., Benigni, A., 2015. Direct reprogramming of human bone marrow stromal cells into functional renal cells using cell-free extracts. Stem Cell Rep. 4, 685–698. https://doi.org/10.1016/j.stemcr.2015.02.002

Perico, N., Remuzzi, G., 2012. Chronic kidney disease: a research and public health priority. Nephrol. Dial. Transplant. 27, iii19-iii26. https://doi.org/10.1093/ndt/gfs284

Pollack, A.L., Runyan, R.B., Mostov, K.E., 1998. Morphogenetic mechanisms of epithelial tubulogenesis: MDCK cell polarity is transiently rearranged without loss of cell-cell contact during scatter factor/hepatocyte growth factor-induced tubulogenesis. Dev. Biol. 204, 64–79. https://doi.org/10.1006/dbio.1998.9091

Pons, B.E., 2013. Symmetry: Culture and Science. Gen. Self-Contacting Symmetric Fractal Trees 21, 333–351.

Porteous, S., Torban, E., Cho, N.P., Cunliffe, H., Chua, L., McNoe, L., Ward, T., Souza, C., Gus, P., Giugliani, R., Sato, T., Yun, K., Favor, J., Sicotte, M., Goodyer, P., Eccles, M., 2000. Primary renal hypoplasia in humans and mice with PAX2

mutations: evidence of increased apoptosis in fetal kidneys of Pax2(1Neu) +/- mutant mice. Hum. Mol. Genet. 9, 1–11.

Priolo, C., Henske, E.P., 2013. Metabolic reprogramming in polycystic kidney disease. Nat. Med. 19, 407–409. https://doi.org/10.1038/nm.3140

Prozialeck, W.C., Lamar, P.C., Appelt, D.M., 2004. Differential expression of E-cadherin, N-cadherin and beta-catenin in proximal and distal segments of the rat nephron. BMC Physiol. 4, 10. https://doi.org/10.1186/1472-6793-4-10

Qiao, J., Bush, K.T., Steer, D.L., Stuart, R.O., Sakurai, H., Wachsman, W., Nigam, S.K., 2001. Multiple fibroblast growth factors support growth of the ureteric bud but have different effects on branching morphogenesis. Mech. Dev. 109, 123–135.

Qiao, J., Sakurai, H., Nigam, S.K., 1999a. Branching morphogenesis independent of mesenchymal-epithelial contact in the developing kidney. Proc. Natl. Acad. Sci. U. S. A. 96, 7330–7335.

Qiao, J., Uzzo, R., Obara-Ishihara, T., Degenstein, L., Fuchs, E., Herzlinger, D., 1999b. FGF-7 modulates ureteric bud growth and nephron number in the developing kidney. Dev. Camb. Engl. 126, 547–554.

Raghavan, V., Rbaibi, Y., Pastor-Soler, N.M., Carattino, M.D., Weisz, O.A., 2014. Shear stress-dependent regulation of apical endocytosis in renal proximal tubule cells mediated by primary cilia. Proc. Natl. Acad. Sci. U. S. A. 111, 8506–8511. https://doi.org/10.1073/pnas.1402195111

Reif, G.A., Yamaguchi, T., Nivens, E., Fujiki, H., Pinto, C.S., Wallace, D.P., 2011. Tolvaptan inhibits ERK-dependent cell proliferation, Cl^- secretion, and in vitro cyst growth of human ADPKD cells stimulated by vasopressin. Am. J. Physiol. Renal Physiol. 301, F1005-1013. https://doi.org/10.1152/ajprenal.00243.2011

Riella, C., Czarnecki, P.G., Steinman, T.I., 2014. Therapeutic advances in the treatment of polycystic kidney disease. Nephron Clin. Pract. 128, 297–302. https://doi.org/10.1159/000368244

Rindler, M.J., Chuman, L.M., Shaffer, L., Saier, M.H., 1979. Retention of differentiated properties in an established dog kidney epithelial cell line (MDCK). J. Cell Biol. 81, 635–648.

Rodrigues-Díez, R., Benedetti, V., Remuzzi, G., Xinaris, C., 2017. Tissue Engineering of Renal Tissue (Kidney), in: Hasan, A. (Ed.), Tissue Engineering for Artificial Organs. Wiley-VCH Verlag GmbH & Co. KGaA, Weinheim, Germany, pp. 575–602.

Rosines, E., Sampogna, R.V., Johkura, K., Vaughn, D.A., Choi, Y., Sakurai, H., Shah, M.M., Nigam, S.K., 2007. Staged in vitro reconstitution and implantation of engineered rat kidney tissue. Proc. Natl. Acad. Sci. U. S. A. 104, 20938–20943. https://doi.org/10.1073/pnas.0710428105

Roth, M., Obaidat, A., Hagenbuch, B., 2012. OATPs, OATs and OCTs: the organic anion and cation transporters of the SLCO and SLC22A gene superfamilies. Br. J. Pharmacol. 165, 1260–1287. https://doi.org/10.1111/j.1476-5381.2011.01724.x

Rothenpieler, U.W., Dressler, G.R., 1993. Pax-2 is required for mesenchyme-to-epithelium conversion during kidney development. Dev. Camb. Engl. 119, 711–720.

Rowe, I., Chiaravalli, M., Mannella, V., Ulisse, V., Quilici, G., Pema, M., Song, X.W., Xu, H., Mari, S., Qian, F., Pei, Y., Musco, G., Boletta, A., 2013. Defective glucose metabolism in polycystic kidney disease identifies a new therapeutic strategy. Nat. Med. 19, 488–493. https://doi.org/10.1038/nm.3092

Ruggenenti, P., Remuzzi, A., Ondei, P., Fasolini, G., Antiga, L., Ene-Iordache, B., Remuzzi, G., Epstein, F.H., 2005. Safety and efficacy of long-acting somatostatin treatment in autosomal-dominant polycystic kidney disease. Kidney Int. 68, 206–216. https://doi.org/10.1111/j.1523-1755.2005.00395.x

Saigusa, T., Bell, P.D., 2015. Molecular pathways and therapies in autosomal-dominant polycystic kidney disease. Physiol. Bethesda Md 30, 195–207. https://doi.org/10.1152/physiol.00032.2014

Sainio, K., Suvanto, P., Davies, J., Wartiovaara, J., Wartiovaara, K., Saarma, M., Arumäe, U., Meng, X., Lindahl, M., Pachnis, V., Sariola, H., 1997. Glial-cell-line-derived neurotrophic factor is required for bud initiation from ureteric epithelium. Dev. Camb. Engl. 124, 4077–4087.

Sakurai, H., Barros, E.J., Tsukamoto, T., Barasch, J., Nigam, S.K., 1997. An in vitro tubulogenesis system using cell lines derived from the embryonic kidney shows dependence on multiple soluble growth factors. Proc. Natl. Acad. Sci. U. S. A. 94, 6279–6284.

Santos, O.F., Barros, E.J., Yang, X.M., Matsumoto, K., Nakamura, T., Park, M., Nigam, S.K., 1994. Involvement of hepatocyte growth factor in kidney development. Dev. Biol. 163, 525–529. https://doi.org/10.1006/dbio.1994.1169

Santos, O.F., Nigam, S.K., 1993. HGF-induced tubulogenesis and branching of epithelial cells is modulated by extracellular matrix and TGF-beta. Dev. Biol. 160, 293–302. https://doi.org/10.1006/dbio.1993.1308

Saxén, L., 1987. Organogenesis of the kidney, Developmental and cell biology series. Cambridge University Press, Cambridge [Cambridgeshire] ; New York.

Schmidt-Ott, K.M., 2010. ROCK inhibition facilitates tissue reconstitution from embryonic kidney cell suspensions. Kidney Int. 77, 387–389. https://doi.org/10.1038/ki.2009.488

Schumacher, K.M., Phua, S.C., Schumacher, A., Ying, J.Y., 2008. Controlled formation of biological tubule systems in extracellular matrix gels in vitro. Kidney Int. 73, 1187–1192. https://doi.org/10.1038/ki.2008.20

Schwartz, G.J., Al-Awqati, Q., 1985. Carbon dioxide causes exocytosis of vesicles containing H+ pumps in isolated perfused proximal and collecting tubules. J. Clin. Invest. 75, 1638–1644. https://doi.org/10.1172/JCI111871

Serra, A.L., Poster, D., Kistler, A.D., Krauer, F., Raina, S., Young, J., Rentsch, K.M., Spanaus, K.S., Senn, O., Kristanto, P., Scheffel, H., Weishaupt, D., Wüthrich, R.P.,

2010. Sirolimus and kidney growth in autosomal dominant polycystic kidney disease. N. Engl. J. Med. 363, 820–829. https://doi.org/10.1056/NEJMoa0907419

Shah, M.M., Sampogna, R.V., Sakurai, H., Bush, K.T., Nigam, S.K., 2004. Branching morphogenesis and kidney disease. Dev. Camb. Engl. 131, 1449–1462. https://doi.org/10.1242/dev.01089

Shakya, R., Watanabe, T., Costantini, F., 2005. The role of GDNF/Ret signaling in ureteric bud cell fate and branching morphogenesis. Dev. Cell 8, 65–74. https://doi.org/10.1016/j.devcel.2004.11.008

Sharmin, S., Taguchi, A., Kaku, Y., Yoshimura, Y., Ohmori, T., Sakuma, T., Mukoyama, M., Yamamoto, T., Kurihara, H., Nishinakamura, R., 2016. Human Induced Pluripotent Stem Cell-Derived Podocytes Mature into Vascularized Glomeruli upon Experimental Transplantation. J. Am. Soc. Nephrol. JASN 27, 1778–1791. https://doi.org/10.1681/ASN.2015010096

Shen, C., Meng, Q., Zhang, G., 2013. Increased curvature of hollow fiber membranes could up-regulate differential functions of renal tubular cell layers. Biotechnol. Bioeng. 110, 2173–2183. https://doi.org/10.1002/bit.24874

Shen, C., Zhang, G., Wang, Q., Meng, Q., 2015. Fabrication of Collagen Gel Hollow Fibers by Covalent Cross-Linking for Construction of Bioengineering Renal Tubules. ACS Appl. Mater. Interfaces 7, 19789–19797. https://doi.org/10.1021/acsami.5b05809

Shillingford, J.M., Murcia, N.S., Larson, C.H., Low, S.H., Hedgepeth, R., Brown, N., Flask, C.A., Novick, A.C., Goldfarb, D.A., Kramer-Zucker, A., Walz, G., Piontek, K.B., Germino, G.G., Weimbs, T., 2006. The mTOR pathway is regulated by polycystin-1, and its inhibition reverses renal cystogenesis in polycystic kidney disease. Proc. Natl. Acad. Sci. U. S. A. 103, 5466–5471. https://doi.org/10.1073/pnas.0509694103

Siegel, J.F., Delakas, D., Rai, S., Kushner, L., 1996. Unilateral Nephrectomy Induces the Expression of the Wilms Tumor Gene in the Contralateral Kidney of the Adult Rat. J. Urol. 156, 688–692. https://doi.org/10.1016/S0022-5347(01)65786-0

Siegel, N., Rosner, M., Unbekandt, M., Fuchs, C., Slabina, N., Dolznig, H., Davies, J.A., Lubec, G., Hengstschläger, M., 2010. Contribution of human amniotic fluid stem cells to renal tissue formation depends on mTOR. Hum. Mol. Genet. 19, 3320–3331. https://doi.org/10.1093/hmg/ddq236

Sigurbjörnsdóttir, S., Mathew, R., Leptin, M., 2014. Molecular mechanisms of de novo lumen formation. Nat. Rev. Mol. Cell Biol. 15, 665–676. https://doi.org/10.1038/nrm3871

Sims-Lucas, S., Schaefer, C., Bushnell, D., Ho, J., Logar, A., Prochownik, E., Gittes, G., Bates, C.M., 2013. Endothelial Progenitors Exist within the Kidney and Lung Mesenchyme. PLoS ONE 8, e65993. https://doi.org/10.1371/journal.pone.0065993

Steer, D.L., Bush, K.T., Meyer, T.N., Schwesinger, C., Nigam, S.K., 2002. A strategy for in vitro propagation of rat nephrons. Kidney Int. 62, 1958–1965. https://doi.org/10.1046/j.1523-1755.2002.00694.x

Steer, D.L., Nigam, S.K., 2004. Developmental approaches to kidney tissue engineering. Am. J. Physiol. Renal Physiol. 286, F1-7. https://doi.org/10.1152/ajprenal.00167.2003

Subramanya, A.R., Ellison, D.H., 2014. Distal Convoluted Tubule. Clin. J. Am. Soc. Nephrol. 9, 2147–2163. https://doi.org/10.2215/CJN.05920613

Sullivan, L.P., Wallace, D.P., Grantham, J.J., 1998. Epithelial transport in polycystic kidney disease. Physiol. Rev. 78, 1165–1191.

Sun, Y., Zhou, H., Yang, B., 2011. Drug discovery for polycystic kidney disease. Acta Pharmacol. Sin. 32, 805–816. https://doi.org/10.1038/aps.2011.29

Sweeney, W.E., Avner, E.D., 2011. Diagnosis and management of childhood polycystic kidney disease. Pediatr. Nephrol. Berl. Ger. 26, 675–692. https://doi.org/10.1007/s00467-010-1656-1

Sweet, D.H., Eraly, S.A., Vaughn, D.A., Bush, K.T., Nigam, S.K., 2006. Organic anion and cation transporter expression and function during embryonic kidney development and in organ culture models. Kidney Int. 69, 837–845. https://doi.org/10.1038/sj.ki.5000170

Taal, M.W., Chertow, G.M., Marsden, P.A., Skorecki, K., Yu, A.S.L., Brenner, B.M., 2011. Brenner and Rector's The Kidney. Elsevier Health Sciences, London.

Taguchi, A., Kaku, Y., Ohmori, T., Sharmin, S., Ogawa, M., Sasaki, H., Nishinakamura, R., 2014. Redefining the in vivo origin of metanephric nephron progenitors enables generation of complex kidney structures from pluripotent stem cells. Cell Stem Cell 14, 53–67. https://doi.org/10.1016/j.stem.2013.11.010

Takahashi, K., Tanabe, K., Ohnuki, M., Narita, M., Ichisaka, T., Tomoda, K., Yamanaka, S., 2007. Induction of pluripotent stem cells from adult human fibroblasts by defined factors. Cell 131, 861–872. https://doi.org/10.1016/j.cell.2007.11.019

Takahashi, K., Yamanaka, S., 2006. Induction of pluripotent stem cells from mouse embryonic and adult fibroblast cultures by defined factors. Cell 126, 663–676. https://doi.org/10.1016/j.cell.2006.07.024

Takasato, M., Er, P.X., Becroft, M., Vanslambrouck, J.M., Stanley, E.G., Elefanty, A.G., Little, M.H., 2014. Directing human embryonic stem cell differentiation towards a renal lineage generates a self-organizing kidney. Nat. Cell Biol. 16, 118–126. https://doi.org/10.1038/ncb2894

Takasato, M., Er, P.X., Chiu, H.S., Little, M.H., 2016. Generation of kidney organoids from human pluripotent stem cells. Nat. Protoc. 11, 1681–1692. https://doi.org/10.1038/nprot.2016.098

Takasato, M., Er, P.X., Chiu, H.S., Maier, B., Baillie, G.J., Ferguson, C., Parton, R.G., Wolvetang, E.J., Roost, M.S., Chuva de Sousa Lopes, S.M., Little, M.H., 2015. Kidney organoids from human iPS cells contain multiple lineages and model human nephrogenesis. Nature 526, 564–568. https://doi.org/10.1038/nature15695

Taylor, T.D., 2007. Golden Fractal Trees, in: Proceedings of the 2007 Bridges Conference on Mathematical Connections in Art, Music, and Science. Sarhangi, R. & Barallo, J, pp. 181–188.

Thomson, J.A., Itskovitz-Eldor, J., Shapiro, S.S., Waknitz, M.A., Swiergiel, J.J., Marshall, V.S., Jones, J.M., 1998. Embryonic stem cell lines derived from human blastocysts. Science 282, 1145–1147.

Torres, V.E., Chapman, A.B., Devuyst, O., Gansevoort, R.T., Grantham, J.J., Higashihara, E., Perrone, R.D., Krasa, H.B., Ouyang, J., Czerwiec, F.S., TEMPO 3:4 Trial Investigators, 2012. Tolvaptan in patients with autosomal dominant polycystic kidney disease. N. Engl. J. Med. 367, 2407–2418. https://doi.org/10.1056/NEJMoa1205511

Torres, V.E., Harris, P.C., 2006. Mechanisms of Disease: autosomal dominant and recessive polycystic kidney diseases. Nat. Clin. Pract. Nephrol. 2, 40–55. https://doi.org/10.1038/ncpneph0070

Torres, V.E., Wang, X., Qian, Q., Somlo, S., Harris, P.C., Gattone, V.H., 2004. Effective treatment of an orthologous model of autosomal dominant polycystic kidney disease. Nat. Med. 10, 363–364. https://doi.org/10.1038/nm1004

Tufro, A., Norwood, V.F., Carey, R.M., Gomez, R.A., 1999. Vascular endothelial growth factor induces nephrogenesis and vasculogenesis. J. Am. Soc. Nephrol. JASN 10, 2125–2134.

Unbekandt, M., Davies, J.A., 2010. Dissociation of embryonic kidneys followed by reaggregation allows the formation of renal tissues. Kidney Int. 77, 407–416. https://doi.org/10.1038/ki.2009.482

Vainio, S., Lin, Y., 2002. Organogenesis: Coordinating early kidney development: lessons from gene targeting. Nat. Rev. Genet. 3, 533–543. https://doi.org/10.1038/nrg842

Velagapudi, C., Nilsson, R.-P., Lee, M.J., Burns, H.S., Ricono, J.M., Arar, M., Barnes, V.L., Abboud, H.E., Barnes, J.L., 2012. Reciprocal induction of simple organogenesis by mouse kidney progenitor cells in three-dimensional co-culture. Am. J. Pathol. 180, 819–830. https://doi.org/10.1016/j.ajpath.2011.11.002

Wallace, D.P., 2011. Cyclic AMP-mediated cyst expansion. Biochim. Biophys. Acta 1812, 1291–1300. https://doi.org/10.1016/j.bbadis.2010.11.005

Wallace, D.P., Rome, L.A., Sullivan, L.P., Grantham, J.J., 2001. cAMP-dependent fluid secretion in rat inner medullary collecting ducts. Am. J. Physiol. Renal Physiol. 280, F1019-1029.

Wang, X., Gattone, V., Harris, P.C., Torres, V.E., 2005. Effectiveness of vasopressin V2 receptor antagonists OPC-31260 and OPC-41061 on polycystic kidney disease

development in the PCK rat. J. Am. Soc. Nephrol. JASN 16, 846–851. https://doi.org/10.1681/ASN.2004121090

Wang, Y., Borchert, M.L., DeLuca, H.F., 2012. Identification of the vitamin D receptor in various cells of the mouse kidney. Kidney Int. 81, 993–1001. https://doi.org/10.1038/ki.2011.463

Watanabe, T., Costantini, F., 2004. Real-time analysis of ureteric bud branching morphogenesis in vitro. Dev. Biol. 271, 98–108. https://doi.org/10.1016/j.ydbio.2004.03.025

Willey, C.J., Blais, J.D., Hall, A.K., Krasa, H.B., Makin, A.J., Czerwiec, F.S., 2017. Prevalence of autosomal dominant polycystic kidney disease in the European Union. Nephrol. Dial. Transplant. Off. Publ. Eur. Dial. Transpl. Assoc. - Eur. Ren. Assoc. 32, 1356–1363. https://doi.org/10.1093/ndt/gfw240

Wolfe, R.A., Ashby, V.B., Milford, E.L., Ojo, A.O., Ettenger, R.E., Agodoa, L.Y.C., Held, P.J., Port, F.K., 1999. Comparison of Mortality in All Patients on Dialysis, Patients on Dialysis Awaiting Transplantation, and Recipients of a First Cadaveric Transplant. N. Engl. J. Med. 341, 1725–1730. https://doi.org/10.1056/NEJM199912023412303

Xia, Y., Nivet, E., Sancho-Martinez, I., Gallegos, T., Suzuki, K., Okamura, D., Wu, M.-Z., Dubova, I., Esteban, C.R., Montserrat, N., Campistol, J.M., Izpisua Belmonte, J.C., 2013. Directed differentiation of human pluripotent cells to ureteric bud kidney

progenitor-like cells. Nat. Cell Biol. 15, 1507–1515. https://doi.org/10.1038/ncb2872

Xia, Y., Sancho-Martinez, I., Nivet, E., Rodriguez Esteban, C., Campistol, J.M., Izpisua Belmonte, J.C., 2014. The generation of kidney organoids by differentiation of human pluripotent cells to ureteric bud progenitor-like cells. Nat. Protoc. 9, 2693–2704. https://doi.org/10.1038/nprot.2014.182

Xinaris, C., Benedetti, V., Novelli, R., Abbate, M., Rizzo, P., Conti, S., Tomasoni, S., Corna, D., Pozzobon, M., Cavallotti, D., Yokoo, T., Morigi, M., Benigni, A., Remuzzi, G., 2016. Functional Human Podocytes Generated in Organoids from Amniotic Fluid Stem Cells. J. Am. Soc. Nephrol. JASN 27, 1400–1411. https://doi.org/10.1681/ASN.2015030316

Xinaris, C., Benedetti, V., Rizzo, P., Abbate, M., Corna, D., Azzollini, N., Conti, S., Unbekandt, M., Davies, J.A., Morigi, M., Benigni, A., Remuzzi, G., 2012. In vivo maturation of functional renal organoids formed from embryonic cell suspensions. J. Am. Soc. Nephrol. JASN 23, 1857–1868. https://doi.org/10.1681/ASN.2012050505

Xinaris, C., Brizi, V., Remuzzi, G., 2015. Organoid Models and Applications in Biomedical Research. Nephron 130, 191–199. https://doi.org/10.1159/000433566

Xinaris, C., Yokoo, T., 2014. Reforming the kidney starting from a single-cell suspension. Nephron Exp. Nephrol. 126, 107. https://doi.org/10.1159/000360682

Yamaguchi, T., Nagao, S., Wallace, D.P., Belibi, F.A., Cowley, B.D., Pelling, J.C., Grantham, J.J., 2003. Cyclic AMP activates B-Raf and ERK in cyst epithelial cells from autosomal-dominant polycystic kidneys. Kidney Int. 63, 1983–1994. https://doi.org/10.1046/j.1523-1755.2003.00023.x

Yang, Z., Zimmerman, S., Brakeman, P.R., Beaudoin, G.M., Reichardt, L.F., Marciano, D.K., 2013. De novo lumen formation and elongation in the developing nephron: a central role for afadin in apical polarity. Dev. Camb. Engl. 140, 1774–1784. https://doi.org/10.1242/dev.087957

Yasuda, G., Jeffries, W.B., 1998. Regulation of cAMP production in initial and terminal inner medullary collecting ducts. Kidney Int. 54, 80–86. https://doi.org/10.1046/j.1523-1755.1998.00990.x

Yokoo, T., Ohashi, T., Shen, J.S., Sakurai, K., Miyazaki, Y., Utsunomiya, Y., Takahashi, M., Terada, Y., Eto, Y., Kawamura, T., Osumi, N., Hosoya, T., 2005. Human mesenchymal stem cells in rodent whole-embryo culture are reprogrammed to contribute to kidney tissues. Proc. Natl. Acad. Sci. U. S. A. 102, 3296–3300. https://doi.org/10.1073/pnas.0406878102

Yokoyama, H., Anzai, N., Ljubojevic, M., Ohtsu, N., Sakata, T., Miyazaki, H., Nonoguchi, H., Islam, R., Onozato, M., Tojo, A., Tomita, K., Kanai, Y., Igarashi, T., Sabolic, I., Endou, H., 2008. Functional and immunochemical characterization of a novel organic anion transporter Oat8 (Slc22a9) in rat renal collecting duct. Cell. Physiol. Biochem. Int. J. Exp. Cell. Physiol. Biochem. Pharmacol. 21, 269–278. https://doi.org/10.1159/000129385

Young, E.W.K., Beebe, D.J., 2010. Fundamentals of microfluidic cell culture in controlled microenvironments. Chem. Soc. Rev. 39, 1036–1048. https://doi.org/10.1039/b909900j

Yu, J., Thomson, J.A., 2008. Pluripotent stem cell lines. Genes Dev. 22, 1987–1997. https://doi.org/10.1101/gad.1689808

Yuri, S., Nishikawa, M., Yanagawa, N., Jo, O.D., Yanagawa, N., 2017. In Vitro Propagation and Branching Morphogenesis from Single Ureteric Bud Cells. Stem Cell Rep. 8, 401–416. https://doi.org/10.1016/j.stemcr.2016.12.011

Zhu, Y., Ma, N., Li, H.-X., Tian, L., Ba, Y.-F., Hao, B., 2014. Berberine induces apoptosis and DNA damage in MG-63 human osteosarcoma cells. Mol. Med. Rep. 10, 1734–1738. https://doi.org/10.3892/mmr.2014.2405

CHAPTER 7 - APPENDICES

7.1 Contribution to the thesis by other researchers

Part of this study was performed in collaboration with other researchers and scientists of the IRCCS - Istituto di Ricerche Farmacologiche 'Mario Negri', Bergamo (Italy), of the Università degli Studi di Genova, Genova (Italy), and of the Azienda Socio-Sanitaria Territoriale (ASST) Papa Giovanni XXIII, Bergamo (Italy) as follows:

- Dr. Valentina Benedetti, Laboratory of Cell Biology and Regenerative Medicine, IRCCS - Istituto di Ricerche Farmacologiche 'Mario Negri', helped me with most of the experiments, particularly in establishing the tubule engineering system, the engineered tubules' 3D culture conditions, and with quantification and statistical analyses.
- PDMS scaffold design and fabrication was carried out by Dr. Patrizia Guida, Dr. Elena Angeli and Professor Ugo Valbusa, Nanomed Laboratories, Dipartimento di Fisica, Università degli Studi di Genova.
- Professor Andrea Remuzzi, Laboratory of Tissue Engineering for Regenerative Medicine, IRCCS - Istituto di Ricerche Farmacologiche 'Mario Negri', kindly provided MDCK type II cells.
- Dr. Marta Todeschini and Dr. Marilena Mister, Laboratory of Immunology of Organ Transplantation, IRCCS - Istituto di Ricerche Farmacologiche 'Mario Negri', performed the isolation of the patient's peripheral blood mononuclear cells.
- Dr. Susanna Tomasoni, Dr. Osele Ciampi and Dr. Lorena Longaretti, Laboratory of Gene Therapy and Cellular Reprogramming, IRCCS - Istituto di Ricerche Farmacologiche 'Mario Negri', generated and characterised every iPSC line used in this research.
- Dr. Ursula Giussani and Dr. Paolo Fruscella, Laboratory of Genetic Medicine, ASST Papa Giovanni XXIII conducted patient-derived iPSC karyotype analysis.

The PhD Student, Valerio Brizi, carried out every other experiment by applying the technologies and procedures described in the Materials and Methods section of this thesis.

7.2 Full list of publications by the candidate

Benedetti V.*****, **Brizi V.***, Guida P.*****, Tomasoni S., Ciampi O., Angeli E., Valbusa U., Benigni A., Remuzzi G. and Xinaris C. *Engineered kidney tubules for studying patient-specific developmental disorders, disease modelling and drug discovery*. **Under Revision.**

***Equal contribution.**

Benedetti V.*****, **Brizi V.***, and Xinaris C. *Generation of functional kidney organoids in vivo starting from a single-cell suspension*. Methods Mol Biol 2016 Aug 19. [Epub ahead of print].

***Equal contribution.**

Xinaris C., **Brizi V.**, and Remuzzi G. *Organoid models and applications in biomedical research*. Nephron (Experimental Nephrology and Genetics: Review) 2015 Jun 25; 130: 191-199.

Ciocca L., Surace C., Digilio M.C., Roberti M.C., Sirleto P., Lombardo A., Russo S., **Brizi V.**, Grotta S., Cini C., and Angioni A. *Array-CGH characterization and genotype-phenotype analysis in a patient with a ring chromosome 6*. BMC Med Genomics 2013 Feb 11; 6:3.